universität wien

DIPLOMARBEIT

Time Dependent Changes during Hydroxyurea Induced Senescence in *MYCN* Amplified Neuroblastoma

angestrebter akademischer Grad

Magistra der Naturwissenschaften (Mag. rer.nat.)

Verfasserin / Verfasser:	Heide-Marie Binder
Matrikel-Nummer:	0048925
Studienrichtung (lt. Studienblatt):	A490
Betreuerin / Betreuer:	Assoc. Prof. Heinrich Kovar, PhD

Wien, am 08.08.08

Acknowledgement

I would like to express my gratitude to Assoc. Prof. Peter F. Ambros, PhD for giving me the possibility to be part of his working group and to explore the field of tumour cell senescence. I would like to thank him and his wife Inge M. Ambros, MD for support, valuable discussions and guidance. Many thanks also to Assoc. Prof. Heinrich Kovar, PhD who was supervisor of my diploma thesis and to Prof. Helmut Gadner for giving me the opportunity to do my diploma thesis at the CCRI.

I want to thank my colleagues at the CCRI for encouragement and for making my stay at the CCRI memorable. Further I want to thank all who supported me with ideas, discussion, methods, antibodies, good mood and nice moments during my diploma thesis.

I want to thank all colleagues at the Henry Wellcome Laboratory for Biogerontology Research in Newcastle upon Time, especially Prof. Thomas von Zglinicki and João Passos for the refreshing athmosphere in the stormy North.

My special thankfulness to my family and Reinhard who supported me immensely throughout my studies and supplied me with motivation and an ambience to relax from exhausting times.

My honour to my friends and my colleagues from university for supplying me with a balancing framework and for keeping me in a good mood.

Kurzfassung

Neuroblastoma ist die häufigste Art von extracranialen, soliden Tumoren bei Kindern. Häufig treten Amplifikationen des *MYCN* Gens auf, die im Zellkern als double minute chromosomes oder als homogenous staining region vorliegen.

Durch Behandlung mit niedrigen Dosen von Hydroxyurea (HU) können die amplifizierten *MYCN* Genkopien selektiv aus dem Zellkern geschleust werden und in Mikrokernen nachgewiesen werden. Außerdem wurde in den malignen Neuroblastomzellen nach einer sechswöchigen niedrig dosierten Behandlung mit HU zelluläre Seneszenz nachgewiesen. In gutartigen humanen Zellen wird diese zelluläre Veränderung durch irreversiblen Proliferationsstillstand gekennzeichnet, was durch cyclin dependent kinases inhibitors (CDKI) und Aktivierung von p53 und pRb bedingt wird. Weiters wird Seneszenz durch erhöhte mitochondriale Radikalfreisetzung und Änderung der Komponenten der Kernmatrix- und -membran gekennzeichnet.

Das Ziel dieser Diplomarbeit war es Kandidaten-Signalwege zu erforschen, die im Prozess der Hydroxyurea induzierten Seneszenzentstehung in *MYCN* amplifizierten Neuroblastomazellen wichtig sind.

Dafür wurden zeitliche Veränderungen des Zellzyklus, des zellulären Sauerstoffradikalgehalts und der mitochondrialen Begebenheiten wie Membranpotential und Masse während der HU Behandlung mittels Durchflußzytometrie ermittelt. Mit Immunfluoreszenz-Mikroskopie wurden zusätzlich die Kernmorphologie und Komponenten der nukleären Matrix ermittelt. Proteinanalysen der CDKIs sowie von assoziierten Proteinen und von MYCN erfolgten mittels Western Blot.

Wesentliche Resultate zeigten, dass nach 3-5 Tagen HU Behandlung die Zellen in der S-Phase des Zellzyklus akkumulierten. Im gleichen Zeitfenster wurde p16 reduziert und p53 erhöht nachgewiesen. Von Tag 10 an wurde eine Reduktion des MYCN- und pRb-Proteinlevels nachgewiesen und die Anzahl der Zellen die sich in G1-Phase befanden erhöhte sich. Zusätzlich stieg der p21 Proteingehalt an und p16 erhöhte sich wieder.

Während der achtwöchigen Behandlung akkumulierten stetig Sauerstoffradikale zu einem 13-fachen Anstieg. Auch die Mitochondrien erreichten eine 3.4-fache Masse und hatten ein zur Hälfte reduziertes Membranpotential. Zuvor fehlendes Lamin A/C wurde in 67% der 8 Wochen behandelten Zellen gefunden und die Kernhülle dieser Zellen war verformt und lobuliert.

In HU behandelten MNA-NB Zellen könnte Seneszenz durch Akkumulation von oxidativem Stress, durch p21-p53 Induktion, durch Aufhebung der *MYCN* Expression und durch Änderung der Kernstruktur entstehen.

Abstract

Neuroblastoma (NB) is the most common extra-cranial solid childhood tumour, frequently associated with *MYCN* amplification (MNA). Selective expulsion of double-minute chromosomes, carrying the amplified gene can be induced by low dose hydroxyurea (HU) treatment. Moreover, chronic low-dose HU induces senescence after six weeks in malignant neuroblastoma cells. In benign human cells, key pathways of senescence-associated irreversible proliferation arrest involve cyclin dependent kinases inhibitors (CDKI) and activation of p53 and pRb. In addition, cellular changes in senescent cells include increased mitochondrial radical levels and alterations of components of the nuclear lamina.

The aim of this study was to investigate candidate pathways involved in HU-induced senescence of MNA NB cells.

Thus, time dependent changes of cell cycle, reactive oxygen species (ROS), mitochondrial mass and membrane potential $\Delta\psi m$ were assessed by flow cytometry. Furthermore, nuclear morphology and lamina composition was monitored by immune fluorescence microscopy. Expression of CDKIs and associated proteins was determined by western blotting together with MYCN.

We found that cells accumulated in S-phase 1 – 5 days after treatment accompanied by decrease in p16 and increase in p53 expression. From day 10 onwards a descent in MYCN and pRb was found and the proportion of cells in the G1-phase increased. Additionally, p21 rose and p16 recovered. ROS levels accumulated steadily to13-fold after 8 weeks and mitochondria were increased 3.4-fold in mass with 50% decrease in mitochondrial membrane potential. Previously lacking lamin A/C was expressed in 67% and the nuclear envelope was lobular in senescent cells after 8 weeks HU-treatment.

In MNA NB cells, senescence may be induced by accumulating oxidative stress leading to p53-p21 induction, abrogation of MYCN expression and finally changes in nuclear structure.

Table of Content

1 Introduction

Tumour cells acquire their transforming behaviour by accumulating mutations and/or changing regulation patterns that would normally keep the cells under high suppression and control. Mechanisms like evasion of apoptosis, independency on intra- and extra-cellular stimuli, change in functionality comprising angiogenesis, tissue invasion, increased proliferative capacity and limitless replicative potential lead to a selective advantage of these cells (Figure 1) (Hanahan and Weinberg 2000).

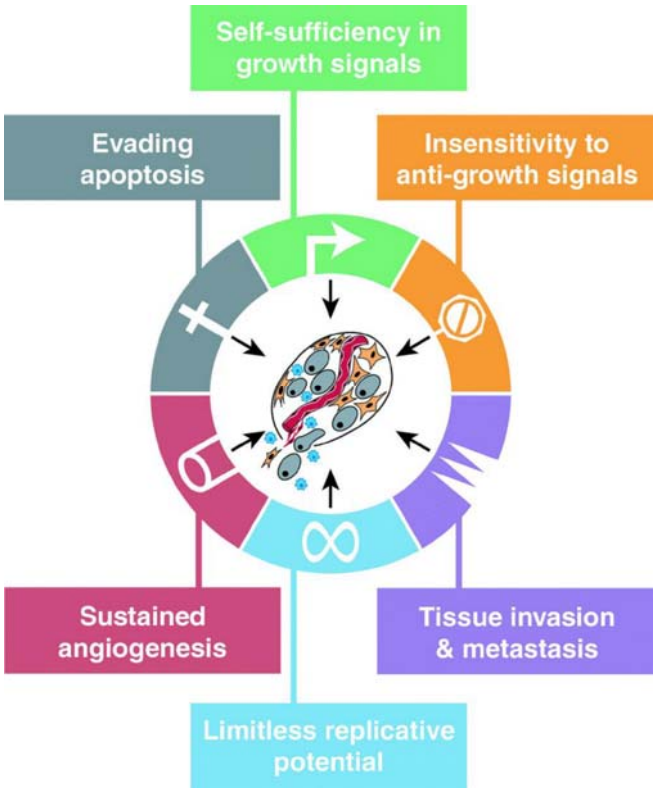

Figure 1 **Acquired Capabilities of Cancer.** (Hanahan and Weinberg 2000)

1.1 Neuroblastoma

1.1.1 General features

Neuroblastoma is the most common solid extra cranial childhood tumour. It is an embryonic neoplasm of the postganglionic sympathetic nervous system. The frequency of detection in children with less than 15 years of age is rated 1 in 100000 (Ladenstein, Berthold et al. 2006), with an average age of diagnosis of 18 month. The real number of incidences may be much higher due to a high frequency of spontaneous regression as indicated by mass screening programs in Japan,

Canada, and Europe (Brodeur 2003; Ladenstein, Berthold et al. 2006).

The clinical hallmark of this neoplasm is heterogeneity. Some tumours may undergo spontaneous regression or maturation/differentiation to a benign neoplasm. Others exhibit an extremely malignant phenotype with regional or disseminated disease which frequently is resistant to intensive therapy (Brodeur 2003). Conflicting opinions exist about the multitude of genetic aberrations, interactions and their usage as prognostic markers. These range from 1p loss of heterogeneity (Caron 1995), allelic loss of the long arm of chromosome 11 (White, Maris et al. 1997), 14q deletions (Thompson, Seifried et al. 2001) to *MYCN* amplification. Moreover, to date only one hereditary neuroblastoma predisposition gene (*HNB1*) has been found which was linked to locus 16p12-13 and was suggested to be *PHOX2B* (Weiss, Guo et al. 2000; Bourdeaut, Trochet et al. 2005).

Next to genetic aberrations, gene expression changes have been observed in neuroblastomas. Signals important for the development of the sympathetic nervous system like the neurotrophins are deregulated in neuroblastoma. TrkA downregulation as well as TrkB upregulation is related to *MYCN* amplification, aggressive tumour behaviour and unfavourable outcome (Nakagawara, Arima et al. 1992; Suzuki, Bogenmann et al. 1993; Nakagawara, Azar et al. 1994). Moreover, drug resistance progressively increases with therapy in neuroblastomas by induction of *MDR1* and *ABCC1* (Keshelava, Seeger et al. 1997).

Spontaneous regression of neuroblastoma may be related to delayed onset of apoptotic pathways (Oue, Fukuzawa et al. 1996). Bcl-2 is supposed to contribute to survival of cells in neurogenesis by inhibiting apoptosis and is, in neuroblastoma, strongly correlated with *MYCN* amplification and aggressive tumour behaviour (Castle, Heidelberger et al. 1993). Another important fact is that 94% of all neuroblastomas revealed telomerase expression. High activity was related to *MYCN* amplification and to poor prognosis, while low telomerase activity was associated with good prognosis (Hiyama, Hiyama et al. 1995).

1.1.2 *MYCN*

1.1.2.1 *MYCN* Amplification (MNA)

MYCN was identified as amplified genetic region in neuroblastoma cell lines as well as in a primary tumour, with partial homology to the *MYC* proto-oncogene (Kohl, Kanda et al. 1983; Schwab, Alitalo et al. 1983). *MYCN* is situated on the short arm of chromosome 2 (2p24) from where it is amplified as extrachromosomal double minute chromosomes (dmin) that may be linearized and

further integrate randomly into the genome to form homogenously staining regions (hsr)(Kohl, Kanda et al. 1983). One *MYCN* copy is retained at its original locus on chromosome 2 (Seeger, Brodeur et al. 1985; Corvi, Amler et al. 1994). Amplified *MYCN* copies are associated with rapid progression of disease in untreated neuroblastomas (Brodeur, Seeger et al. 1985; Seeger, Brodeur et al. 1985). 70 percent of patients whose tumour comprised only one *MYCN* copy had progression-free survival eighteen month after diagnosis, whereas 95 percent of patients with 10 and more copies per diploid genome displayed advanced disease (Corvi, Amler et al. 1994). MNA is detected in about 30 percent of untreated neuroblastomas and suggests an intrinsic biologic property that is found in a subset of neuroblastomas already at time of diagnosis, demonstrating a powerful predictor of poor prognosis (Brodeur, Hayes et al. 1987).

1.1.2.2 *MYCN* Expression and Function

Expression of *MYCN* proto-oncogene is normally restricted to the nervous system and selected other tissues of the developing embryo. The 49,6 kD oncoprotein (Wu, Apweiler et al. 2008) is a member of the superfamily of transcription factors (Slamon, Boone et al. 1986). Like other members of the MYC family, MYCN contains a basic DNA binding region (BR), a helix-loop-helix (HLH) and a leucine zipper motif at the carboxy-terminus and an amino-terminal transactivation domain (MYC box) (Wenzel, Cziepluch et al. 1991). This nuclear protein has a short half-life and acts as a transcription factor only in heterodimerized form. MAX, another ubiquitously expressed nuclear protein with basic helix-loop-helix/leucine zipper motif (bHLH-LZ) and long half-life is its binding partner. MYCN and MAX heterodimerize via their bHLH-LZ motifs to form a complex that can bind to the DNA sequence CACGTG (Wenzel and Schwab 1995), also called E-Box. The MYC/MAX complex acts as transcriptional activator and is suggested to influence cell growth and proliferation through direct activation of genes involved in DNA synthesis, RNA metabolism and cell-cycle progression (Grandori and Eisenman 1997). In contrast, the homodimerized MAX-complex as well as heterodimers formed with nuclear proteins MAD and MXI1 are transcriptional repressive. Moreover, these two members of the MYC-related bHLH-LZ family of proteins compete with MYCN to form a complex with MAX (Lahoz, Xu et al. 1994; Foley and Eisenman 1999).

MYCN exerts its oncogenic effects through transcriptional upregulation of numerous target genes including *ABCC1* (Norris, Bordow et al. 1997), *MCM7* (Shohet, Hicks et al. 2002), the p53 inhibitor *MDM2* (Slack and Shohet 2005), *HMGA1* (Giannini, Cerignoli et al. 2005) and repression of *DKK* genes (Koppen, Ait-Aissa et al. 2007; Koppen, Ait-Aissa et al. 2008).

1.1.2.3 Prognostic Implications of *MYCN*

Commonly, *MYCN* amplification correlates with high levels of MYCN protein and aggressive tumour behaviour (Nakagawara, Arima et al. 1992) but also non-*MYCN*-amplified cell lines can express high levels of MYCN. In these cells alternations in the protein degradation pathway might lead to a long half-life of MYCN proteins (Cohn, Salwen et al. 1990).
High-resolution restriction mapping of the *MYCN* locus suggests that a 130kb core domain is amplified, containing no other expressed gene constantly amplified in human neuroblastomas (Reiter and Brodeur 1996; Reiter and Brodeur 1998). Still, *DDX1* and *NAG* were found co-amplified repeatedly with *MYCN* in cell lines and primary tumours (George, Kenyon et al. 1996; Wimmer, Zhu et al. 1999). Moreover, increased expression of genes in the vicinity of *MYCN*, like *ALK*, were demonstrated (Stock, Bozsaky et al. 2008).

1.1.2.4 Nuclear Organization and Expulsion of Amplified Genetic Material

Like in many cancer cells, also in neuroblastoma amplified genes are present as dmin or hsr (Benner, Wahl et al. 1991). Dmin are minichromosomal genetic elements with circular, few megabase sized DNA. They lack functional centromeres and telomeres, and frequently dmin are autonomously replicating. Dmin are found to localize to peripheral nuclear sites after nuclear membrane breakdown. Further localisation during the cell cycle was revealed in Table 1. Studies analysing primary MNA neuroblastomas conclude that more than 90% of the amplified DNA is present as dmin (Benner, Wahl et al. 1991; Moreau, McGrady et al. 2006).

Cell cycle phase	**location and nature of dmin**
S-phase	relocated to the centre or expelled by budding, colocalization with lamins
G2	dmin are uncoupled
Anaphase	lag behind
Prometaphase	locate near the chromosome rosettes at the periphery

Table 1 **Location and nature of dmin chromosomes during the cell cycle** (Deng, Zhang et al. 2006).

It has been concluded that dmin, chromosome fragments and lagging genetic material can give rise to micronuclei (Schiffmann and De Boni 1991). Micronuclei are intracellular compartments

surrounded by a nuclear membrane and localize near the nucleus.

There are at least two different pathways explaining how dmin are incorporated into micronuclei. The classical pathway describes lagging acentric chromosomes that are enclosed into nuclear membranes after mitosis, when the nuclear membrane forms again (Ford, Schultz et al. 1988). The other mechanism was found to take place during S-phase selectively, when dmin are situated to the periphery of the nucleus (Tanaka and Shimizu 2000). These spatially defined dmin have been shown to associate with lamins during S-phase (Itoh and Shimizu 1998; Tanaka and Shimizu 2000). These associated complexes of dmin and lamins form extrusions often referred to as nuclear buds that evolve into micronuclei that are rich in dmin genetic material during metaphase/anaphase transition (Shimizu, Itoh et al. 1998).

Micronuclei are inducible by many different mutagens including clastogens - substances that cause breakage of chromosomes - and aneugens – substances that affect cell division and the mitotic spindle apparatus. Additionally, also ionizing radiation induces micronuclei by means of double strand breaks (DSB) (Schoenlein, Barrett et al. 2003). Prolonged cell cycle duration, higher incidence of double strand breaks and a reduced DNA repair are typical incidences in premature and physiological aging. Cells from patients with premature aging syndromes and from aged, healthy controls show an elevated formation of micronuclei (Weirich-Schwaiger, Weirich et al. 1994).

The mechanism and function of selective expulsion of extrachromosomal material is still not clear. Moreover, the effects micronuclei exert in the cytoplasm and whether they are degraded or expulsed from the cell are to be explored.

1.2 Cellular Senescence

Somatic cells face different stresses during their lifespan. Dependent on the species, tissue and cell type diverse counter mechanisms have evolved that let the organism cope with cellular stress. One option is apoptosis with the intention of eliminating stress-damaged cells actively. Another possible outcome is differentiation to change the cellular function as means of adaption. Alternatively, stressed cells may enter senescence which introduces a permanent proliferation arrest. An example for such differences are damaged epithelial cells and fibroblasts which have been shown to senesce, while damaged lymphoblasts activate the apoptotic pathway (Campisi and d'Adda di Fagagna 2007). The predictions of why a cell gets committed for either counter mechanism are still to be clarified.

More than 45 years ago Hayflick first coined the term replicative cellular senescence and referred to it as a programmed intracellular event. He showed that normal human cells (embryonic fibroblasts) have a limited proliferative capacity in culture. In his *in vitro* experiments he observed a change in phenotype of the fibroblast cell culture: These cells had a segregation blockage but remained alive for a prolonged period of time before dying (Hayflick and Moorhead 1961; Hayflick 1965).

From then on research in this field emerged. Gerontology focused on many theories about the coherence of cellular and organismal aging, as well as on theories explaining the onset of senescence. The theories established try to explain the molecular, genetic and biologic changes observed along with upcoming senescence but still no concordance in ideas could be brought about. The major problem reflecting this topic is the extreme heterogeneity between different cell types, species and inducers of senescence (Figure 2) which leave possible explanations high. Still, in the following chapter accredited general features, markers, the main theories of senescence and the pathways leading to its onset are resumed.

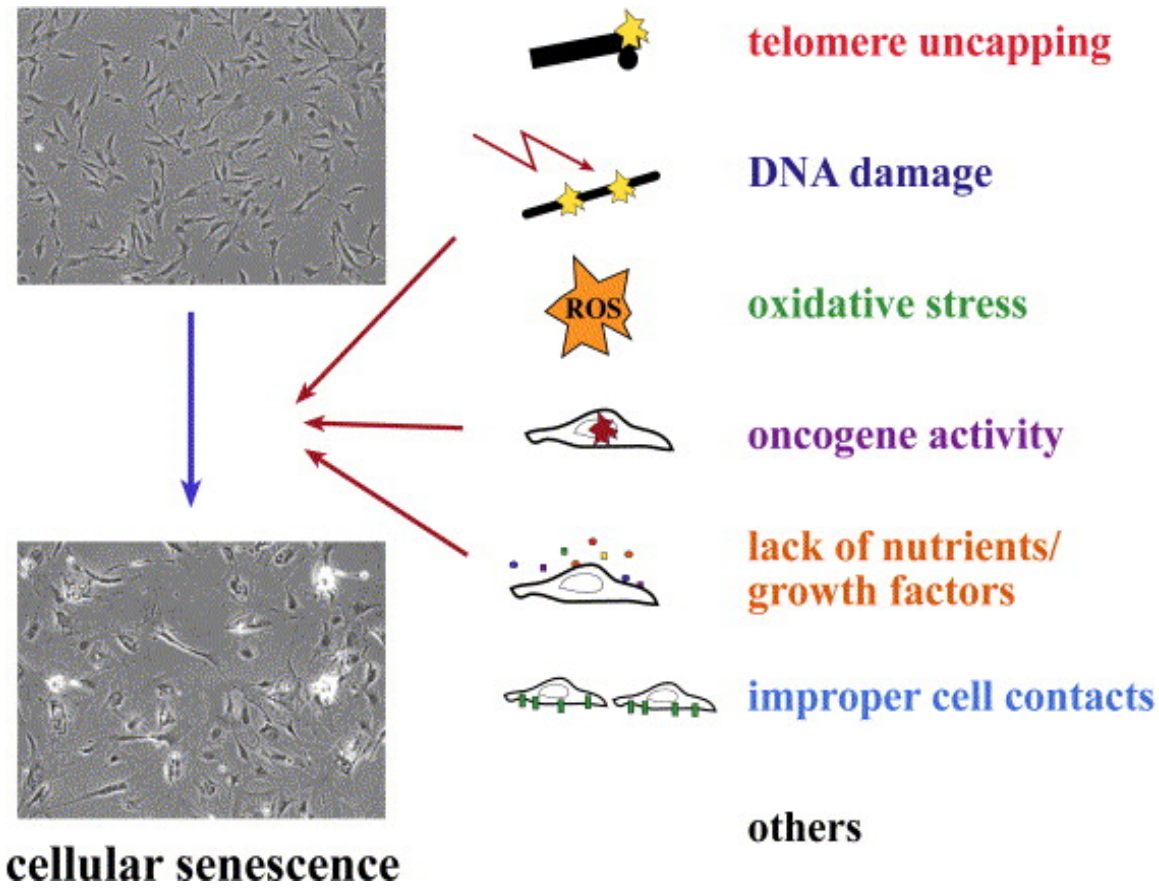

Figure 2 **Inducers of senescence.** Multiple types of stresses can induce cells to undergo senescence. The combined levels of stress determine how rapidly the entry into senescence will occur (Ben-Porath and Weinberg 2005).

1.2.1 General Features of Senescence and their Approval

With ongoing senescence, cells undergo several changes listed in Table 2. Whether these changes in morphology, expression and metabolism induce senescence or whether this is just the consequence of the senescent phenotype still remains unknown.

Feature
irreversible replication blockage
morphology remodelling increased cell volume increased granularity loss of original shape increased adherence cell-cell contact inhibition
change in gene expression
metabolism change
prolonged viability
chromatin silencing
senescent-associated heterochromatic foci (SAHF)
shortened telomeres
increased ROS
dysfunctional mitochondria

Table 2 **Features of senescence.** Summarized from (Goldstein 1990; Dimri, Lee et al. 1995; Toussaint, Medrano et al. 2000; Ben-Porath and Weinberg 2004; Ben-Porath and Weinberg 2005; Campisi and d'Adda di Fagagna 2007; Itahana, Campisi et al. 2007; Zhang 2007).

1.2.2 Theories of Senescence

In this chapter only the main theories of senescence are described. A high convergence in between theories is often found, which makes it even harder to differentiate between either of them. Just to mention, there are - next to replicative senescence, stress induced premature senescence, like oncogene induced and free radical induced aging - theories dealing with the accumulation of damage (Kirkwood 2005), accumulation of waste and mitochondrial theory of aging . Replicative senescence, was found to result in an DNA damage response (DDR). Also free radicals and accumulated damage, elucidate a DDR, which is a connecting part in nearly all theories. (Guo, Deng et al. 2007; Passos, Saretzki et al. 2007; Deng, Chan et al. 2008)

Thus, all theories of senescence simplify this complex cellular network but are probably giving an

incomplete description of cellular senescence. Of course for every theory there are experimental back up but perhaps not reliable in other systems. Thus, an overlap of all theories depending on the species, cell type and senescence inducers may explain the senescence phenomenon more adequately.

1.2.2.1 Replicative Senescence – Role of Telomeres

Telomeres are heterochromatic, nucleoprotein like structures at the chromosome ends (de Lange 2005). The function of telomeres is capping and protecting chromosomes from being recognized as double strand breaks (DSB), from fusion of chromosome ends and to provide stability to chromosomes.

Replication shortens the telomeric repeats up to 50-100 basepairs each S-phase (Alberts Bruce 2002). Moreover, oxidative stress leads to telomere uncapping and erosion (Passos and von Zglinicki 2005; Passos, Saretzki et al. 2007; Passos, Saretzki et al. 2007). Telomerase, an enzyme containing an RNA template for telomeric repeats is able to extend the telomere length. Like this, the proliferative capacity of a cell is increased. Tumour cells highjack this mechanism often in order to prevent proliferation arrest. Short or uncapped telomeres lead to a situation that resembles damaged DNA at the end of linear chromosomes: Chromatin ends are not looped and a free double strand is exposed to the surrounding which immediately induces a DNA repair mechanism leading to apoptosis or senescence (Deng, Chan et al. 2008).

1.2.2.2 Stress-Induced-Premature Senescence

In cells which still have long, capped and protected telomeres senescent features can be induced prematurely. This type of senescence is referred to as stress-induced premature senescence (SIPS), evolves usually much faster than replicative senescence and many subtypes belong to it. SIPS varies dependent on the type of endo- and exogenous stimuli that commit the cells to the senescence pathway and often these stresses are cumulative. Oxidative stress, ultra violet radiation (UV), ionizing radiation (IR) and chemotherapeutic agents change the point of time and approach to undergo senescence when a critical level of stress is acquired. Source and severity of subcytotoxic doses of the stressor, the cell type and species influence the molecular mechanisms underlying the decision between cell death, differentiation or senescence. In the following chapter the main stimuli that induce SIPS are explained and different schemes will be presented. The function of stress induced premature senescence seems to be a halt of further proliferation. Thereby stress induced damage cannot segregate to daughter cells. This is thus seen as a parallel mechanism to apoptosis or

differentiation. Like in replicative senescence, a DDR triggers further responses related to senescence. (Ben-Porath and Weinberg 2005; von Zglinicki, Saretzki et al. 2005; Campisi and d'Adda di Fagagna 2007; Suzuki and Boothman 2008)

1.2.2.3 Oncogene Induced Senescence (OIS)

One of the key steps in cellular transformation of cells is immortalization which is done by expression of telomerase or by alternative lengthening of telomeres (ALT). Further hallmarks are the dominant gain of function of oncogenes and/or recessive loss of function of tumor suppressor genes which lead to a deregulation of proliferation and apoptosis. (Hanahan and Weinberg 2000; Campisi 2005; Zhang 2007)

Serrano et al found that oncogenic RAS induces a G1 arrest in primary human and rodent cells (Serrano, Lin et al. 1997). From then on many other oncogenes, which are summarized in Table 3, were found to induce senescence when upregulated. These include components of the RAS pathway and lead to an increased proliferation by growth factor signaling. Overexpression of E2F transcription factors also induces premature senescence as cell cycle proceeds unregulated. Activation and overexpression of downstream targets of the TGF-β pathway like SMAD3 or SMURF2 lead to a senescent phenotype (Funayama and Ishikawa 2007). These *in vitro* and *in vivo* studies lead to the suggestion that senescence is a cell-intrinsic mechanism suppressing the transformation of a benign lesion to a highly proliferative tumor. (Campisi 2005; Di Micco, Fumagalli et al. 2007; Zhang 2007)

It is thought that the level of oncogene expression, at least for RAS correlates with the strength of the senescence response. The mechanisms leading to OIS include hyperproliferation and altered DNA replication. This induces replication stress like firing of the DNA replication origins more than once per cell cycle resulting in stalled replication forks. Finally, the replication forks collapse leading to damaged DNA (Campisi 2005; Mallette and Ferbeyre 2007; Zhang 2007).

Name	Pathway	Type and function
TGF-β	TGF signalling pathway	Cytokine
Interferon-β	Antiviral response	Cytokine
XMRK	Growth factors signalling pathway	EGFR
PTEN	Inhibitor of growth factors signalling pathway	Protein or lipid phosphatase
RAS	Growth-factor signalling pathway	Membrane-associated small GTPase
RAC1	Growth-factor signalling pathway	Small GTPase
RAF	Growth-factor signalling pathway	Protein kinase
MOS	Growth-factor signalling pathway	Protein kinase
MEK	Growth-factor signalling pathway	Protein kinase
SMURF2	TGF signalling pathway	SMAD-specific E3 ubiquitin ligase
CDC6	DNA replication	DNA replication licensing factor
CYCLIN E	Cell-cycle regulation	CDK modulator
STAT5	Growth-hormone signalling pathway	Transcription factor
MYC	Transcription and DNA replication	Transcription factor
E2F	Transcription	Transcription factor

Table 3 **List of OIS inducers** (Di Micco, Fumagalli et al. 2007)

1.2.2.4 Mitochondrial Damage and Free Radical Theory

In 1972 Dan Harman was the first to link aging with an increase in free radicals inside the cell. He based his theory on the concept that irradiation, which introduces free radicals in cells leads to mutations, aberrations, cancer and aging. Free radicals produced as an intermediate of mitochondrial respiration and cell metabolism throughout the life, thus should also imply in the mechanisms concerning aging. (Harman 1956)

Free radicals or radical species (RS) are highly unstable molecules with an unpaired electron. The free electron reacts with organic molecules in the cell and thus modifies their original function.

Reactive oxygen species (ROS) and reactive nitrogen species (RNS) are comprised of oxidizing agents that include a radical atom themselves or easily form radicals. The major RS are summarized in Table 4 (Wink and Mitchell 1998; Halliwell 2007)

ROS	radical centred molecules	hydroxyl radicals	$OH^{\bullet}$
		superoxide radicals	$O_2^{\bullet-}$
		peroxyl radicals	$-OO^{\bullet}$
	non-radical molecules	peroxynitrite	$ONOO^-$
		hypochlorus acid	$HOCl^-$
		singlet oxygen	$1O_2$
		hydrogen peroxide	H_2O_2
RNS	radical centred molecules	nitric oxide	$NO^{\bullet}$
	non-radical molecules	nitrogen dioxide	NO_2
		nitryl chloride	NO_2Cl
		nitroxyl anion	NO^-

Table 4 **Reactive oxygen and nitrogen species.**

Endogenous ROS are intermediates produced by oxidative enzymes of the electron transport chain during mitochondrial respiration (Figure 3). Oxidative phosphorylation establishes a membrane potential ($\Delta\psi_m$) along the inner mitochondrial membrane which is used for producing adenosin triphosphate (ATP). Also cellular metabolism with enzymatic reactions generates RS. Production of RS is used in signalling cascades and also in defence against microorganisms and inflammatory response by inducible nitric oxide synthase (iNOS) (Wink and Mitchell 1998; Starcevic, Diotte et al. 2003; Passos and Von Zglinicki 2006).

Environmental RS reach from ionizing radiation, to UV light, but also include air pollution, smoking and toxic substances like asbestos. *In vitro* culturing of cells at 20% oxygen results in high oxidative stress and this situation resembles an *in vivo* hyperoxic situation. The effects of RS on the cells are numerous, including aggregation of lipid peroxidation, misfolded proteins, and DNA damage (Starcevic, Diotte et al. 2003).

Lipid peroxidation disturbs cellular function as steroid hormones, fat soluble vitamins like retinoic

acids and prostaglandins, which connect surface receptors to the membrane and the cellular membranes themselves, are oxidized. This influences gene expression, protein synthesis and can even lead to protein cross linking. (Voss and Siems 2006)

Oxidation of proteins primarily modifies amino acids and produces protein bound carbonyls which disrupt protein function and folding. Oxidized proteins are normally repaired or degraded by proteasomes. When damage occurs faster than proteins are repaired and degraded, oxidized proteins aggregate. A positive feed-back loop is started, as aggregates block the protease activity. The accumulated damaged proteins, also known as lipofuscin or age pigment, aggregate in cellular compartments (lysosomes). Lipofuscin binds transition metal irons and has autofluorescence capacity. Moreover, protein aggregates like Lewy bodies are involved in neurodegenerative diseases. Important for protein function is also their secondary and tertiary structure which is changed by RS. Oxidation of cysteine dissociates the important disulfide bridges found in many proteins. Metal irons, which are often coupled to active centres of enzymes, change their valence and thus the enzyme is inactivated. (Terman and Brunk 2006; Voss and Siems 2006)

DNA is prone for oxidation. Next to direct DSB and single strand breaks (SSB), bases are damaged. The most known biomarker for oxidative damaged DNA is 8OHdG, which results from oxidation of guanine. When repair mechanisms are leaky, mutations result and these accumulate during cells age. Oxidized DNA forms adducts with organic molecules, further leading to DNA damage. Another important fact is that telomeres not only shorten each replicative cycle, but also are eroded because of oxidative stress. Mitochondrial DNA (mtDNA) is less protected than nuclear DNA and thus more prone for damage. Moreover, as no repair mechanisms exist for SSB in mitochondria, damage accumulates and results in dysfunction. This again starts a feed-back loop as damaged mitochondria show a higher risk of releasing radical intermediates which then in turn again damage the cell. (Passos, Saretzki et al. 2007)

Cells have a variety of defence mechanisms to protect themselves from oxidative damage. The glutathione system, uric acid, vitamins and many enzymes with antioxidative properties are usually regulated according to the oxidative status of the cell. MnSOD, GPx1 and others are regulated by various stress sensoring proteins like p53. Still, the levels of oxidants and antioxidants determine the overall situation in the cells and deregulation leads to damage.

Only lately methods have been found to measure oxidative stress in cells. This is done with reduced fluorescent dyes that are oxidized to their fluorescent form by RS. Moreover, dyes to prove functionality and mass of mitochondria have been developed. As explained before, dysfunctional mitochondria are inefficient as they release higher amounts of free radicals and produce less

amounts of ATP. Moreover, mitochondrial size increases and higher amounts of free radicals are produced, starting a positive feedback loop (Kurz, Decary et al. 2004). Mitochondrial membrane potential $\Delta\psi_m$ is measured with cationic dyes that change upon membrane potential shifts.

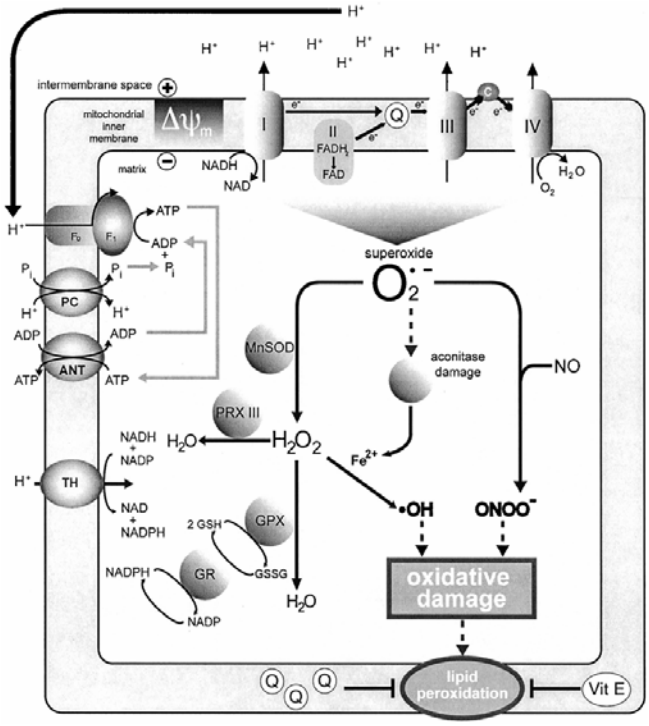

Figure 3 **Mitochondrial radical production and oxidative damage.** Production of ATP in the mitochondria is linked to the establishment of a membrane potential ($\Delta\psi_m$) by the respiratory chain. Superoxide radicals are produced which damage metal-binding enzymes like aconitase. $O_2^{\bullet-}$ are scavenged via several steps by superoxide reductase, MnSOD, peroxiredoxin PrxIII and glutathione peroxidase GPX. Further, this radical is reacting to produce hydroxyl radicals or, together with nitric oxide produce peroxynitrite. Oxidative stress leads to mtDNA damage, lipid peroxidation and aggregation of oxidized mitochondrial proteins.(Smith, Kelso et al. 2003)

1.2.3 Pathways leading to Senescence

Senescence is dependent on two major pathways: the p53-p21^{CIP} and the p16^{INK4A}-retinoblastoma (pRb) pathways (Toussaint, Medrano et al. 2000; Itahana, Campisi et al. 2007). The two pathways block proliferation independently but there is also cross talk between them as shown in Figure 4. In general, telomere shortening/erosion and other signals leading to a DNA damage response trigger the p53-p21 dependent pathway, which as a second step involves the p16-pRb pathway. On the other hand, senescence onset can act primarily through the p16-pRb pathway like in oxidative stress or oncogene induced senescence (Toussaint, Medrano et al. 2000). In the latter, especially oncogenic RAS leads to increased mitogenic signalling through the mitogen-activated protein kinase (MAPK) cascade.

Which pathway is primarily activated is dependent on the different cell types and senescence inducers. Epithelial cells rather induce the p16-pRb pathway while fibroblasts prefer the p53-p21 cascade. Interestingly, in cultured cells it was shown that there is a high heterogeneity in between the same population as cells expressing mainly p16 were found next to cells expressing primarily p21. Inactivation of either or both pathways leads to an extended proliferative capacity of cells and tumour cells often show mutations in proteins involved in these pathways. (Itahana, Campisi et al. 2007)

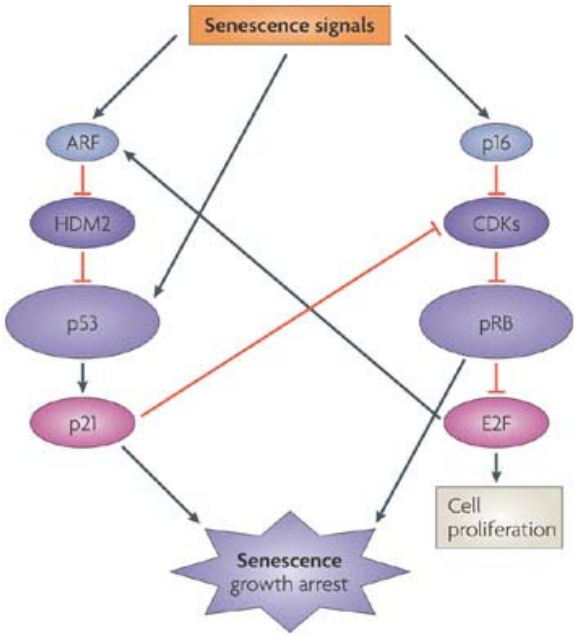

Figure 4 **Pathways leading to senescence and their interaction.** (Ben-Porath and Weinberg 2004)

1.2.3.1 DNA Damage Response and Repair

Damage of DNA is a chemical and structural modification of genomic material. Carcinogenic substances induce DNA adduct formation by alkylation, oxidation, deamination and dimerization, but also SSB and DSB occur. Moreover, epigenetic patterns are changed leading to deregulation of gene expression. The most complicated damage to DNA is the DSB as it bears the danger to induce chromosomal aberrations and leads to the formation of micronuclei. (Holland, Frei et al. 2003; Obe and Vijayalaxmi 2007)

There are six major mechanisms of DNA repair. DSB are mainly repaired by homologous recombination (HR) during late S-and G2-phase, or by non-homologous end joining (NHEJ). The other damages are repaired by direct DNA repair, mismatch repair, nucleotide- and base-excision repair.(Holland, Frei et al. 2003)

Genomic integrity can only be maintained when DNA damage repair mechanisms are efficient.

Several diseases have been found to be linked to mutations in DNA repair signalling proteins like in ataxia-telangiectasia (AT), Bloom syndrome, Xeroderma pigmentosum and Fanconi anemia. Patients with these diseases have a higher risk of developing neoplasms and show premature aging compared to people showing normal DNA repair mechanisms. (Holland, Frei et al. 2003)

Generally, for DNA damage repair like in Figure 2, sensor molecules like H2AX recognize the lesion. ATM and ATR are activated and recruited to the site of damage. These upstream kinases transduce the damage signal to mediator molecules (e.g. MDC1), downstream kinases (e.g. Chk1 and Chk2) and to effector molecules (e.g. p53 and cdc25). Several mechanisms and signalling cascades are started, which result in blockage of the cell cycle, change of gene transcription, execution of apoptosis or senescence and of course in induction of different repair mechanisms.(Zhou and Elledge 2000; Campisi and d'Adda di Fagagna 2007)

By experiments with fluorescence-tagged proteins the choreography of damage repair has been studied in detail. These damage repair proteins assemble at focal sites where DSB or HU induced replication stallings occur. (Lisby, Barlow et al. 2004; Lisby and Rothstein 2004; Lisby and Rothstein 2005)

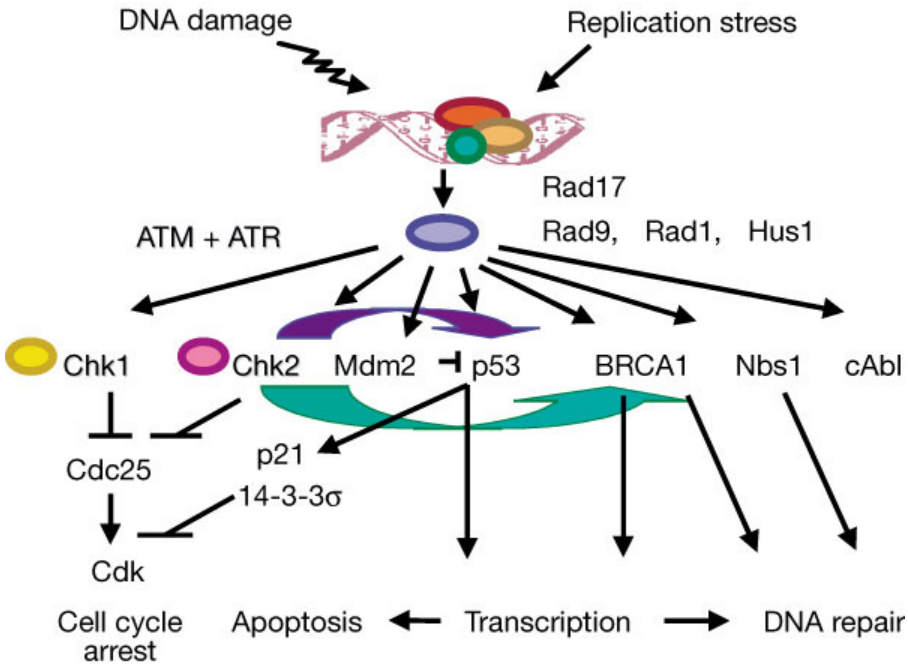

Figure 5 **The DNA damage response.** Many direct and indirect targets like kinases are involved in responding to damaged DNA. This then leads to cell cycle arrest and transcriptional change further on triggering apoptosis or repair (Zhou and Elledge 2000).

1.3 Experimental System: Senescence in *MYCN* Amplified Neuroblastoma Cell Lines

In neoplasms, senescence is an important issue as many tumour cells overcome it to immortalize. This is achieved among others by increased telomerase activity, by oncogene amplification or by overriding apoptosis induction. Expression of tumour suppressor genes and growth inhibitor factors push the cell into a senescent phenotype. What has been shown in the past decade is that also oxidative stress, cytotoxic therapy and radiation therapy induce senescence in tumour cells. (Schmitt, Fridman et al. 2002; Roninson 2003)

Senescence was suggested to be an antagonistic mechanism to tumour establishment (Campisi 2005). It aroused high interest when in cultured neuroblastoma cell lines cells with morphologically senescent phenotype were found to occur spontaneously (Ambros and Ambros 2000).

Generally, in MNA neuroblastoma cell lines morphologically distinct cell types - neuronal (N-cells) and flat (F-cells) cells - occur and sometimes also an intermediate type (I-cells) occurs. The published cell types show different cell morphology, proliferative capacity and expression patterns. (Ross, Spengler et al. 1983; Ambros, Rumpler et al. 1997; Spengler, Lazarova et al. 1997; Ross, Biedler et al. 2003)

N-cells are morphologically described as cells with small cytoplasms. They show a phenotype with neuritic outgrowth and neurofilament triplet protein expression. More than 60% of the N-cells harbour high numbers of *MYCN* copies in the nucleus (Ambros, Rumpler et al. 1997). They also show *MYCN* positive micronuclei. Moreover, N-cells show high proliferative capacity with more than 40% of cells incorporating BrdU (120 minutes pulse). Transforming activities include a high telomerase activity abrogating replicative senescence and leading to limitless proliferative potential of these tumour cells. Moreover, the neoplastic feature of blocking apoptotic pathways in these neuroblastoma N-cells is suggested to result from epigenetic silencing of caspase 8 and from overexpression of Bcl-2, survivin and NM23. (Ambros, Rumpler et al. 1997; van Noesel and Versteeg 2004).

N-cells can convert into another cell type - termed spontaneous senescent F-cells - without changing culturing parameters. This cell type forms up to 30 % of the untreated population (Ross, Spengler et al. 1983; Ambros, Rumpler et al. 1997). The conversion involves expulsion of amplified *MYCN* dmin into micronuclei. Thus spontaneous senescent cells are characterized by low *MYCN* copies and a flat morphology (Ambros, Rumpler et al. 1997). Their BrdU uptake decreases, suggesting them to have reduced proliferative capacities. Spontaneous senescent cells upregulate CD44 - a

favourable prognostic factor - and MHC-1 - which suggests acquired immunocompetent features. SA-β-Gal activity in spontaneous F-cells underscores the senescence phenotype. Together this suggests that spontaneous senescent cells are tumour revertant (Ambros and Ambros 2000).
Additionally, continual low dose HU treatment of cultured neuroblastoma cells induces the spontaneous senescent population and this population is referred to as induced senescent cells (Narath, Ambros et al. 2007). During treatment, an increase in micronuclei was observed which is suggested to lead to the loss of amplified *MYCN* (unpublished observations of our working group). Like spontaneous senescent cells, also the induced senescent cells showed decreased *MYCN* copy number. The generation of a pure induced senescent cell population was shown to take 6-8 weeks of continuous HU treatment. Similar to spontaneous senescent cells, also induced senescent cells showed features of tumour revertance: They incorporated less BrdU compared to an untreated population composed primarily of N-cells. Additionally, spontaneous senescent cells were shown to express CD44 and MHC-I, whereas telomerase activity was abrogated and telomeres were shortened. Induced senescent cells were, like spontaneous senescent cells, positive for the senescence marker SA-β-Gal. Narath et al. argued that senescence was established in induced senescent cells by replicative senescence as telomeres were shortened. Additionally, another unknown mechanism was suggested to contribute to MNA neuroblastoma cell senescence as replicative senescence takes longer than the 8 weeks, which were needed for induced senescent cells to form a pure population. (Narath, Ambros et al. 2007)

1.4 Hydroxyurea, a Ribonucleotide Reductase Inhibitor

Hydroxyurea (HU) is a drug that was first synthesized in 1869 and its mode of action was first described 1928. This small molecule shown in Figure 6 is used to treat patients with myeloproliferative diseases like chronic myelogenous leukemia. In solid tumours, HU is used alone or in combination with other genotoxic substances and IR to inhibit neoplastic proliferation. Further, in sickle-cell anaemia its usage prevents patients from crisis. Lately, HU was found to inhibit human immunodeficiency virus (HIV) type I DNA synthesis, suggesting an anti-viral application. (Szekeres, Fritzer-Szekeres et al. 1997; Holland, Frei et al. 2003)

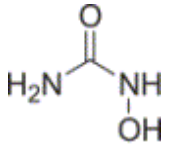

Figure 6 **Chemical structure of Hydroxyurea** (King 2003)

The mechanism of its action is only partly known. A recent study shed light on its in vivo metabolism and found that it produces nitric oxide (NO) (King 2003): Urease, an exclusively bacterial enzyme found in the gastric tract degrades HU to hydroxylamine, which can then be further reduced to NO *in vivo*. Moreover, both horseradish peroxidase and catalase catalyze the rapid formation of NO and nitroxyl (HNO) from HU. Heme or iron-bound proteins like cytochrome P450, catalase, aconitase and ribonucleotide reductase are inactivated. NO also reacts rapidly with superoxide (O_2^-) to form peroxynitrite, which disrupts protein structures through the nitration of protein tyrosine residues. The reaction generating NO and its intermediates is schematically shown in Figure 7. Moreover, production of peroxynitrite from mitochondrial superoxide and NO leads to depletion of ATP generation by blocking the electron transport chain. (Wink and Mitchell 1998; Holland, Frei et al. 2003; King 2003)

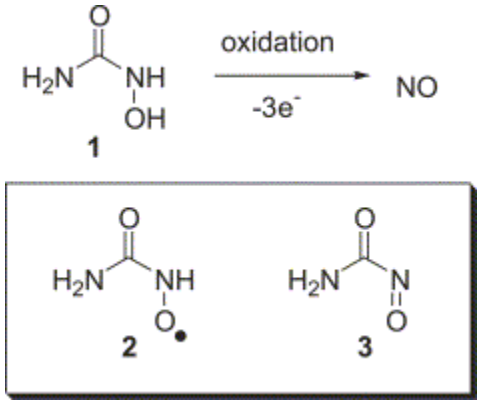

Figure 7 **Chemical oxidation of hydroxyurea** (1) to NO and structures of the proposed intermediates: the nitroxide radical (2) and *C*-nitrosoformamide (3).(King 2003)

HU enters the cell via passive diffusion. The main intracellular mode of action is inhibition of the enzyme ribonucleotide reductase (RNR). RNR catalyses the formation of deoxyribonucleotide triphosphate (dNTPs) from corresponding ribonucleotide triphosphate (NTPs), a reaction essential for DNA synthesis and repair in all living cells (Schrell, Rittig et al. 1997; Szekeres, Fritzer-Szekeres et al. 1997).

Active RNR is composed of 2 subunits, the large (RRM1) and optionally the small (RRM2) subunit in cycling cells or the p53 inducible subunit (RRM2B) during DNA repair and in G0/G1 arrested cells (Pontarin, Ferraro et al. 2007). The RRM1 gene was mapped to chromosome band 11p15.4 and is cell cycle independently expressed. It contains a pair of thiol groups (-SH) at the catalytic site and has two allosteric sites for binding ATP and the small subunit RRM2. RRM2, encoded on chromosome band 2p25.1, is cell cycle specifically expressed. Levels rise in late G1- phase and peak in S-phase until in late mitosis it is ubiquitylated by the anaphase-promoting-complex (APC) followed by degradation.

RRM2B, located on chromosome 8p22.3 and its transcription is dependant on p53 induced by ultraviolet light, γ-irradiation or DNA-damaging agents. Other studies suggest a role of RRM2B in mitochondrial DNA replication, as cells with a mutated form show severe mtDNA depletion.(Bourdon, Minai et al. 2007)

Both homologs, RRM2 and RRM2B harbour two iron binding centres and a stable organic free radical bound to a tyrosine in a hydrophobic pocket. Thus the main function in both is conserved, with the only difference that RRM2B was found to have lower affinities for binding RRM1.

Two RRM1 and two RRM2 subunits assemble to form the active enzyme. The conversion of NTPs to dNTPs is a radical-based reaction step limiting in S-phase DNA synthesis, accomplished by reduction of the thioredoxin disulfide.

HU is an iron chelator and radical scavenger. It inactivates both ribonucleotide small subunits by directly reducing the tyrosyl radical to a normal tyrosine residue via one-electron transfer from the drug. Moreover, also reduction of the iron centre leads to the release of this ferric compound from the protein. The inhibition is reversed significantly in the presence of iron, dithiothreitol (DTT) and oxygen. The regeneration was much more marked for RRM2B, resulting in a selective inhibition of RRM2 as compared to RRM2B.(Nordlund, Sjoberg et al. 1990; Holland, Frei et al. 2003; King 2003; Shao, Zhou et al. 2006)

1.5 Change in Nuclear Structure - Lamins

The nucleus, the biggest compartment of the eukaryotic cell, is in charge of hosting the genetic material of the cell. Moreover, it serves as workspace for biosynthesis by transcription and splicing, and also contains numerous RNAs and proteins that conduct interactions in the cell. This highly specific organelle is surrounded by a nucleoskeleton comprising a nuclear envelope with nuclear pores, the outer nuclear membrane and the inner nuclear membrane. On the nucleoplasmic side of the inner nuclear membrane, a meshwork of proteins makes up the nuclear lamina. The proteins incorporated are the lamins, intermediate filaments of group V and lamin-associated proteins. The main function of the nuclear lamina is providing nuclear structure and organization. Lamin binding proteins serve as connection between chromatin and the nuclear envelop by which localisation and function of chromatin is regulated (Figure 8)(Foisner 2001; Mattout, Dechat et al. 2006).

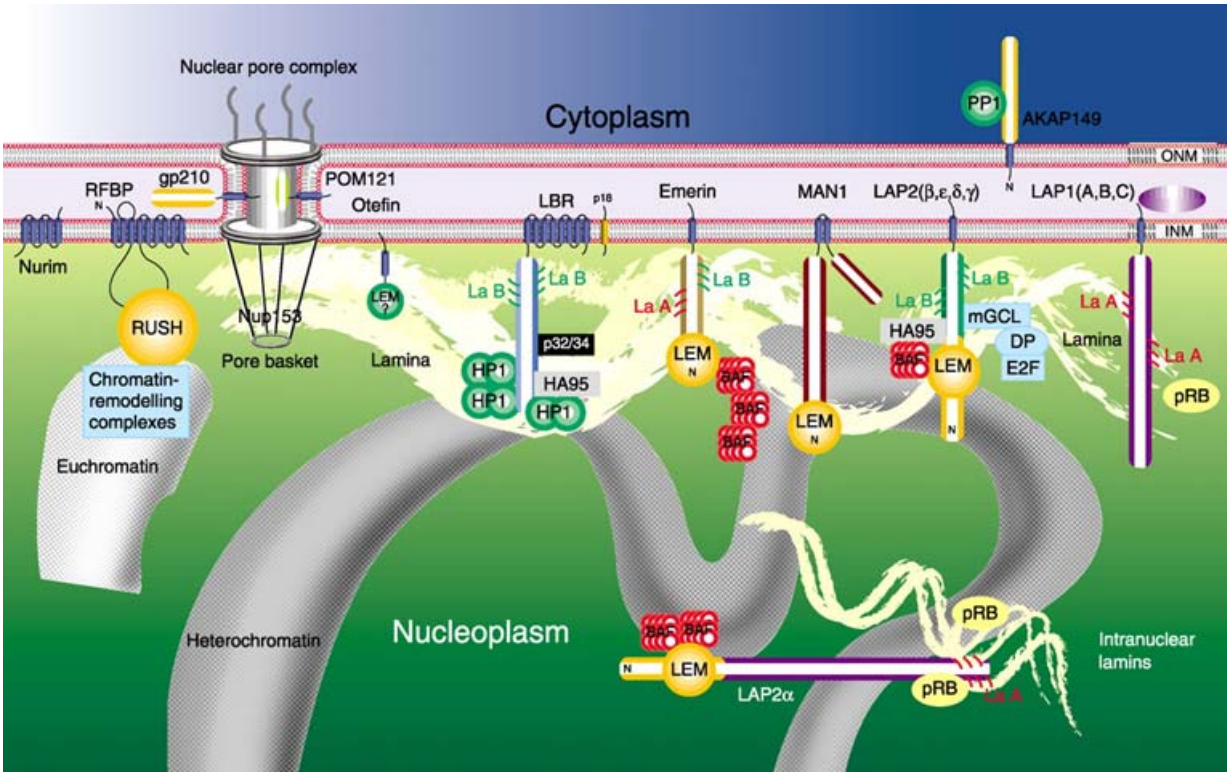

Figure 8 **Interconnections between lamins**, associated proteins and chromatin at the nuclear envelope and in the nucleoplasm. (Foisner 2001)

The structure of lamins and other intermediate filaments is a central helical rod domain flanked by a variable globular head and a globular tail domain (Figure 9) (Shumaker, Kuczmarski et al. 2003; Mattout, Dechat et al. 2006).

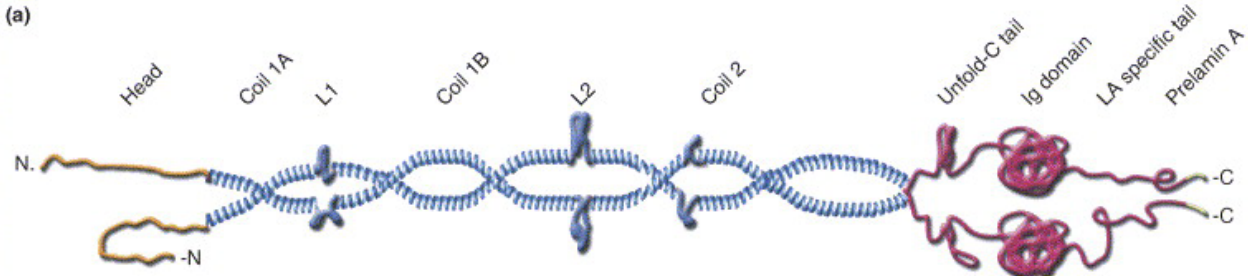

Figure 9 **Structure of Lamin A**. The short, N-terminal head domain is shown in yellow, the central rod-like domain in blue, the C-terminal globular domain in red. The C-terminal truncated domain of prelamin A is shown in green.

Lamins are encoded by 3 genes, *LMNA*, *LMNB1* and *LMNB2* that are located to chromosome band 1q21.2-q21.3, 5q23.3-q31.1 and 19p13.3. They are grouped in A type and B type lamins according to their biochemical properties and function during mitosis. Generally, lamins depolymerise during mitosis. Neutral A type lamins are soluble during mitosis, while acidic B type lamins stay bound to the nuclear membrane. Shortly after cytokinesis, the nuclear lamina reassembles, lamin A getting incorporated later in G1-phase. (Gruenbaum, Margalit et al. 2005)

LMNA gives rise to four isoforms by variable splicing: lamin A, lamin AΔ10, lamin C and lamin C2(Constantinescu, Gray et al. 2006). By post transcriptional modification steps of farnesylation and truncation of 18 amino acids of the C-terminal tail by the zinc metalloproteinase Ste24 (Zmpste24), lamin A is processed into its mature form (Figure 10). Lamin A is primarily found in differentiated cells. Hematopoietic cell lines, embryonic cells and stem cells such as F9 teratocarcinoma do not express lamin A/C (Rober, Sauter et al. 1990). This suggests the importance of cell plasticity to be negatively correlated with lamin A/C expression and thus its expression marks the stage of differentiation a cell has undergone. (Rober, Sauter et al. 1990; Constantinescu, Gray et al. 2006; Liu and Zhou 2008)

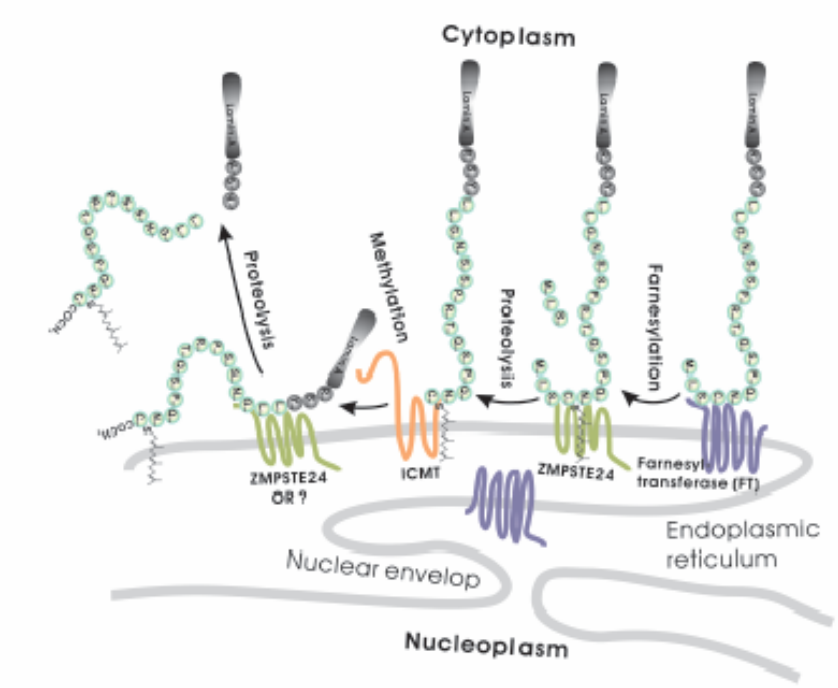

Figure 10 **The maturation of lamin A.** Farnesyl-protein transferasere recognize the Cystein-aaX domain and adds a farnesyl group. This is the signal for the zinc metalloprotease Zmpste24, which cuts off the 3 C-terminal amino acids (aaX) before a methylation step is performed. This step leads to a truncation of 15 amino acids at the C-terminal tail domain by Zmpste24. (Kudlow, Kennedy et al. 2007) (Vlcek and Foisner 2007)

LMNB1 and *LMNB2* give rise to the proteins lamin B1, B2 and B3. B1- and B2-type lamins are expressed ubiquitously in all cells. The non-canonical Lamin B3 is only expressed in spermatocytes.(Constantinescu, Gray et al. 2006; Liu and Zhou 2008)

Many lamin binding proteins with a high range of functions have been found and suggest heterogeneous functions also for lamins. Next to LEM-domain proteins like emerin, LAP2α and LAP2β also BAF and LBR show functions related to senescence. LAP2α is one of three splicing variants encoded by the thymopoietin (*TMPO*) gene mapped to chromosome 2p22 (Harris, Andryuk

et al. 1994). The splicing product of *TMPO* gives rise to the 75kD nucleoplasmic protein thymopoietin alpha, or lamin associated protein alpha (LAP2α) and 5 transmembrane proteins, LAP2β - ζ. LAP2α is involved in the intranuclear chromatin architecture. Its N-terminal domain is conserved with the other LAP2 splicing variants, while the remaining LAP2α structure differs. By dimerization Lap2α binds to lamin A/C. The formed coiled-coil structures interact with pRb and thus plays a role in cell cycle regulation (Markiewicz, Dechat et al. 2002; Shumaker, Kuczmarski et al. 2003; Dechat, Gajewski et al. 2004; Dorner, Vlcek et al. 2006; Naetar, Hutter et al. 2007; Snyers, Vlcek et al. 2007)

1.5.1 Lamins and Aging

Monogenic hereditary diseases involved in premature or early aging are called progeroid syndromes. Mutated, progeroid-involved genes give insight into the mechanisms of aging. Hutchinson-Gilford progeria (HGPS) resembles a time-lapse aging phenotype but shows no signs of raised cancer rate or neurodegenerative diseases, as associated with physiological aging (Lans and Hoeijmakers 2006). The gene mutated in this autosomal dominant disorder is *LMNA* (predominantly G608G)(Liu and Zhou 2008). This mutation leads to a cryptic splicing site that serves as proteolytic cleavage site for Zmpste4 and results in an unmodified, truncated prelamin A, called progerin. Also many other mutations in the *LMNA* gene cause diseases and are summarized as laminopathies. The search of *LMNA* in the Online Mendelian Inheritance in Man database (OMIM) with the entry ID MIM *150330 links HGPS, limb girdle muscular dystrophy, dilated cardiomyopathy 1A, Emery-Dreifuss muscular dystrophy, familial partial lipodystrophy, lipoatrophy, Charcot-Marie-Tooth disease, Werner syndrome, mandibuloacral dysplasia and restrictive dermopathy (RD) to mutations in the *LMNA* gene (McKusick 2007).

Lately, it was found that farnesylated lamin A is toxic to cells and leads to abnormal structure of the nuclear lamina with envelope interruptions and chromatin extrusions (Fong, Ng et al. 2004). Fibroblasts of HGPS patients show nuclear accumulated prelamin A leading to decreased exchange of lamin fibres (Gilchrist, Gilbert et al. 2004).

Several lines of evidence suggest an involvement of *LMNA* in physiological aging processes. The connection of lamin A expression and physiological aging arose when premature aging in the HGPS was correlated with a mutation in the *LMNA* gene. Cleaved, farnesylated prelamin A is found in cells from HGPS patients. The same phenomena could be observed to a smaller extent in cells from old organisms, which also showed misshaped nuclei with lobes and invaginations. (Haithcock, Dayani et al. 2005; Lans and Hoeijmakers 2006; Scaffidi and Misteli 2006)

Usually, heterochromatic regions are structurally fixed and linked to the nuclear lamina. In HGPS patients, but also in late passage fibroblasts less heterochromatic markers are found which suggests lamin A to be associated with the epigenetic control of heterochromatin. Moreover, HGPS and late passage cells show loss of heterochromatin. (Shumaker, Kuczmarski et al. 2003; Gruenbaum, Margalit et al. 2005)

2 Material and Methods

2.1 Cell Culture

Neuroblastoma cell line STA-NB-9 (MNA, dmin) and STA-NB-10 (MNA, dmin) were cultivated in RPMI 1640 GlutaMAX (Gibco-BRL, Grand Island, New York, USA) supplemented with 10% fetal calf serum (FCS, PAA Laboratories GesmbH, Pasching, Austria), 2.5% HEPES (Gibco), 1% Sodium-Pyruvate (PAA Laboratories GesmbH), 0.6% Penicillin (10.000 U/ml)/Streptomycin (10 mg/ml) (PAA Laboratories GesmbH) at 37°C in 5% CO_2 until confluence. Splitting of the control cells occurred on average once a week.

Cells were harvested by washing with phosphate-buffered saline (PBS, Invitrogen) following incubation with 0.5 - 2ml of Accutase (PAA Laboratories GesmbH) according to flask size at 37°C. The detached cells were resuspendend in a volume of medium at least triple amount of Accutase used. Cells are washed with PBS, or Accutase is inactivated by and kept in basic sorting buffer (PBS (Ca/Mg^{++} free), 1mM EDTA (Invitrogen), 25mM HEPES pH 7.0, 1%FCS, 0.02µm filter sterilized (Pall Life Sciences)).

2.1.1 Hydroxyurea Treatment

STA-NB-10 cells were treated with 150µM HU for 1 day to 10 weeks, whereas STA-NB-9 cells were treated with 75µM of HU when subconfluent. HU was renewed by changing half of the medium supplemented with freshly thawed HU at least once a week. In the control cells medium was changed averagely every 7 days.

2.1.2 Comparison of H_2O_2 and HU Treatment in STA-NB-9

STA-NB-9 cells were grown in a separate T-25 flask for each condition analyzed. Control cells were treated as explained and are referred to as untreated cells. H_2O_2 treatment was performed at a concentration of 75µM from a fresh stock dilution for 24 hours before harvesting the cells which are referred to as H_2O_2 induced cells. 24 hours treatment with HU was done in parallel and cells are referred to as induced cells. Thawed senescent cells were generated by 8 weeks HU induction followed by 3 weeks cultivation in HU-free medium before freezing and are referred to as induced senescent cells.

Morphology change and SA-β-Gal activity, cell cycle and ROS level detection (MitoSox and DHE staining) were performed with the harvested population.

2.1.3 Time Course of STA-NB-10 Treated with HU for 0 – 70 days

For each time point, STA-NB-10 cells were grown in a separate T-75 flask. Time points were at 0, 1, 5, 10, 15, 56 and 70 days. Control cells were grown in parallel in a separate flask and are referred to as untreated cells. Cells treated for 1 – 15 days with HU are referred to as induced cells (induced). Additionally, the time of treatment is indicated. The following analyses were performed with the same cell population from one flask: cell cycle (until day 56), *MYCN*-FISH (0, 1, 10 and 70 days), SA-β-Gal (until day 56), cellular superoxide levels (until day 56), lamin A/C and lamin B double fluorescence staining and protein isolation for western blotting (until day 56).
For each time-point the flask was harvested, 1/10 of the cells were seeded in the original flasks to test for SA-β-Gal activity. From the remaining 9/10 of the population 1/10 was used to prepare cytospins (at least 2), 2/10 were used for superoxide assessment, and 2/10 were used for cell cycle analysis. The remaining 4/10 of the population were shock frozen as pellet and stored at -80°C for western blotting.

2.1.4 Time Course of STA-NB-10 Treated with HU for 0 – 10 days

For each time point, STA-NB-10 cells were grown in 6-well plates. Time points were at 0, 3, 6, 8 and 10 days. Control cells were grown in parallel in separate wells and are referred to as untreated cells. Cells treated for 1 – 10 days with HU are referred to as induced cells. Cell cycle and growth curve were determined for each time point for treated and untreated cells.

2.1.5 ROS Monitoring in STA-NB-9 (Newcastle)

For ROS detection and analysis of mitochondrial function in STA-NB-9, untreated STA-NB-9 (referred to as untreated cells), approximately 30-40 days HU treated cells (referred to as induced cells), and thawed senescent cells (referred to as induced senescent cells) were used. Senescent cells were generated by 8 weeks HU induction followed by 3 weeks cultivation in HU-free medium before freezing. Control cells, low passage MRC5 fibroblasts and senescent cells were cultivated in HU-free medium which was changed once a week. HU renewal was achieved by changing half the medium supplemented with 37.5µM HU every 4 days. Low passage MRC5 fibroblasts were a kind gift of the work group of T. von Zglinicki, Henry Wellcome Laboratory for Biogerontology Research in Newcastle. Experiments were also performed in the laboratory of T. von Zglinicki, supervised by J. Passos.

2.2 Microscopy Techniques

2.2.1 Cytospin Preparation

Accutase treated cells were harvested in PBS or basic sorting buffer and stored on ice until usage. Filter, funnel and holder were assembled on the glass slides and fixed with clamps. Filters were prewetted and then filled with 50 - 500µl of prevortexed cell suspension. With the cytocentrifuge (Shandon, Cheshire, United Kingdom) the cells were applied onto the slides at 500 rpm for 8 minutes. The slide and filter/clipboard were cautiously taken apart and the slide was dried over night in provided boxes. Storage of these preparations was done either at RT for up to two weeks or at -20°C for several years in appropriate boxes.

2.2.2 *MYCN*-Status Analysis

When the thawed cell line was split the first time an aliquot of cell suspension was used for preparation of cytospins and a *MYCN*/2p FISH (see 2.2.3) was done to confirm that the amplified *MYCN* is present in the form of dmin.

2.2.3 Double-target FISH

Cytospin slides were fixed in 4% paraformaldehyde in PBS for 20 minutes at 4° C. After washing 2 x 5 minutes in PBS cells are dehydrated in an EtOH series (70%, 90%, 95% EtOH for each 3 minutes; further on referred to as EtOH series) and air dried. 1.5µl nick-labelled *MYCN*-dig and 2p-bio probes (see 2.2.4) were applied to the cell spot, covered with a coverslip and sealed with rubber cement. Denaturation of the probe was achieved on the heating plate at 78°C for 8 minutes. The slides were hybridized overnight in a moist chamber in the heater at 37° C. Washing was performed 5 minutes in 2 x SSC at RT, followed by 15 minutes 50% formamide in 2 x SSC at 42° C and 2 x 7 minutes washing in 2 x SSC at 42°C. The probes were detected with antibodies against digoxigenin and biotin in 2% BSA (Sigma-Aldrich)/PBS by incubation in a moist chamber at 37° C for 30 minutes followed by washing 2 x 7 minutes in 4 x SSC supplemented with 0.1% Tween 20 at 42° C. Secondary antibodies in 2% BSA/PBS were incubated in a moist chamber at 37°C for 30 minutes followed again by the washing procedure described before. Fixation of the staining was achieved by incubation of the slides in 4% paraformaldehyde in PBS for 20 minutes at 4° C, followed by washing twice 5 minutes in PBS followed by dehydration in EtOH as above and air drying in the dark. Slides were mounted with Vectashield supplemented with DAPI and sealed with

rubber cement. Slides were analyzed with an Axioplan fluorescence microscope (Zeiss, Austria).

2.2.4 Nick-labeling of FISH Probes

The bacterial clones RP11-355H10 (AC010145, *MYCN*) and 08–103-1 (chromosome2p) were obtained from Dr. M. Rocchi (Resources for Molecular Cytogenetics, University of Bari, Italy). 2µg of extracted DNA, *MYCN* or 2pter, were combined with either DIG-Nick Translation Mix (Roche, Vienna, Austria) containing 0.08 mM digoxigenin-11-dUTP or Biotin-Nick Translation Mix (Roche, Vienna, Austria) containing 0.08 mM biotin-16-dUTP respectively and filled up with ddH_2O to a total volume of 40µl. For direct labeling of *MYCN* with spectrum green the following labeling mix was prepared: 1,52µg *MYCN* DNA, 5µl DTT (Fisher Scientific, Applichem), 5µl 10x nick-translation buffer (0.5M Tris-HCl ph 8.0, 50mM MgCl, 0.5 mg/ml BSA pH 7.8), 5µl nucleotides (Sigma-Aldrich), 1µl Spectrum Green-dUTP (Abbott, Vysis), 5µl DNase (1:1000) (Roche), 1,5µl DNA Polymerase (8U/µl) (Promega) filled up to a total volume of 50µl with water. The solutions were incubated for 120 minutes at 16°C (direct labeling 2h at 15°C). To verify labeling and size (*MYCN*: 200 Kb) of the probes, a 1.2% agarose gel was run 40 minutes at 100V and 500mA with 5µl sample added to 1µl loading buffer. Meanwhile the probes were kept on ice so that further nick labeling remains possible. The reaction was stopped by addition of 30µg of COT human DNA (Roche Diagnostics GmbH, Mannheim, Germany), a volume of NaAc (3M, pH 5.5) calculated as 1/10 of the probe volume plus the COT DNA volume and 2.5 times the volume of the solution of 100% EtOH. Precipitation of labeled DNA probes is achieved by incubation at -70° for a minimum of 30 minutes followed by a centrifugation step (30 minutes at 13000 rpm at 4°C). After removal of the supernatant the pellet was resuspended in 70% EtOH followed by centrifugation for 15 minutes at 13000 at 4°C. The supernatant was removed carefully and the DNA pellet was dried. Resuspension of the probe was done in 40µl of hybridization mix (200µl formamide, 100µl 20x SCC, 200µl dextransulfate and 200µl distilled water).

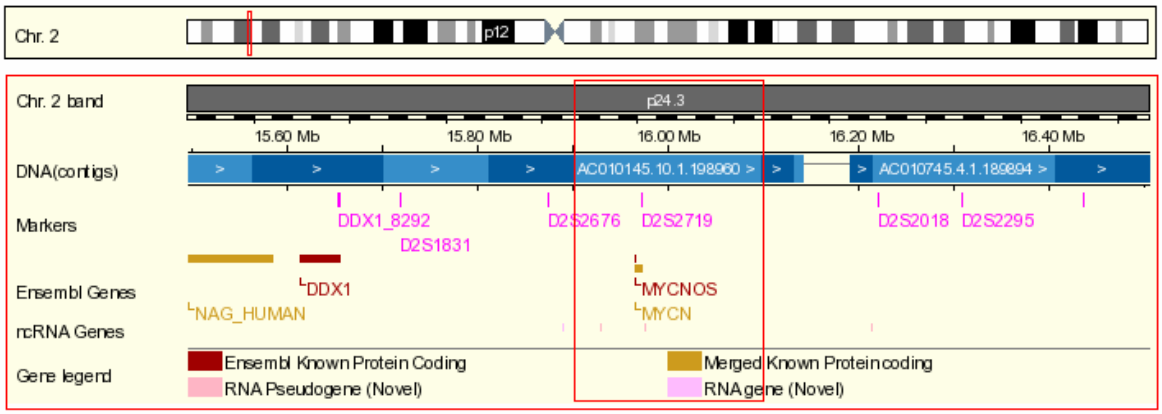

Figure 11 **Ensembl chromosome map** showing the location of the *MYCN* clone used in FISH experiments.

2.2.5 Interphase FISH with Simultaneous Immunofluorescence

Cytospin slides were incubated in PBS for 5 minutes and afterwards fixed in 4% precooled paraformaldehyde (Roth, Austria) at 4°C for 20 minutes. After 5 steps of each 3 minutes washing in PBS (further defined as washing step) the preparations were incubated with filtered (pore size: 0.2µm) 5% BSA in PBS for 30 minutes in a humid chamber at 37°C. Further on the cells were incubated with the lamin A/C or lamin B antibody diluted 1:100 in the 5% BSA solution for 60 - 120 minutes in a humid chamber at 37°C. Following the washing step the cells were incubated with the secondary rabbit anti mouse-TRITC antibody for 30 minutes (37°C, humid chamber), followed by another washing step. The immune fluorescence staining was then fixed in 4% paraformaldehyde for 20 minutes. After 2 x 5 minutes washing with PBS the preparations were dehydrated (EtOH series) and air dried (in the dark). 1.5µl of the direct-spectrum green labeled MYCN-probe were applied onto the cells, covered with a coverslip and sealed with fixogum. DNA denaturation was accomplished by putting the slides onto a heating plate (78°C) for 8 minutes, followed by hybridization over night in a humid chamber at 37°C. After removing the coverslip form the slide, the cells were washed 5 minutes in 2xSSC at room temperature, 5 minutes at 50% formamide in 2xSSC at 42°C and another 5 minutes in 2xSSC at 42°C. Before dehydration (EtOH series), the cells were washed 5x3 minutes in PBS. After drying of the preparations, the slides were mounted with Vectashield supplemented with DAPI and cover slips were sealed with rubber cement (Fixogum). Slides were analyzed with an Axioplan 2 fluorescence microscope (Zeiss, Austria) using the Metafer4-MetaCyte and Isis software (both MetaSystems, Altlussheim, Germany).

2.2.6 Immunofluorescence microscopy

Cytospin slides and grown cell preparations were fixed in 4% paraformaldehyde in PBS for 20 minutes at 4° C. After washing (3 x 5 minutes in PBS) unspecific binding sites were blocked in 2% BSA in PBS at 37°C for 30 minutes in a humid chamber. Primary antibody incubation was performed for 1 hour at 37°C in a humid chamber. After 3 washing steps, each 5 minutes in PBS the fluorophore-conjugated secondary antibody was incubated for 30 minutes in a humid chamber at 37°C. The antibodies and the used concentrations are depicted in Table 5. After 3 passes of washing, cells were mounted with 10µl Vectashield mounting medium supplemented with DAPI (Axxora) and coverslips were sealed with Fixogum rubber cement (Marabu).

According to preexperiments done to determine optimal staining conditions and staining results, different slightly adapted standard immune fluorescence protocols were established. Preexperiments included different fixatives (MeOH, -20°C; EtOH/Acetate, RT; PFA, -4°C or RT), preextraction and permeabilisation steps (different concentrations of Triton X 100 or Tween, different duration).

The above describes standard protocol was used for lamin A/C, lamin B, nuclear pore complex (mAb414), LAP2α, BrdU, *MYCN*-dig and all double stainings with CD44. For prelamin A single staining, preextraction was performed by incubation of rehydrated cytospin preparations with 0.5% TXT for 10 minutes. After the fixation step, permeabilisation was performed in 0.1% TXT100 for 5 minutes at room temperature.

Slides were analyzed with an Axioplan fluorescence microscope (Zeiss, Austria) and images were taken with a high resolution CCD camera with the ISIS software (MetaSystems, Altlussheim, Germany).

2.2.7 Senescence-Associated β-Galactosidase Activity Assay

Cells in flasks were washed with PBS, and the senescence detection kit (BioVision, Mountain View, USA) was used following the protocol supplied by the company as follows: Cells were fixed with 200 µl 0.2% glutaraldehyde for 15 minutes at room temperature. The cells were washed in PBS, covered and incubated with freshly prepared X-gal solution (containing 10 mM phosphate buffer, 150 mM NaCl, 1 mM $MgCl_2$, 3.3 mM $K_4Fe(CN)_6 3H_2O$, 3.3 mM $K_3Fe(CN)_6$, and 0.2% 5-bromo-4-chloro-3-indolyl-b-galactropyranosid) overnight. After rinsing the cells in the flask with PBS cells were analyzed with an Axiovert 135 inverted fluorescence DIC microscope (Zeiss, Austria) and pictures were taken with a CCD camera and the associated software (PixeLINK, Ottawa, USA).

2.3 Flow Cytometry

2.3.1 Growth Curve

5 x 10^5 STA-NB-10 cells were seeded in 6-well-plates. Two days later, the medium was exchanged with HU-supplemented medium (150µM) or for control cells with HU-free medium. After 0, 1, 3, 6, 8 and 10 days cells were harvested and transferred to tubes in basic sorting buffer. 20µl of the cell suspension were mixed with 10 ml Isoton (Beckman Coulter) and 4 drops of ZapoGlobin II lytic reagent (Beckmann Coulter) and cell number was counted in the Coulter counter (Beckmann Coulter). The remaining cells were used for cell cycle analysis. For calculating population doubling time, the following equation was used:

$$T_d = \text{period of time x log (2)/log (population output/population input)}$$

2.3.2 Cell Cycle Analysis

DNA staining according to cell cycle stage was performed with the Cycle Test Plus –DNA reagent kit (Becton Dickinson Co., Mountain View, CA) according to the manufacturer's protocol. A cell pellet of 1x10^6 cells was resuspended in 700µl dimethylsulfoxide (DMSO) in sucrose-sodium citrate. Permeabilisation of the cells was performed by incubation in 125 µl of prewarmed trypsin in spermine tetrahydrochloride detergent buffer 10 minutes at room temperature. Permeabilisation inactivation was done by incubation with 90µl RNase A and trypsin inhibitor in spermine buffer. Staining of DNA was performed with propidium iodide (PI) in spermine buffer for 10 minutes on ice followed by centrifugation of the cells. Detection was performed with a FACScan flow cytometer (Becton Dickinson Co, Mountain View, CA).

2.3.3 Proliferation Assay

5 x 10^5 cells were seeded per well into a 6-well plate. After two days HU supplemented medium was added for STA-NB-9 at a concentration of 75µM and for STA-NB-10 at a concentration of 150µM. 10µM BrdU was added to each well. Control cells were cultivated in HU-free, BrdU containing medium. After 24 hours incubation with both substances cells were harvested and cytospin preparations were prepared. Detection of incorporated BrdU was done according to standard immune fluorescence protocol. BrdU positive cells were counted with an Axioplan fluorescence microscope (Zeiss, Austria).

2.3.4 Analysis of Reactive Oxygen Species (Cellular Superoxide, Cellular Peroxide and Peroxinitrite Levels)

Three tubes with each approximately 2 x 10^5 cells were prepared (negative control and stained sample). Cells were centrifuged at 1500rpm for 3.5 minutes, the supernatant was aspirated and the cells were resuspended in either MitoSOX Red mitochondrial superoxide indicator (5µM, Molecular Probes) or Dihydrorhodamine 123 (DHR, 30µM, Molecular Probes). Incubation time was 10 minutes and 30 minutes, respectively at 37°C followed by centrifugation at 1500rpm for 3.5 minutes. Resuspension of the stained cell pellet was performed in 2ml serum free medium. DHR was excited at 488nm and was detected at 530 nm (FL1). MitoSox was excited at 488 – 514nm and detected at 670 nm (FL3). Median fluorescence intensity was measured with the Partec PAS flow cytometer (Partec GmbH, Münster, Germany) and analysed with the Partec FloMax software (Partec GmbH, Münster, Germany). The flow cytometer was calibrated using fluorescent beads. All data are mean ± standard error of mean from 5 independent experiments with measurements in duplicate.

For the time course experiment with STA-NB-10 (chapter 2.1.3) and for STA-NB-9 experiment comparing HU to H_2O_2 (chapter 2.1.2) only MitoSox Red was used. The procedure was the same as described above except for using a FACScan flow cytometer (Becton Dickinson Co, Mountain View, CA) for detection and analysis.

2.3.5 Analysis of Mitochondrial Membrane Potential and Mitochondrial Mass

Cells were harvested, counted and three tubes with each 2 x 10^5 cells were prepared (negative control and stained sample). Cells were centrifuged at 1500rpm for 3.5 minutes, the supernatant was aspirated and the cells were resuspended in either 10-N-nonyl acridine orange (NAO, 10µM, Molecular Probes) or 5,5',6,6'-tetrachloro-1,1',3,3'-tetraethylbenzimidazolyl-carbocyanine iodide (JC-1, 1µg/ml, Molecular Probes). Incubation time was 10 minutes and 30 minutes respectively at 37°C, followed by centrifugation at 1500rpm for 3.5 minutes. Resuspension of the stained cell pellet was performed in 2ml serum free medium. NAO was excited at 488nm and was detected at 530 nm (FL1). JC-1 was excited at 488nm and was detected at 530 nm (FL1) and at 670 nm (FL3). The FL3/FL1 ratio was calculated for JC-1. Analysis was done with the Partec PAS flow cytometer (Partec GmbH, Münster, Germany) and analysed with the Partec FloMax software (Partec GmbH, Münster, Germany). The flow cytometer was calibrated using fluorescent beads. All data are mean ± standard error of mean from 3 independent experiments with measurements in duplicate.

2.4 Protein Analysis

2.4.1 Western Blot

Cells were harvested, centrifuged at 1100 rpm for 10 minutes and washed once with PBS before shock freezing the pellet in liquid nitrogen. After thawing, the cell pellets were lysed and resuspended in 100 – 150µl of 2x loading buffer plus the same volume of PBS followed by boiling the sample for 15 minutes at 95°C. To define the amount of proteins in the probes a 10% SDS gel was loaded with samples diluted to half the concentration with 1x loading buffer and run at 70mV(limiting) for 1 hour. The samples were prepared as following: 10µl 2x sample buffer was added to 10µl lysed protein or 5µl of broad band range prestained protein marker (Biolabs, Ipswich, UK), 15 minutes at 95°C (only 5 minutes for the marker), 5 minutes at 13000 rpm. Blotting of the gel was performed with a nitrocellulose membrane between 3 filter papers soaked in transfer buffer. Blotting was achieved at constant 400mV/gel for 1.5 hours on ice. The membrane was stained with ponceau, the staining was scanned and integrated intensity measurements were performed using ImageJ software. Protein levels present in the samples were calculated and normalized.

Equal amounts of protein from each lysate were resolved by SDS–PAGE and transferred to the membrane and stained with ponceau as described above. Unspecific binding sites were blocked with 1% skim milk in PBS for at least 60 minutes, shaking at RT. The membrane was incubated with the primary antibodies in 0.5% skim milk over night at 4°C shaking. The blots were washed 6 times 10 minutes with TBS-Tween. Incubation with the secondary antibody (Pierce Biotechnology) diluted in ODYSSEY blocking buffer was performed for 1 hour at room temperature shaking. The antibodies and the used concentrations are depicted in Table 5. The blots were washed again 6 times 15 minutes with TBS-Tween. Detection was performed with the LI-COR ODYSSEY system. Further, integrated density measurements were performed with ImageJ. As senescent cells change their gene expression for most reference house-keeping genes as indicated by microarray analysis, the integrated density of the ponceau staining was taken as loading control.

Antibody against	dilution	species	Company
LaminA/C (636)	1:100	mouse monoclonal	Santa Cruz biotechnology, Inc.
Lamin B (C-20)	1:100	goat polyclonal	Santa Cruz biotechnology, Inc.
prelamin A (C-209)	1:50	goat polyclonal	Santa Cruz biotechnology, Inc.
LAP2a	1:250	rabbit polyclonal	ImmuQuest Ltd
MAb414	1:100	mouse monoclonal	Abcam Ltd
CD44, Phagocytic Glycoprotein-1	1:30	mouse monoclonal	DakoCytomation, Vienna, Austria
MYCN	1:100	mouse monoclonal	Abcam
p53 (DO1)	1:10	mouse serum	B. Vojtesek (Masaryk Memorial Cancer Institute, Brno, Czech Republic).
p21 (F5)	1:70	mouse monoclonal	Santa Cruz biotechnology, Inc
p16 (F12)	1:200	mouse monoclonal	Santa Cruz biotechnology, Inc.
pRb (IF8)	1:200	mouse monoclonal	Santa Cruz biotechnology, Inc.
BrdU	1:100	mouse	BD
digoxigenin- FITC	1:100	sheep	Enzo Life Sciences, Inc., Farmingdale, NY
biotin-TRITC	1:100	mouse	
sheep Ig- FITC	1:100	rabbit	DakoCytomation, Vienna, Austria
mouse Ig- TRITC	1:40	rabbit	DakoCytomation, Vienna, Austria
mouse Ig- FITC	1:60	rabbit	DakoCytomation, Vienna, Austria
goat IgG- TRITC	1:40	rabbit	Jackson Immuno Research
rabbit IgG- TRITC	1:30	swine	DakoCytomation, Vienna, Austria
mouse IgG –DyLight 800 (infrared)	1:8000	goat	Pierce Biotechnology

Table 5. **List of antibodies used.**

3 Aim of the study

The aim of this study was to investigate candidate pathways and changes involved in HU-induced senescence of MNA NB cells.

In the first part of the study the changes brought about by low dose HU treatment of neuroblastoma cells concerning population growth, cell cycle behaviour and *MYCN* copy number were assessed. Additionally, the senescence typical markers SA-β-Gal activity and morphology change were monitored to have an indicator for senescence after low dose HU treatment.

As second part, involvement of ROS and mitochondrial function during the onset of tumour cell senescence after low dose HU treatment was assessed. The idea behind was to find the direct effects of HU treatment on the cell and the indirect effects corresponding to premature senescence onset.

As third part of the study, the composition of the nuclear envelope and associated proteins were assessed following low dose HU treatment of neuroblastoma cells. Additionally, spontaneous F-cells were compared to N-cells to learn about the differences in components of the nuclear lamina and of the nucleoplasm like lamin A/C, prelamin A, lamin B, LAP2α and nuclear pore complexes.

4 Results

4.1 Markers of Senescence: Cell Morphology and SA-β-Gal Activity

To prove that the onset of senescence is induced in neuroblastoma cells by long term low dose treatment with HU, the main marker for senescence, SA-β-Gal activity was assayed on untreated, HU induced and HU induced senescent cell populations. Additionally, the change in morphology was observed. These indicators of senescence were documented by images taken in the phase contrast or bright field of an inverted DIC fluorescence microscope with 10x and 20x magnifying objectives coupled to a CCD camera.

In Figure 12 STA-NB-9 cells treated according to the protocol with X-gal and assayed for positivity are depicted. Terminology and type of treatment are referred to in detail in chapter 2.1.2. Small cells with scant cytoplasms and neurite outgrowth (N-cells) were found to be SA-β-Gal negative, whereas cells with flat morphology and high granularity (F-cells) were found in the induced and senescent population and were positive for SA-ß-Gal staining. In Figure 12A, an untreated population is depicted. Typical N-cells show no blue staining. Spontaneous F-cells, with F-cell morphology were seen infrequently and were positive for SA-β-Gal. In Figure 12B, ind-cells show no significantly higher fraction of F-cells and SA-β-Gal staining - indicated here by the blue staining beneath the N-cell layer. In Figure 12C induced cells are depicted, consisting of cells with flat morphology and showing SA-β-Gal positive staining. In Figure 12D H_2O_2 induced cells show a markedly higher proportion of cells with flat morphology compared to the HU induced cells. In H_2O_2-induced cells, induced cells and induced senescent cells SA-β-Gal staining is shown on cells with flat morphology, while cells with neurite outgrowth and scant cytoplasm are not stained.

To assess the time point of change in morphology and SA-β-gal expression a time course experiment was performed with STA-NB-10 cell line explained in detail in chapter 2.1.2 (Figure 13). The untreated population was compared to induced cells (1, 5, 10 and 15 days after the start of HU treatment) and induced senescent cells. Untreated cells (Figure 13A) contained primarily a population of small cells with scant cytoplasm and neurite outgrowth. Only a low number of cells with flat morphology were observed in the untreated population. N-cells showed no SA-β-Gal staining whereas the flat cells showed blue staining. N-cells pretending to be positively stained were adhering to positive F-cells.

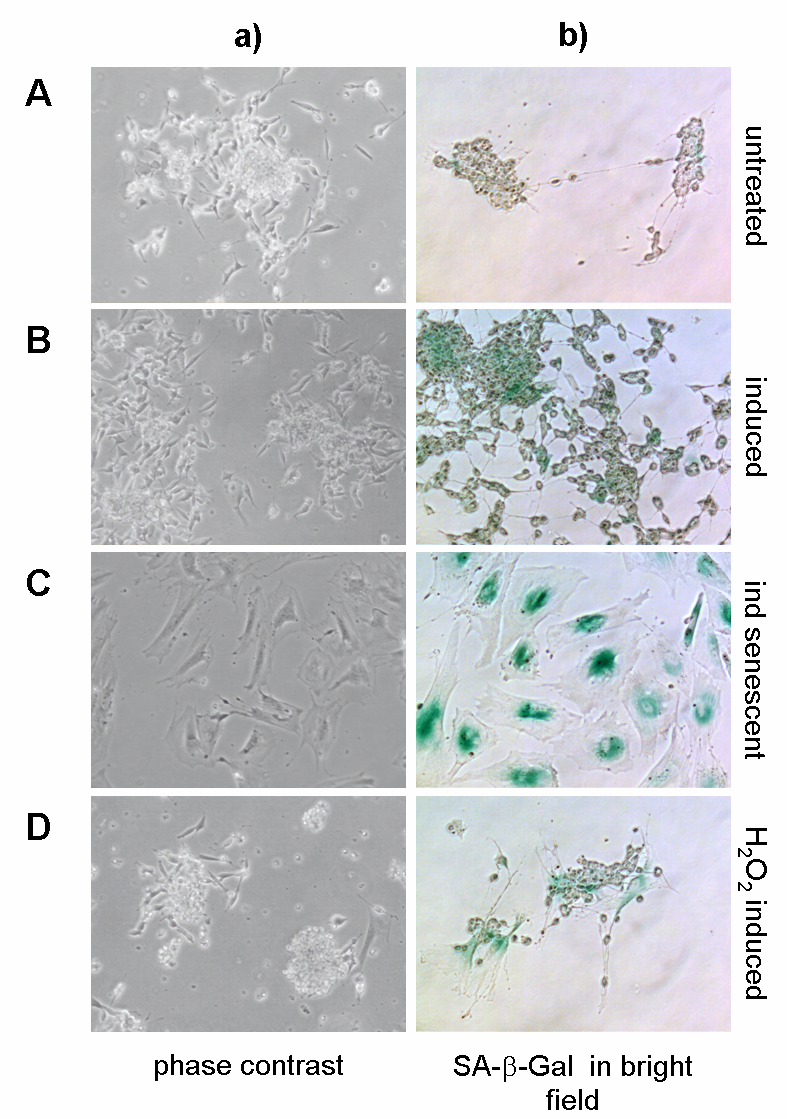

Figure 12 **STA-NB-9 cells acquiring the senescent morphology showed senescence-associated-β-galactosidase activity (SA-β-Gal).** Images of untreated cells **A** induced cells **B** induced senescent **C** and H_2O_2 induced **D** cells were taken with a CCD camera coupled to an inverted fluorescence DIC microscope before staining by phase contrast a) and after SA-β-Gal staining by bright field b) imaging.

With HU treatment, N-cell population of induced cells decreased and a high proportion of cell debris was found in the medium. In cells induced for 10 days (Figure 13D) and 15 days (Figure 13E) a third cell type, next to F-cells and N-cells appeared in the flasks. This cell type clustered and formed neurite networks connecting to the surrounding cells, resembling typical features of differentiating neuroblastoma cells. In induced senescent cells (Figure 13F) a small proportion of cells with differentiating features was present. SA-β-Gal positive staining was in all time points only found in morphological flat cells which did not show neurite outgrowth. The proportion of cell types varied between different flasks for different time points, but a general trend was that cells with neurite outgrowth declined. During treatment the amount of cells with flat morphology and

cells with features of differentiation increased. In late stages of induction - from 6 weeks onwards (only treatment for 56 days is shown) -the amount of differentiating cells decreased and SA-β-Gal positive cells with flat, enlarged morphology remained.

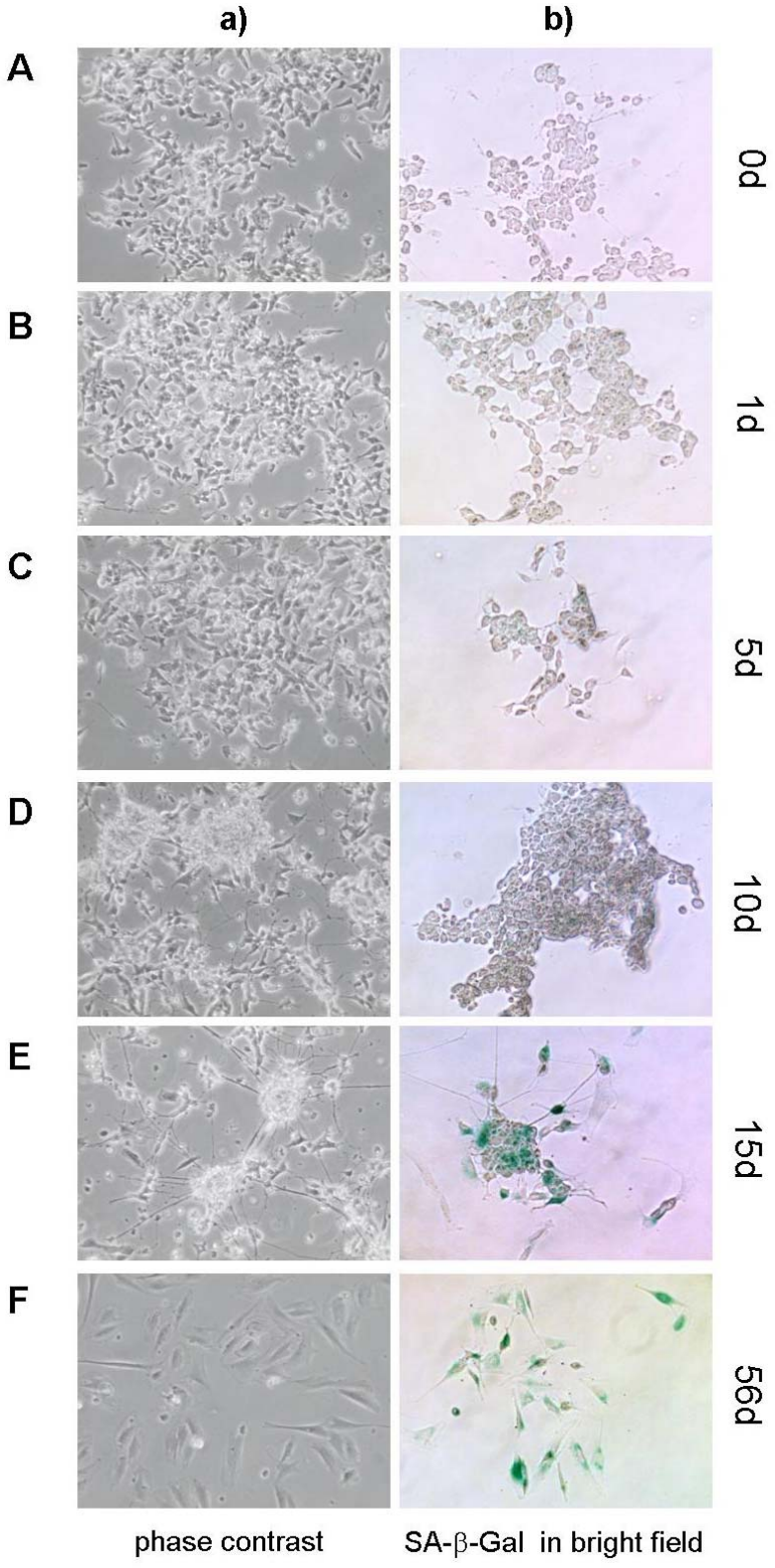

Figure 13. **STA-NB-10 cells acquiring the flat, enlarged morphology showed senescence-associated-β-galactosidase activity (SA-β-Gal).** Images of untreated cells **A** inducedcells treated for 1 day **B**, 5 days **C**, 10 days **D**, and 15 days **E** with HU, as well as of induced senescent cells treated for 56 days **F** were taken with a CCD camera coupled to an inverted fluorescence DIC microscope before staining by phase contrast a) and after SA-β-Gal staining by bright field b) imaging.

4.2 Proliferation, Growth and Cell Cycle Assay, *MYCN* Copy Number

4.2.1 Cell Cycle Analyses

Next to the assessment of the senescence typical morphology and senescence marker SA-β-Gal, the cell cycle was monitored by staining cells with BD cell cycle test and measuring DNA content with flow cytometry.

In Figure 14 the cell cycle of asynchronous STA-NB-9 cells induced for 24 hours with HU (induced) or H_2O_2 (H_2O_2 induced), and induced until senescence with HU (induced senescent) is depicted. Details about the experimental setup are described in chapter 2.1.2. The treatment with either HU or H_2O_2 insignificantly increases the G1-population and decreases the S-phase population. Moreover, HU depletes cells with G2/M-DNA content while in H_2O_2 induced cells this population does not decline. However, induced senescent cells show a high proportion of cells in G1-phase (92%) and only 8% of the cells remain in S-phase. Interestingly, neither induced nor induced senescent cells were detected to have a G2/M-phase DNA content.

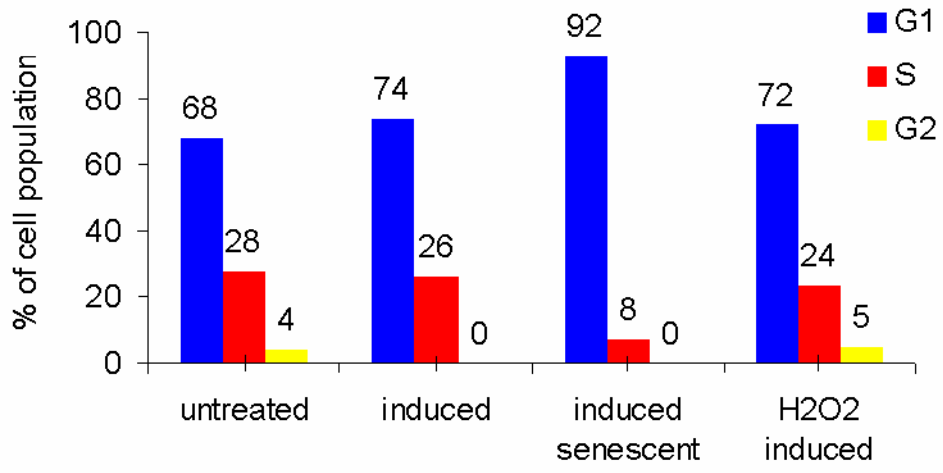

Figure 14. **Cell cycle of STA-NB-9 cells after induction.** Untreated cells, 24 hours HU treated (induced), HU induced senescent cells (induced senescent) and 24 hours H_2O_2 treated cells (H_2O_2 induced) were assessed for G1-phase (G1), S-phase (S) and G2-phase/mitosis (G2) of the cell cycle.

STA-NB-10 cell line was assessed in more detail for changes in the cell cycle with time. In Figure 15 and Figure 16 the amount of cells detected for either G1-, S- or G2/M-phase of the cell cycle were monitored. From the time course experiment explained in detail in chapters 2.1.2, aliquots were monitored for their cell cycle pattern (Figure 15). The untreated population was made up of 66% of cells with G1-phase-, 28% with S-phase- and 6% with G2/M-DNA content. After 1-5 days

of HU induction an increase in the S-phase population was observed (day1 35% and day 5 43%). This shift of the population was observed along with a decrease in G1-phase (d1= 61%, d5=51%). From day 10 of induction, a consistent increase in G1-phase was observed, reaching up to 80% after 56 days. At this time point only 6% of the population remained in S-phase.

In Figure 16 the effect of HU treatment on the first ten days were assessed in detail. 1, 3, 6, 8 and 10 days induced cells were stained with BD cell cycle test and assessed by FACS. Untreated cells were analysed in paralell to compensate for systematic errors (Figure 16A). During the analysis, the untreated cell population showed no significant change in cell cycle. The mean proportion of cells in S-phase were 26% and in G1-phase 70%, while 5% of the cells were in G2/M-phase. When such cell populations were treated with HU (Figure 16B), an increase in the S-phase population was observed on day 1 (S-phase = 51%) with a decrease in G1-phase (G1= 46%). From day 3 of induction, the G1-phase population increased and the proportion of cells in S-phase decreased. After 10 days treatment with HU the cell population showed 73% G1-phase, 20% S-phase and 7% G2/M-phase.

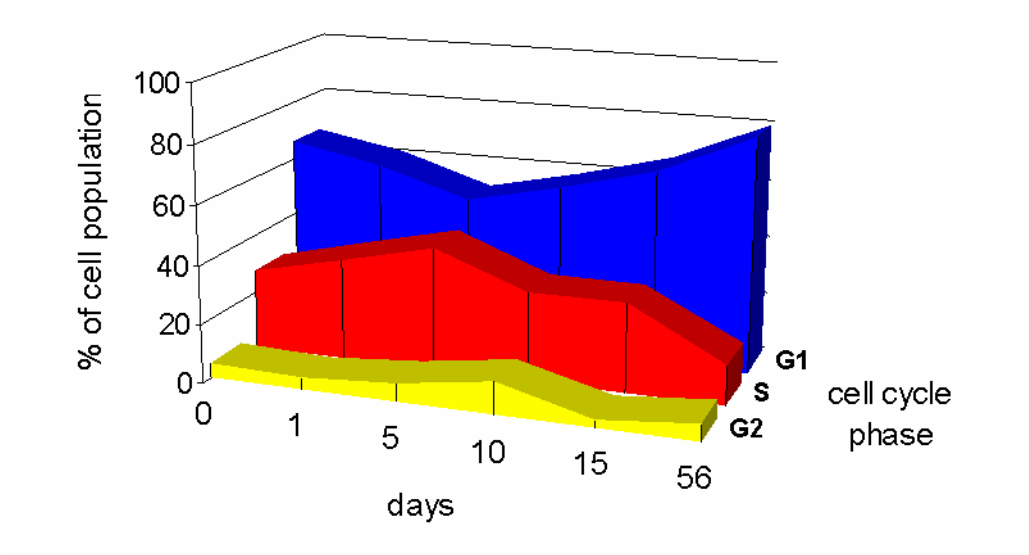

Figure 15 **Cell cycle of STA-NB-10 cells in a time course after induction.** Untreated cells (0 days) and HU induced cells (1 – 56 days) were assessed for G1-phase (G1), S-phase (S) and G2/M-phase (G2) of the cell cycle.

4.2.2 Growth Curve

To assess the growth curve and population doublings of the cells which were taken for the experiment depicted in Figure 16A and B, the cell number was counted with a coulter counter and is shown in Figure 16C. A starting population of 5 x 10^5 cells was assessed over 10 days following HU treatment. In parallel an untreated population was assessed. Doubling of untreated neuroblastoma cells was calculated to occur every 3 days. To the contrary, HU treatment decimates

the cell population to 2.4 x 10^5 cells representing approximately half of the original cell number.

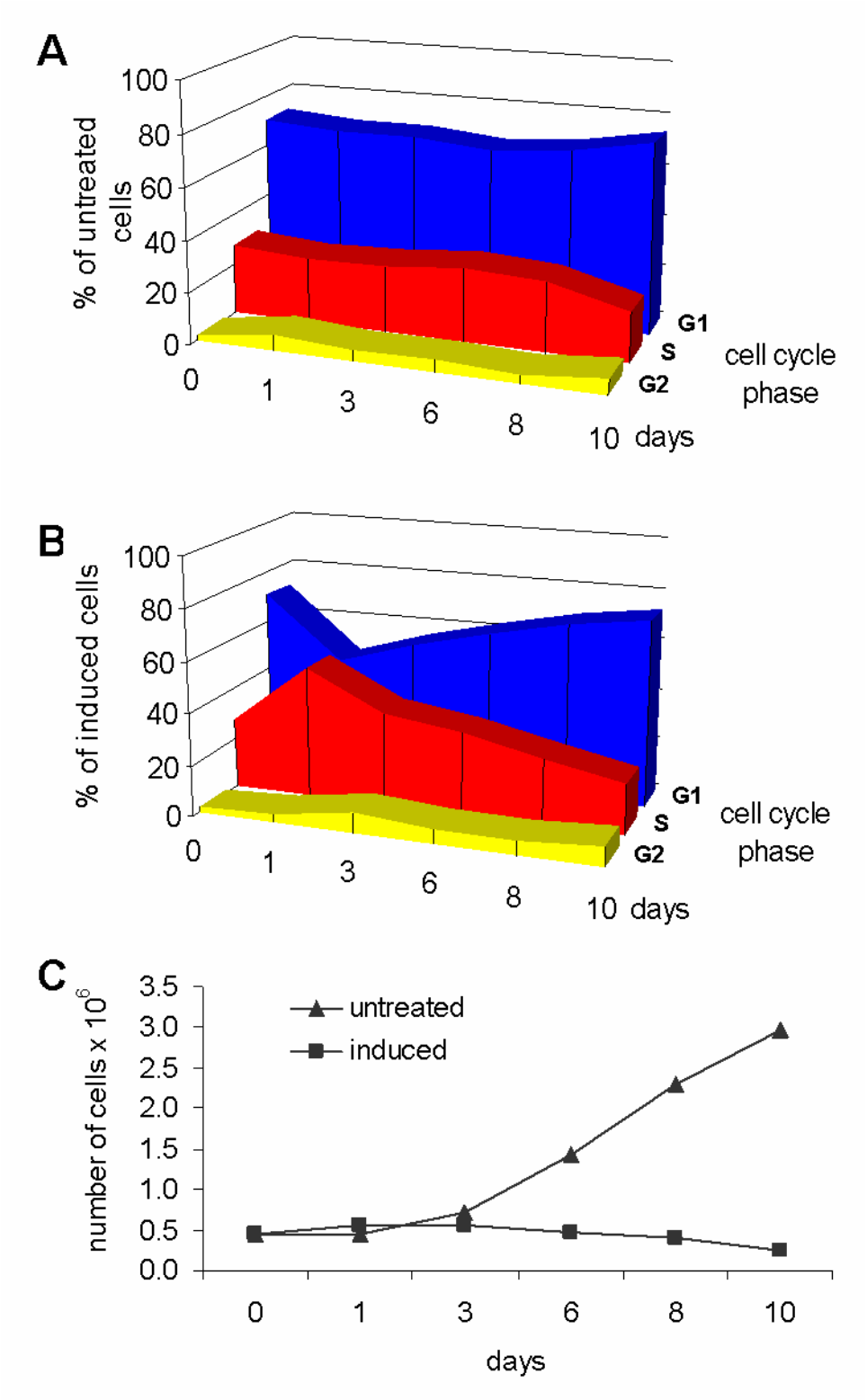

Figure 16 **Cell cycle and growth curve of STA-NB-10 cells for 10 days after induction.** Untreated cells **A** and HU induced cells **B** were assessed for G1-phase (G1), S-phase (S) and G2/M-phase (G2) of the cell cycle in parallel. **C** Growth curve of the untreated cell population (triangle) was compared to HU induced cell population (square) for 10 days.

4.2.2.1 Proliferation Assay

To further assess the high increase in S-phase after the first 24 hours of HU treatment in STA-NB-10 cells, the neuroblastoma cells were assessed for BrdU uptake over 24 hours. In Figure 17 the effects of HU treatment on entering S-phase during 24 hours was compared to untreated control cells (Figure 17). After 24 hours treatment with HU in BrdU supplemented medium cells showed the same proportion of replicating cells as the control. The cells proliferating are for untreated and treated cells approximately 46% of at least 890 cells counted. Around 54% of the cells did not show BrdU positivity.

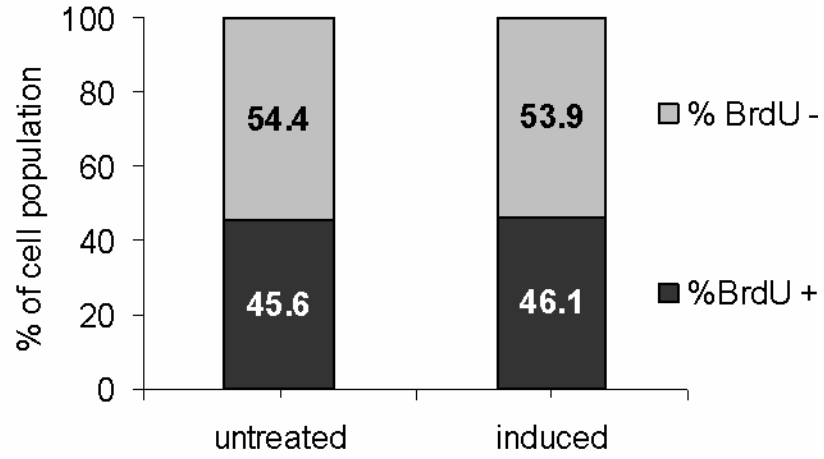

Figure 17. **HU treatment does not affect BrdU incorporation during 24 hours.** Proliferation was assayed in asynchronous STA-NB-10 populations. 1456 HU induced cells and 890 untreated cells were assessed in parallel for BrdU incorporation during 24h. The percentage of the population positive (BrdU+) and negative (BrdU-) for BrdU is depicted.

4.2.3 *MYCN* Amplification Status

The copy number of the *MYCN* gene in the time course of low dose HU treatment (150µM) of the *MYCN* amplified neuroblastoma cell line STA-NB-10 was evaluated (Figure 18). Direct *MYCN*-interphase-FISH was performed on cytospin preparations of the treated cell populations. FISH spot counting was performed by automatic microscopy with the Metafer Metacyte program. Results are shown as percentage of total counted cells which were 709 cells for untreated control, 634 for 1 day treated cells, 481 for 10 days treated cells and 286 cells for 70 days treated cells. Cells are classified according to Ambros et al. with one or two copies being normal, 3 to 8 *MYCN* copies - up to 4-fold increase relative to reference signals - per cell signifying gain of *MYCN* and more than 8 copies - > 4-fold increase relative to reference signals - showing gene amplification (Ambros, Benard et al. 2003). In untreated neuroblastoma cells 73% of the cells had more than 8 copies of *MYCN*, whereas less than 3% of the cells displayed normal *MYCN* copy numbers. 24 hours HU treated cells showed a smaller percentage of amplified cells (67%) and a not significant higher percentage of cells with a *MYCN* gain (from 24.4% to 30.6%). In the 10 days HU treated cell population 26% of the cells show amplified status, whereas 50% show a gain of *MYCN* and 17.5% show a normal phenotype. In

contrast to our expectations, the population treated for 70 days showed a higher percentage of cells with amplification (42.3%) compared to 10 days induced cells. The majority of the 70 days induced cells showed *MYCN* gain. 15.7% of the population showed a normal *MYCN* status, which is a 5.6-fold increase compared to the untreated control.

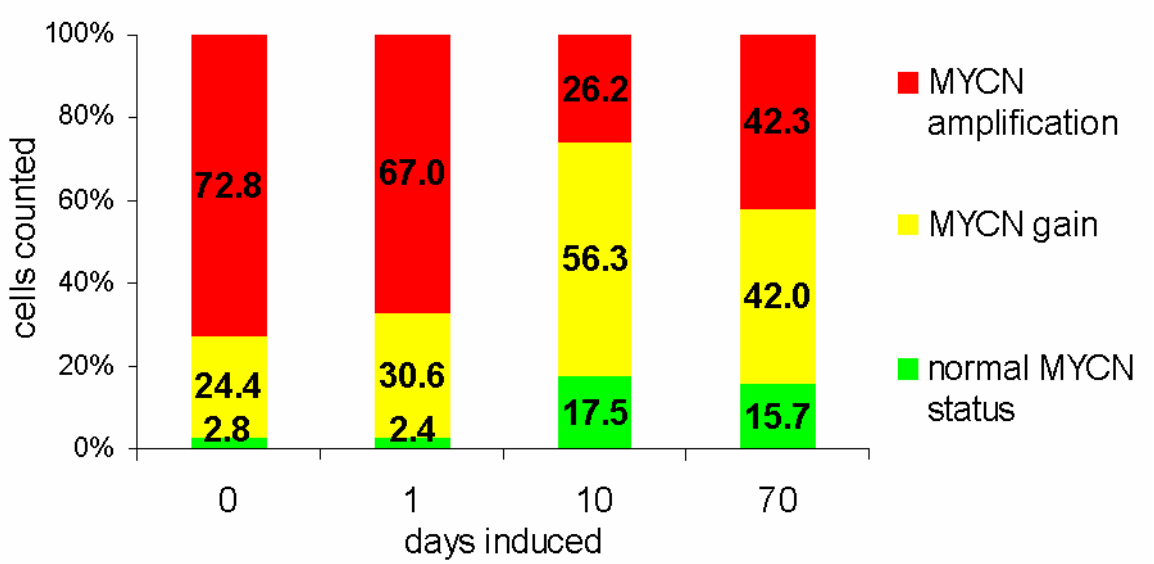

Figure 18 **Decrease of *MYCN* copy number following HU treatment.** Direct *MYCN*-interphase-FISH was performed on cells induced for different periods of time. After HU induction automatic spot counting was performed. Results are shown as percentage of total counted cells.

4.3 Investigation of ROS Involving Mitochondrial Function in Neuroblastoma Cells Undergoing a Senescent Phenotype after HU Treatment

Here we tested whether the treatment with HU and the induction of senescence provokes an increase in superoxide, peroxynitrite, mitochondrial membrane potential $\Delta\psi_m$ and mitochondrial mass. Therefore, cells induced for different amounts of time with HU (or with H_2O_2 for 24 hours), as well as different cell lines (STA-NB-9, STA-NB-10, MRC5) were stained with specific dyes. Analysis was performed by flow cytometry and/or by live cell imaging with a confocal microscope.

4.3.1 Change in Superoxide Levels

To measure superoxide levels (Figure 19), at least 35 days HU treated (induced), induced senescent and control STA-NB-9 (untreated) populations were stained with MitoSox Red mitochondrial superoxide dye. Details about treatment of cells and staining method are described in chapter 2.1.5 and 2.3.4. Flow cytometric analysis (Figure 19A) of induced and induced senescent cells showed a

more than two fold increase (2.4 and 2.7 respectively) in intensity. All data are relative values ± standard error of mean from 5 independent experiments with measurements in duplicate. The asterisk indicates a significant difference to the control ($p < 0.05$) determined by paired two-tailed t-test. Relative fluorescence intensity of untreated cells is comparable to the fluorescence intensity of MRC5 fibroblasts. Slide grown live STA-NB-9 cells (Figure 19B) were imaged by confocal light microscopy.

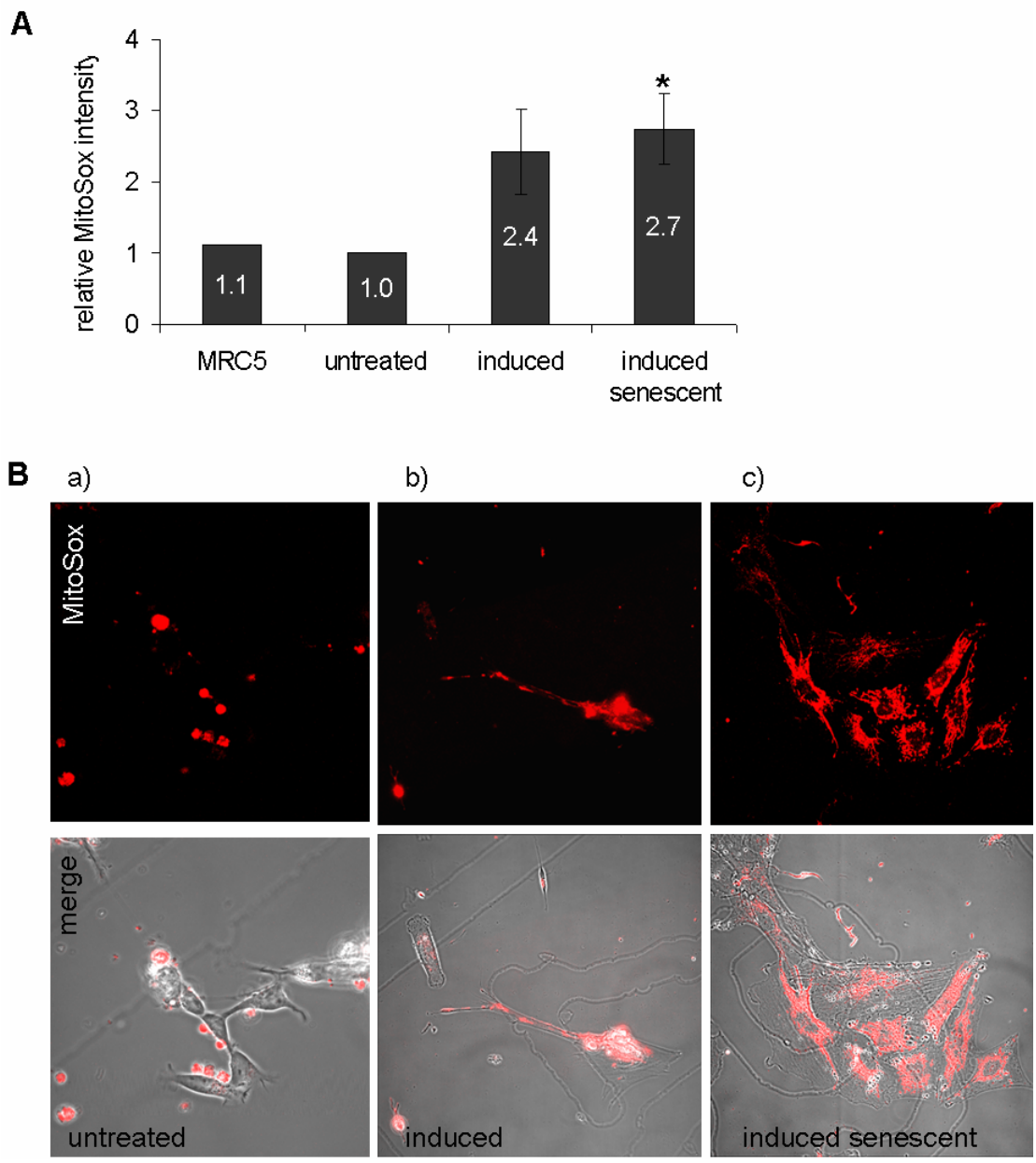

Figure 19. **Increase in superoxide levels. A** Relative fluorescence intensity of MitoSox Red in untreated STA-NB-9 cells (relative fluorescence intensity of 1), HU induced cells (induced), HU induced senescent cells (induced senescent) and MRC5 fibroblasts was measured by FACS. Asterisk indicates significance $p<0.05$. **B** Fluorescence and phase contrast images of untreated a), induced b) and induced senescent c) STA-NB-9 neuroblastoma cells are depicted. Cell debris or apoptotic cells were unspecifically stained).

Typical cells of untreated control cells were taken with a 63x magnification objective while the images of the typical HU treated and induced senescent cells were taken with 40x. Untreated cells show small cytoplasm and neuronal outgrowth. These cells show little MitoSox staining (red), but unspecific background staining shows high fluorescence intensity. Induced cells show increased fluorescence intensity. Moreover, the morphology of induced cells changes to a flat morphology and cytoplasms enlarge compared to untreated cells. Induced senescent cells show the largest cytoplasms of the three compared populations. Bright fluorescent staining is localized to the cytoplasm leaving the nucleus unstained.

day

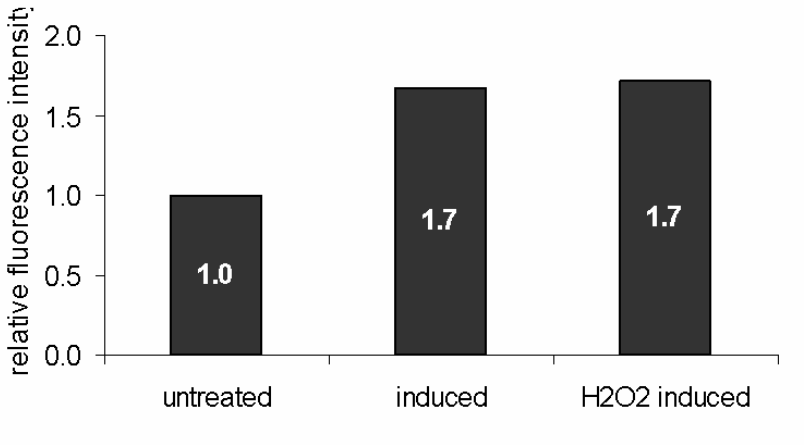

Figure 20. **Increase in ROS after 24 hours treatment.** MitoSOX was measured in STA-NB-9 cells treated for 1 with HU or H_2O_2. Moreover untreated control cells were stained and analysed by FACS. HU shows the same potential to induce cellular superoxide as H_2O_2.

Following the initial experiment, the time of superoxide increase and comparison of the radical inducer H_2O_2 to HU after 24 hours treatment were analysed with the same method. Therefore, STA-NB-9 cells were induced for 24 hours with HU. Hydrogen peroxide (H_2O_2), itself a ROS, was used as a positive indicator of cellular oxidative stress and treatment was done for 24 hours with 75µM H_2O_2. These differentially conditioned cells were stained with MitoSOX Red superoxide indicator according to the protocol (chapter 2.1.1) and were analysed by FACS. In Figure 19Typical cells of untreated control cells were taken with a 63x magnification objective while the images of the typical HU treated and induced senescent cells were taken with 40x. Untreated cells show small cytoplasm and neuronal outgrowth. These cells show little MitoSox, relative values to the untreated control cells are depicted. HU treatment raised the cellular superoxide levels to the same level as for the positive control cells treated with hydrogen peroxide (1.7 fold increase).

A further experiment done with STA-NB-10 cell line to provide information about the superoxide levels in the first two weeks of HU treatment (150µM) is shown in Figure 21. The relative fluorescence intensities measured by FACS are depicted. As expected, HU increased the superoxide levels markedly after 5 days (3.4 fold) and another increase was observed after 15 days (7.3 fold). Highest superoxide levels were observed in STA-NB-10 cells treated for 8 weeks with HU (13

fold).

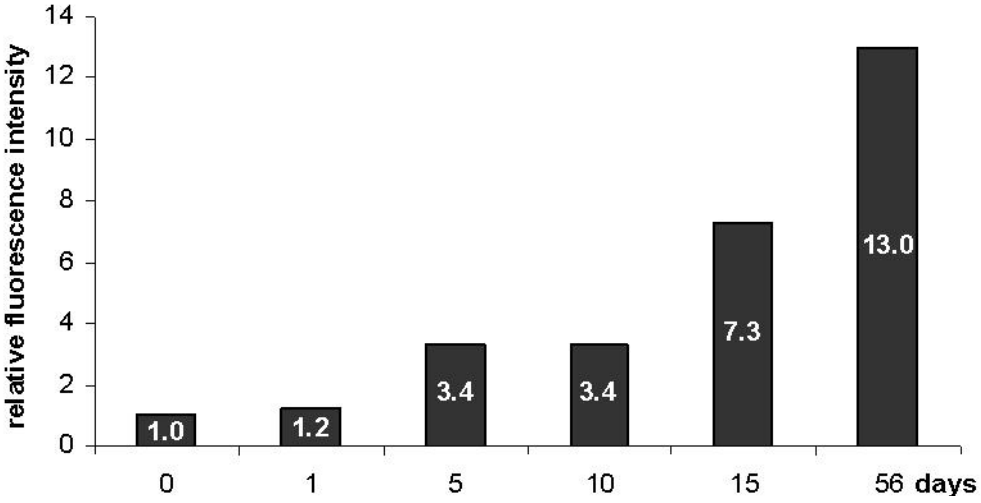

Figure 21. **Increase in superoxide with time after induction of STA-NB-10 cells.** STA-NB-10 cell line was induced with 150µM HU for 1 to 56 days. Speroxide was measured by MitoSox fluorescence intensity measured by FACS and is depicted as relative values to untreated control cells.

4.3.2 Change in Peroxide Levels and Derivatives

To measure the levels of peroxide and its derivatives (Figure 22), 75 µM HU treated (induced), induced senescent and control STA-NB-9 (untreated) populations were stained with DHR. Details about treatment of cells and staining method are described in chapter 2.1.5 and 2.3.4. In Figure 22A induced cells show a 2.4 fold increase of peroxide and derivative levels. Induced senescent cells increase 6.9 fold compared to untreated cells. Results are relative values to the untreated control cells and the standard errors of 5 different experiments are shown. The asterisk indicates a significant difference compared to the control ($p < 0.05$). Relative fluorescence intensity of untreated cells is comparable to the intensity measured in MRC5 fibroblasts. In Figure 22B slide grown live STA-NB-9 cells were imaged by confocal light imaging. Typical cells of untreated control cells were taken with a magnifying objective of 63x while the images of the typical induced and induced senescent cells were taken at 40x. Untreated cells show a small cytoplasm and neuronal outgrowth. These cells show little DHR fluorescence (green). In HU treated cells the fluorescence intensity is faint but increases compared to the control cells. Moreover, the cells get flatter and larger. Induced senescent cells show the enlarged, flattened morphology. Bright fluorescent staining is localized in the cytoplasm at the mitochondria, leaving the nucleus unstained.

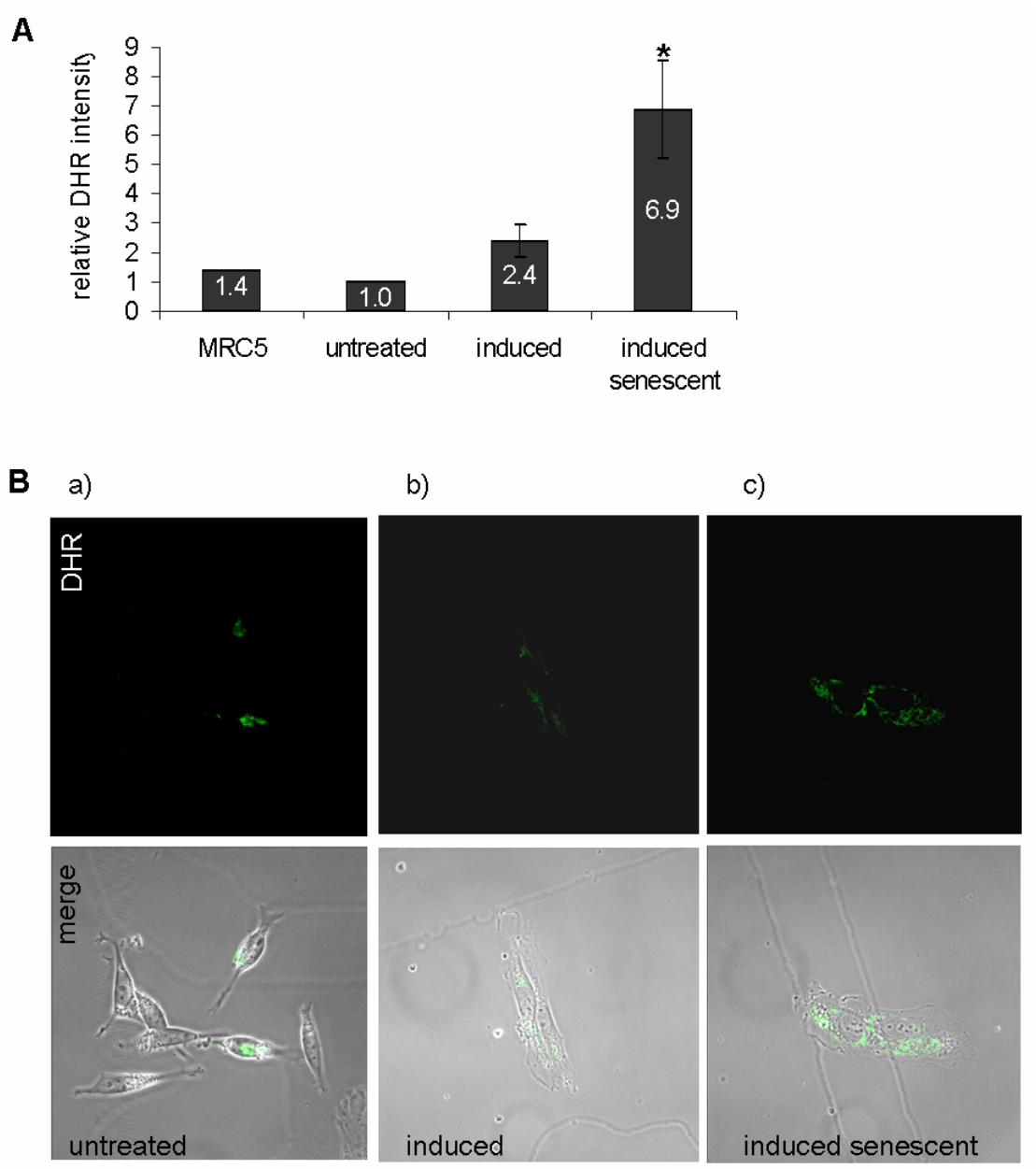

Figure 22. **Increase in peroxide and peroxynitrite levels. A** Relative fluorescence intensity of oxidized DHR in untreated (relative fluorescence intensity of 1), HU induced (induced), HU induced senescent (induced senescent) STA-NB-9 cells and MRC5 fibroblasts was measured by FACS. Asterisk indicates significance $p<0.05$. **B** Fluorescence and phase contrast images of untreated, induced and induced senescent cells are depicted.

4.3.3 Change in Mitochondrial Mass and Mitochondrial Membrane Potential

To measure mitochondrial mass (Figure 23A) 75 µM HU treated, induced senescent and control STA-NB-9 cells were stained with the cardiolipin binding dye NAO and samples were analysed by FACS. Results are relative values to the untreated control cells and the standard errors of 3 different experiments are shown. HU treated and induced senescent cells showed an increase in mitochondrial cardiolipin bound NAO. The MFI of the HU treated cells increases 1.4 times while senescent cells increased 3.4 times compared to control cells. Results are not significant ($p > 0.05$) still an increase in relative fluorescence intensity could be observed in all three experiments.

To measure mitochondrial membrane potential $\Delta\psi_m$ (Figure 23B) 75 µM HU treated, HU induced senescent and control STA-NB-9 cells were stained with JC-1 and were analysed by FACS. Results are shown as ratios of the 530 nm (FL1) and 670 nm (FL3) intensity and are relative values to the untreated control cells. The standard errors of 3 different experiments are shown. HU treated and induced senescent cells showed a decrease in $\Delta\psi_m$. The relative fluorescence intensity of HU treated cells decreases to 0.5 compared to untreated cells with the relative ratio value of 1 and induced senescent cells show a ratio of 0.6.

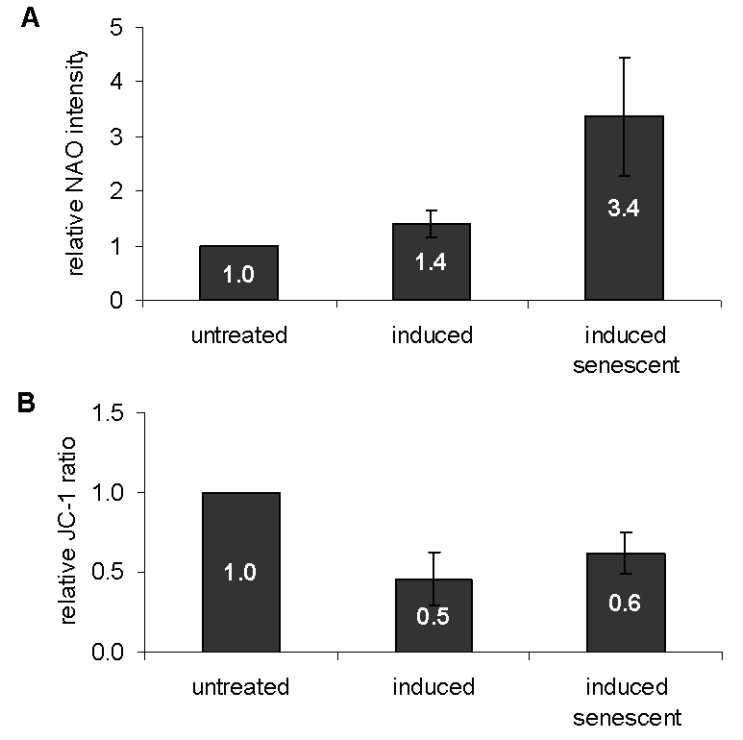

Figure 23. **Increase in mitochondrial mass and decrease in mitochondrial membrane potential $\Delta\Psi_m$.** Mitochondrial mass **A** is measured by FACS as intensity of NAO and is here depicted as relative value to the untreated cells. $\Delta\Psi_m$ **B** is depicted as relative ratio of green (FL3) to red (FL1) fluorescence compared to the control ratio. The standard errors of 3 different experiments are shown.

4.4 Lamin and Associated Proteins

Changes of lamins and lamin associated proteins were found to correlate to normal aging and premature aging syndromes like Hutchinson Gilford progeria and other laminopathies. Therefore, it was assessed whether the HU induced senescent tumour cells showed changes in the composition and timely appearance of nuclear lamina. Moreover, we were interested to characterise the properties of the nuclear lamina of micronuclei that formed spontaneously and which were induced by HU treatment.

In Figure 24 the composition of the lamina of neuroblastoma cells is depicted. Only a small proportion of cells showed lamin A/C staining (Figure 24A), whereas a high percentage of cells showed incorporation of lamin B (Figure 24B) into the nuclear lamina. Mitotic cells indicated by arrows showed association of chromatin (DAPI) with lamin A/C but not with lamin B. Cells with incorporation of lamin A/C often showed lobulated nuclei resembling cells from progeria patients (not shown).

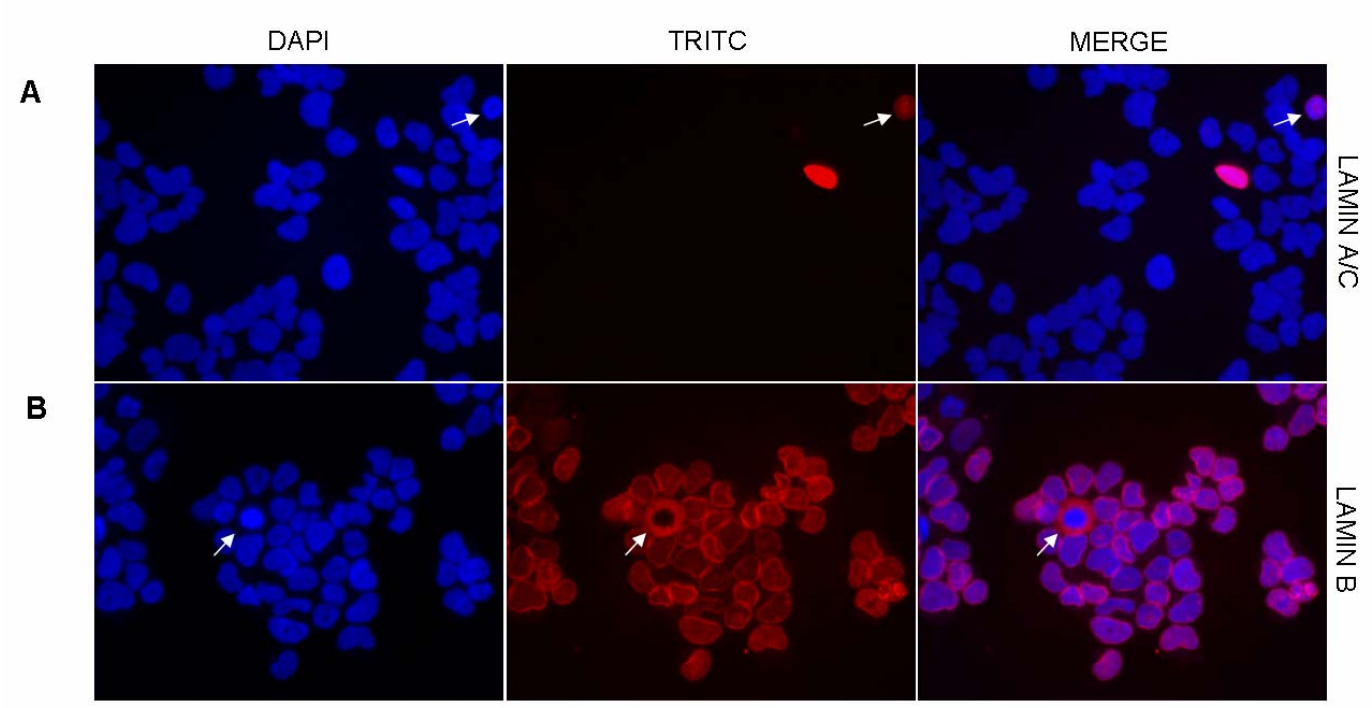

Figure 24 **Lamin expression on untreated neuroblastoma cells.** Untreated STA-NB-10 cells were stained with α-lamin A/C antibody **A** or with α-lamin B antibody **B** and as secondary antibody a TRITC labelled antibody was used. In the left row the DAPI channel is shown in blue. The middle row shows the specific lamin staining in red and the right row shows the merged channels. The images were taken with a 40x objective. Mitotic cells are indicated by arrows.

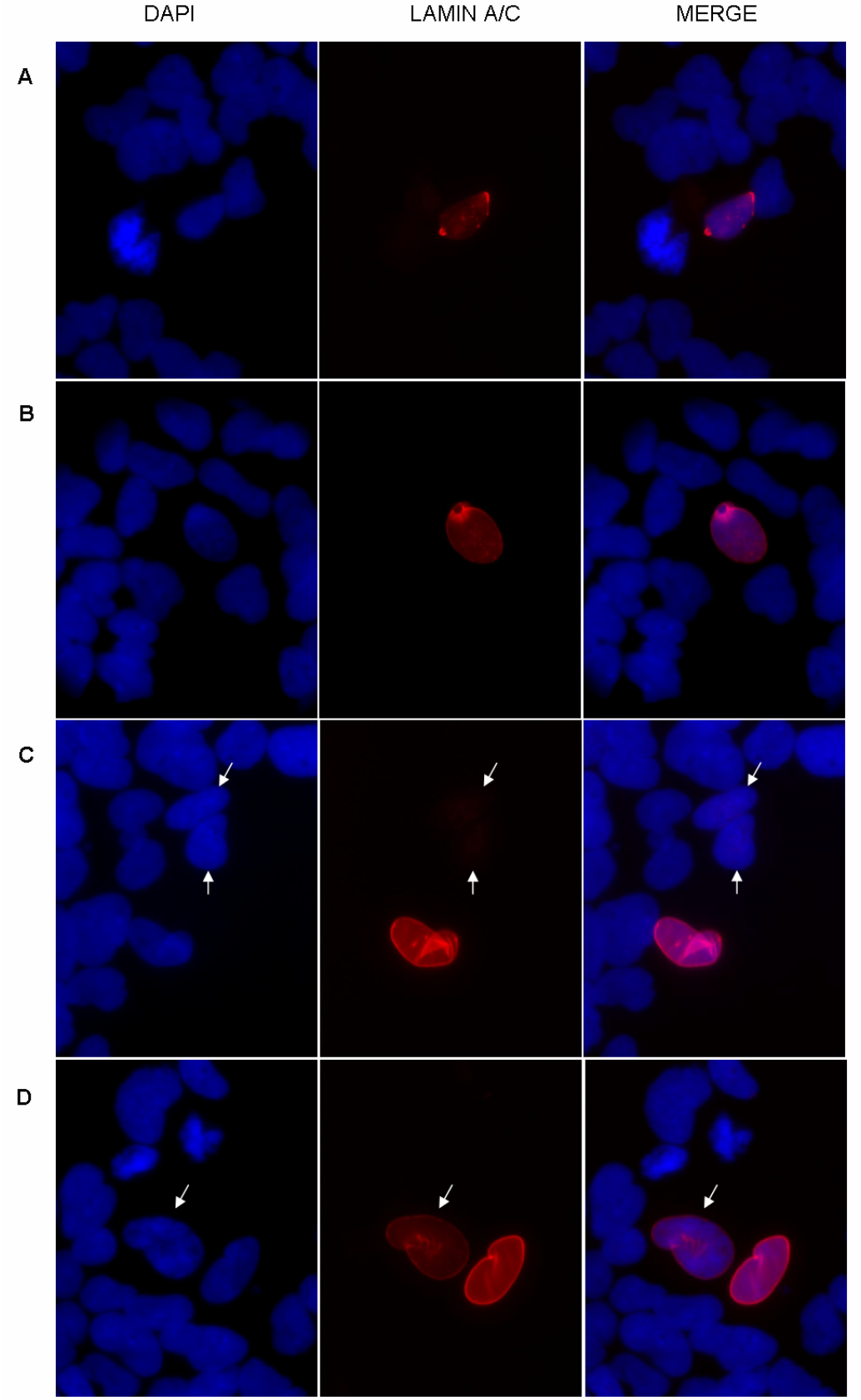

Figure 25. **Untreated STA-NB-10 cell population show only rare cells with incorporation of lamin A/C into the nuclear membrane.** In the first column DAPI staining a), in the second column lamin A/C b) is shown. The third column shows the merged channels c). Images were taken with a Zeiss Axioplan 2 with the 63x objective. Arrows indicate cells with faint positive lamin A/C staining.

The different types of lamin A/C staining found to occur in STA-NB-10 cells are shown in Figure 25. One type of staining found showed lamin A/C incorporation preferentially at the poles of the nuclei (Figure 25A). Double staining with lamin B revealed that these lamin A/C positive poles show no or weak lamin B staining (data not shown). In Figure 25B a cell with a defined, structure-giving accumulation of lamin A/C is shown. This concretion of lamin A/C coincides with a high intensity in DAPI staining. At sites of micronuclear budding cells showed similar structure-giving lamin A/C accumulation (data not shown). In Figure 25C a lobulated nucleus is shown with high lamin A/C intensity at the site of the nuclear membrane and at distinct intranuclear foci. Figure 25D shows the differences in intensities of lamin A/C at the site of the nuclear lamina. The weaker stained cell shows additional intranuclear diffuse staining.

To further assess the composition of the nuclear envelope of neuroblastoma cells the untreated STA-NB-10 cells were stained with a prelamin A antibody recognising the C-terminal tail of uncleaved lamin A (Figure 26A). Further, lamin A/C binding protein LAP2α which is involved in cell cycle regulation was stained (Figure 26B). Nuclear pore complexes were assessed by staining with a monoclonal mAb414 antibody raised against a conserved domain in nucleoporins (Figure 26C). The staining of prelamin A in Figure 26A was found in the nucleus and in the cytoplasm, but not incorporated at the site of the nuclear envelope. The intranuclear staining concentrates to the centres of the nuclei, omitting the outer nuclear regions. Mitotic cells showed cytoplasmic staining. Figure 26B shows that LAP2α is localized in the nucleus. There it forms a pattern that omits regions of the nucleus and accumulates in other regions. Moreover, TRITC intensity is heterogeneous in untreated cells. In mitotic cells LAP2α appears around the condensed DNA. In Figure 26C nuclear pore complexes are found preferentially at the site of the nuclear envelope but also intranuclear patches occurred. Mitotic cells showed nuclear pore staining surrounding the nucleus. Spontaneous F-cells with enlarged cytoplasm also showed cytoplasmic staining.

As there was a high heterogeneity found for different lamin stainings and associated proteins in the untreated cells, double staining was performed. To discriminate for spontaneous senescent F-cells, the untreated population was stained for CD44, a surface marker not expressed on N-cells.

CD44 positive cells in general showed lamin A/C staining and lower lamin B intensity. For double staining with antibodies against the nuclear pore complex and CD44, there was no significant difference in fluorescence intensity observed. There was, however, an increased amount of nuclear pore staining in the cytoplasm of the CD44 positive cells (not shown). In Figure 27 double staining for CD44 and prelamin A is shown. In Figure 27 the line profiles show that the intensity of prelamin A in N-cells is only 30% of total intensity found in the image. In the spontaneous

senescent cell intensities reach from around 55% intensity in the cytoplasm to around 80% in the nucleus. The cytoplasm is encircled by CD44 positive staining marking the membrane bound surface molecule. In the cytoplasm, moreover a micronucleus, indicated by the arrow, shows weaker DAPI staining (55%), around 75% TRITC-prelamin A intensity and 20% FITC-CD44 intensity.

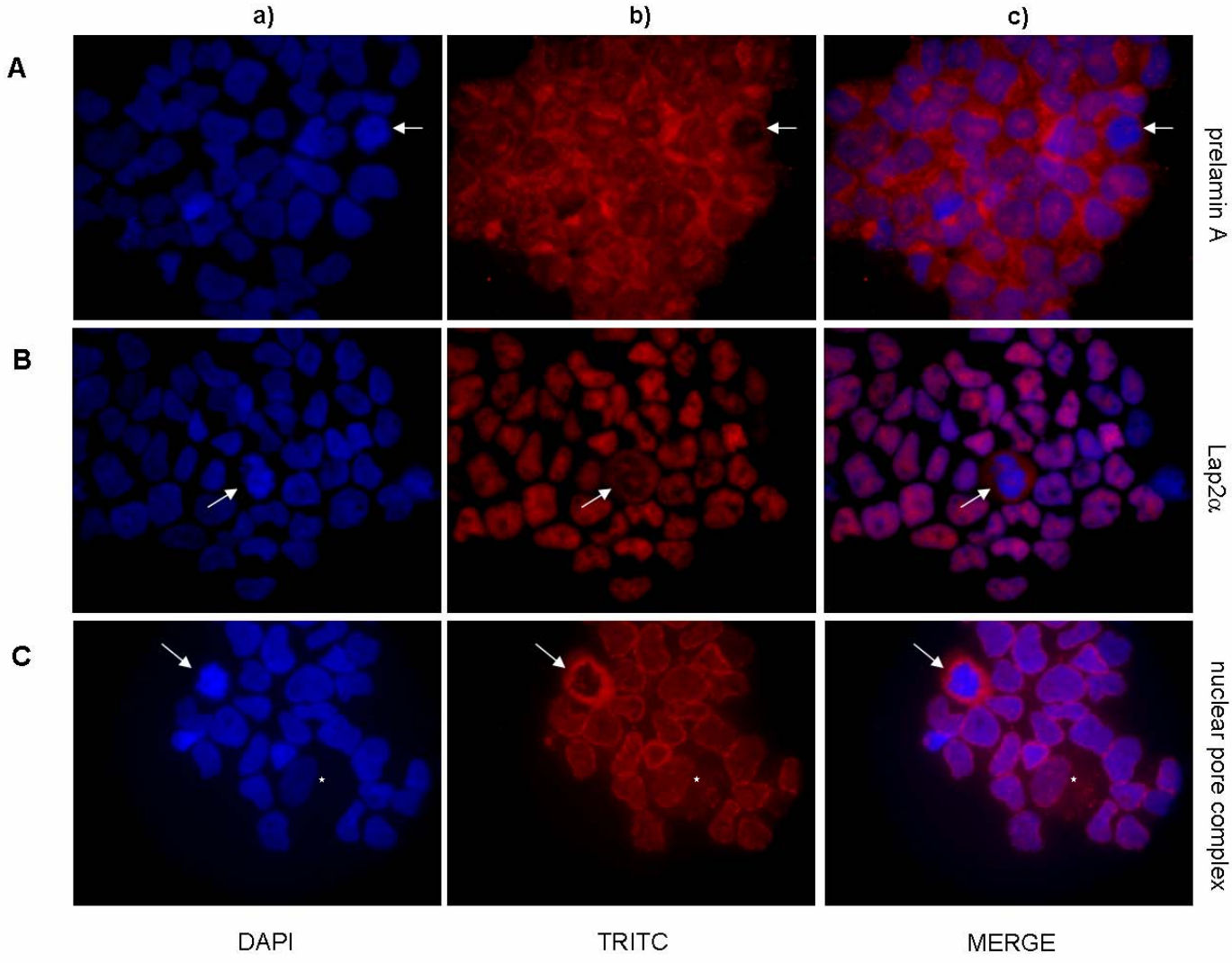

Figure 26 **Lamin and associated proteins in STA-NB-10 cells.** In a) DAPI staining (blue) is shown, in b) the TRITC conjugated secondary antibody staining (red) and in c) the merged channels are shown. Images of cells stained for prelamin A (**A**), LAP2α (**B**) and nuclear pore complex (**C**) are shown. Mitotic cells are indicated by arrows, spontaneous F-cell is indicated by asterisk.

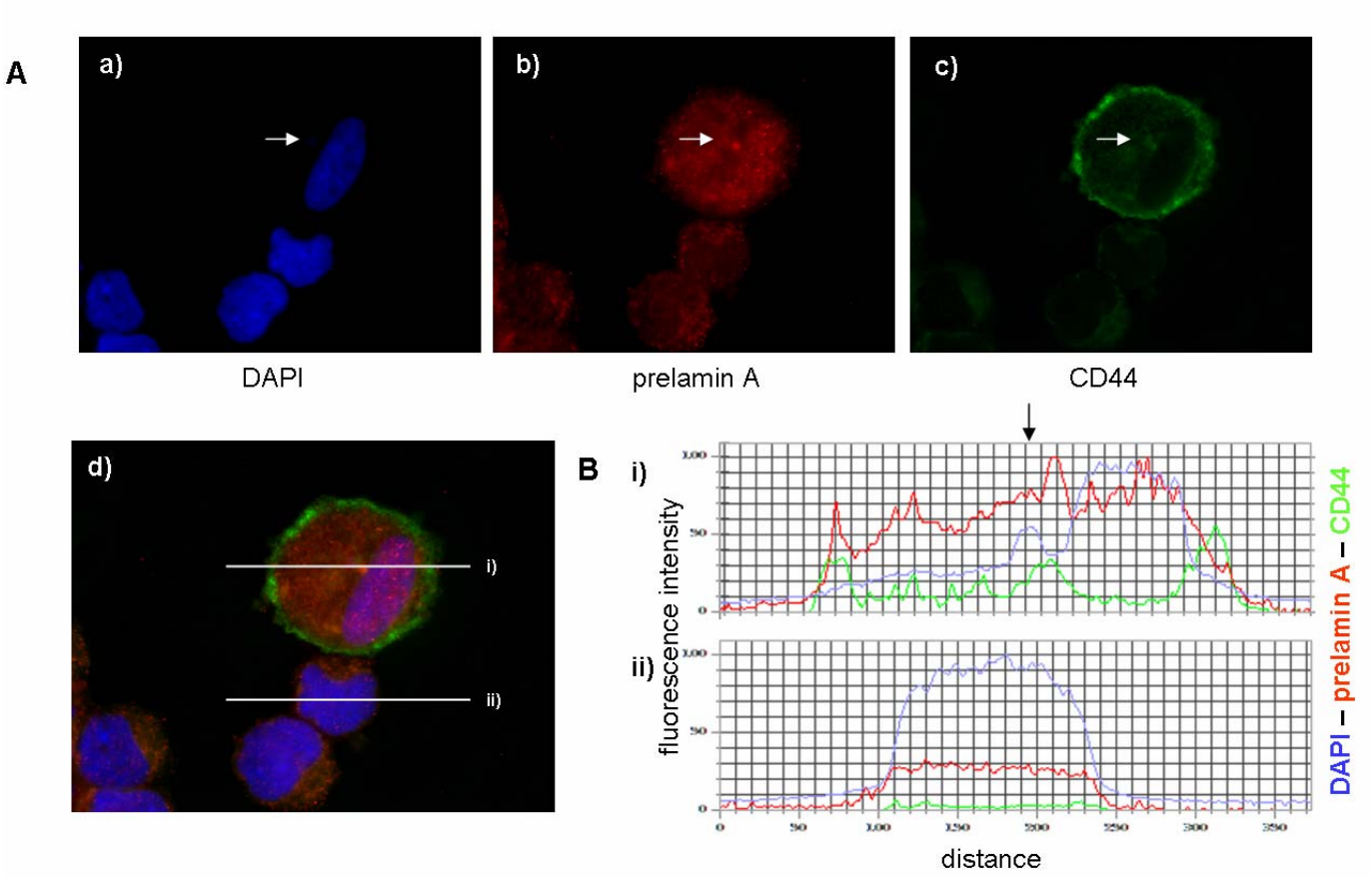

Figure 27 **Accumulation of prelamin A in spontaneous senescent cells. A** Untreated STA-NB-10 cells were stained for **a)** DAPI (blue), **b)** prelamin A (red) and **c)** CD44 (green). The arrows indicate a micronucleus. Merged channels are shown in **d)**. The line traces in white of the CD44 positive cell **i)** and of the CD44 negative cell **ii)** correspond to the profiles in B. In **B** the profile of the two cells shown in Ad) are depicted. x-axis indicates the distance of the white line, whereas the y-axis corresponds to the fluorescence intensity. The arrow in Bi) indicates the site of the micronucleus.

In Figure 28 double staining for CD44 and LAP2α is shown. In Figure 28A the line profiles show that the intensity of LAP2α in N-cells reached from 50% to 100% of total intensity found in the image. In the F-cells intensities reach a maximum in the nucleus of 40% of total intensity. In the profile of N-cells (Figure 28Bi) a negative correlation of heterochromatic, DAPI intensive areas and LAP2α was observed. At position 265 of the line trace nuclear DAPI intensity of this cell was at its peak while nuclear LAP2α reaches its minimum nuclear intensity.

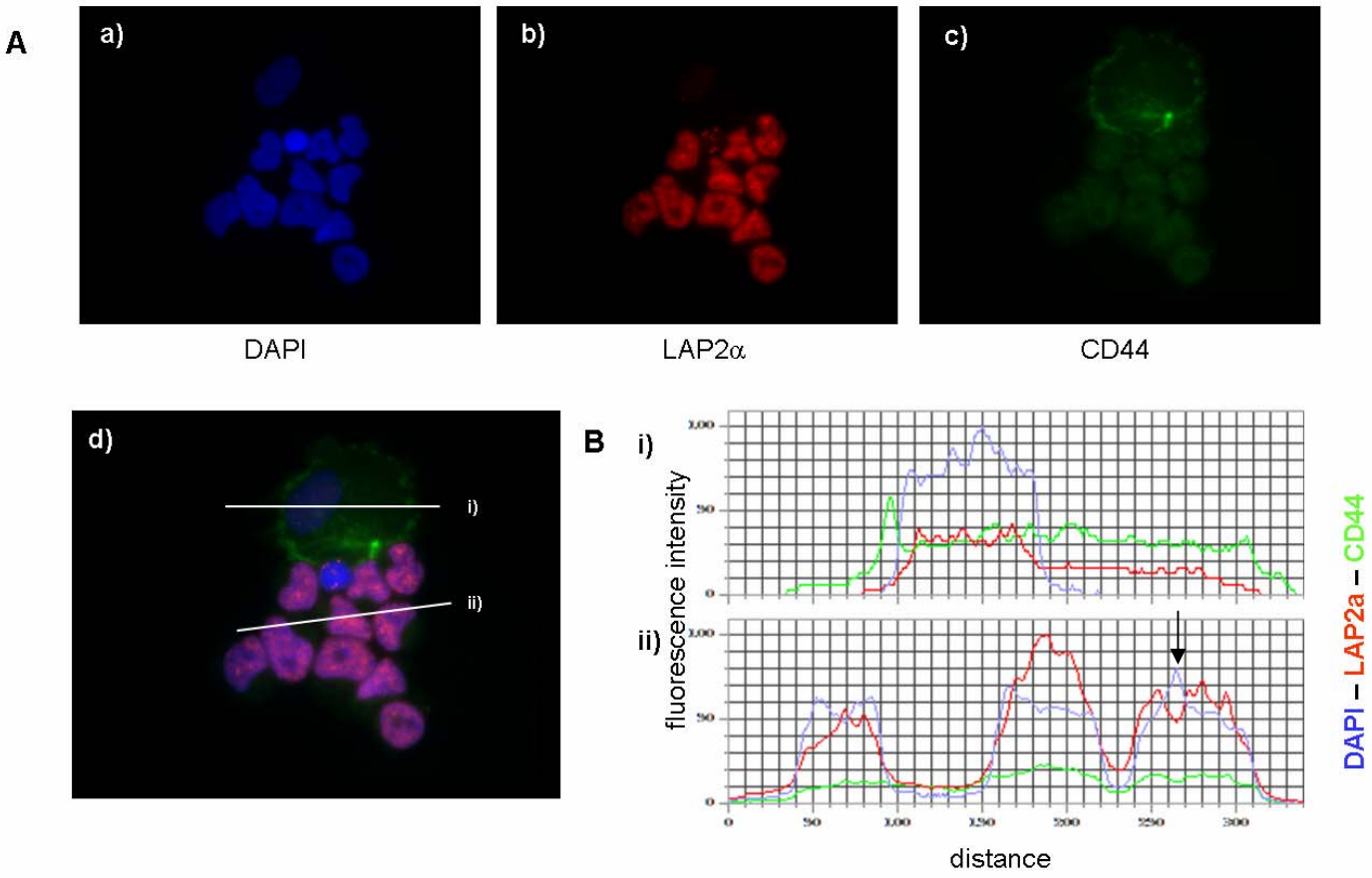

Figure 28 **Reduced LAP2α in spontaneous senescent cells. A** Untreated STA-NB-10 cells were stained for **a)** DAPI (blue), **b)** LAP2α (red) and **c)** CD44 (green). Merged channels are shown in **d)**. The line traces in white of the CD44 positive cell i) and of the CD44 negative cell ii) correspond to the profiles in B. In **B** the profile of the two cells shown in Ad) are depicted. x-axis indicates the distance of the white line, whereas the y-axis corresponds to the fluorescence intensity. The arrow in Bi) indicates the site of high DAPI staining.

In a further experiment the correlation between lamin expression and *MYCN* status of neuroblastoma cells was assessed. Therefore, untreated cells were stained for lamin A/C or lamin B. Following fixation, indirect FISH was done with a BAC clone hybridizing to the *MYCN* gene. In Figure 29 examples of lamin B stained cells (Figure 29A) and lamin A/C stained cells (Figure 29B) are given. Cells with only a low *MYCN* copy number show similar lamin B fluorescence intensities as compared to amplified nuclei. Moreover, the majority of *MYCN* containing micronuclei (indicated with arrow) showed lamin B staining. In Figure 29B images of lamin A/C stained cells are depicted. The intensity of lamin A/C staining is considerably high, which is the reason for the faint nuclear envelope staining shown in the FITC channel (bleed through). These cells show no excess number of *MYCN* copies and lamin A/C staining. Moreover, cells showing high amplification of the oncogene do no express lamin A/C.

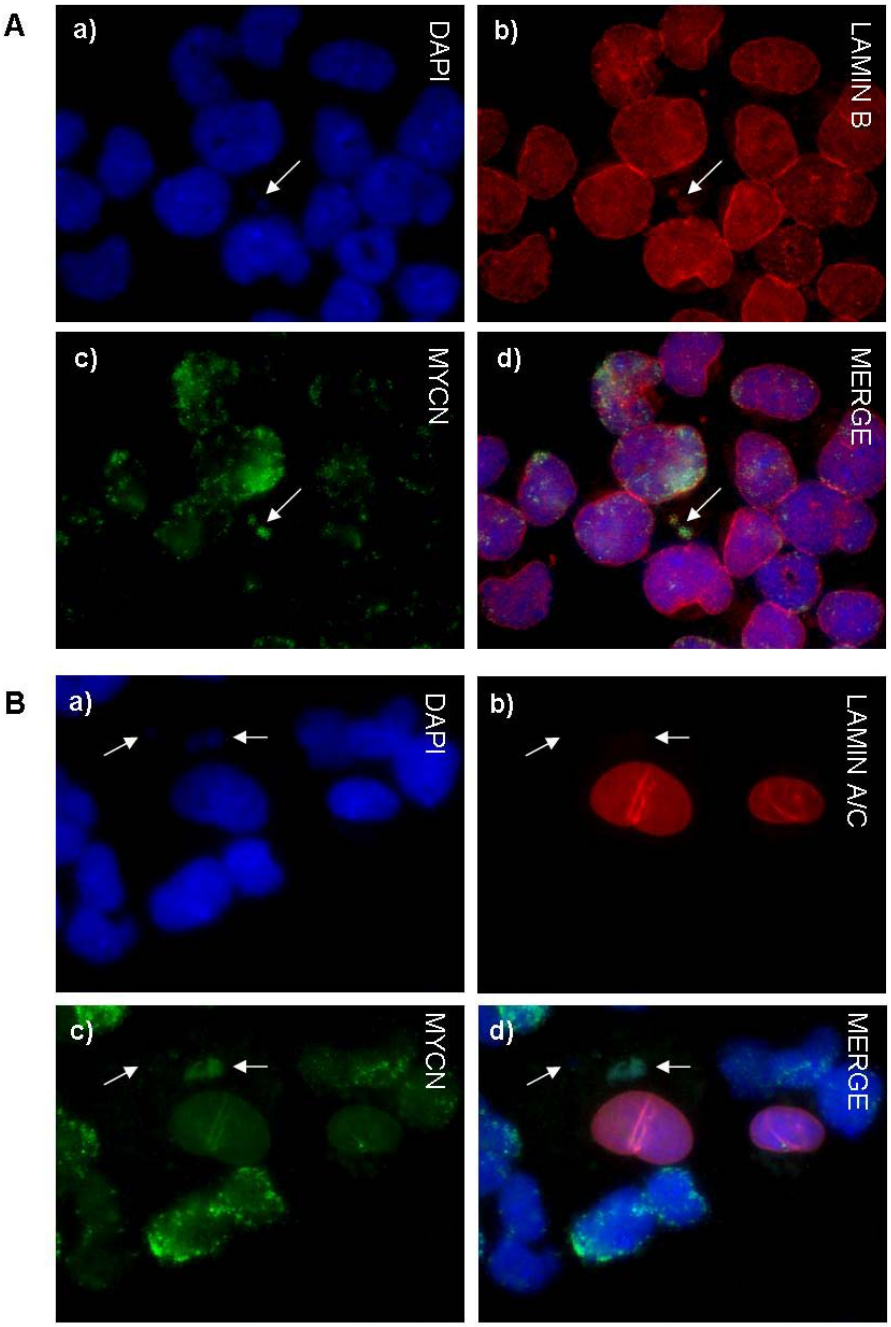

Figure 29 **Interphase *MYCN* FISH on lamin stained untreated STA-NB-10 cells.** Images of cytospin preparations were stained for **a)** DAPI (blue) and **Ab)** lamin B (red) or **Bb)** lamin A/C. An indirect FISH was performed with a *MYCN* probe (green) **c)** to show the amplified *MYCN* copies. In **d)** the merged channels are shown. Micronuclei are indicated by the white arrows.

In order to evaluate the effect of HU on the lamin composition in the nuclear lamina, a time course experiment was carried out treating STA-NB-10 cells with 150µM HU for 10 weeks. In Figure 30 the change in lamin A/C and lamin B incorporation into the nuclear lamina and change in nuclear morphology is depicted in untreated cells (Figure 30A), 5 days treated cells (Figure 30B) and 70 days treated cells (Figure 30C). Only a small proportion of cells showed lamin A/C positive staining, whereas all cells incorporated lamin B into the nuclear lamina. After 5 days of HU treatment, a higher amount of destroyed cells were found on the slides. Moreover, the nuclear area of intact cells enlarged. The small fraction of cells which were positive for lamin A/C showed a

reduced staining intensity in lamin B. After 70 days of treatment with HU a large part of the population showed increased cellular and nuclear areas. An increased part of the population showed lamin B replaced by lamin A/C at the nuclear envelope. Moreover lamin A/C positive cells showed lobulations and invaginations of the nuclear lamina.

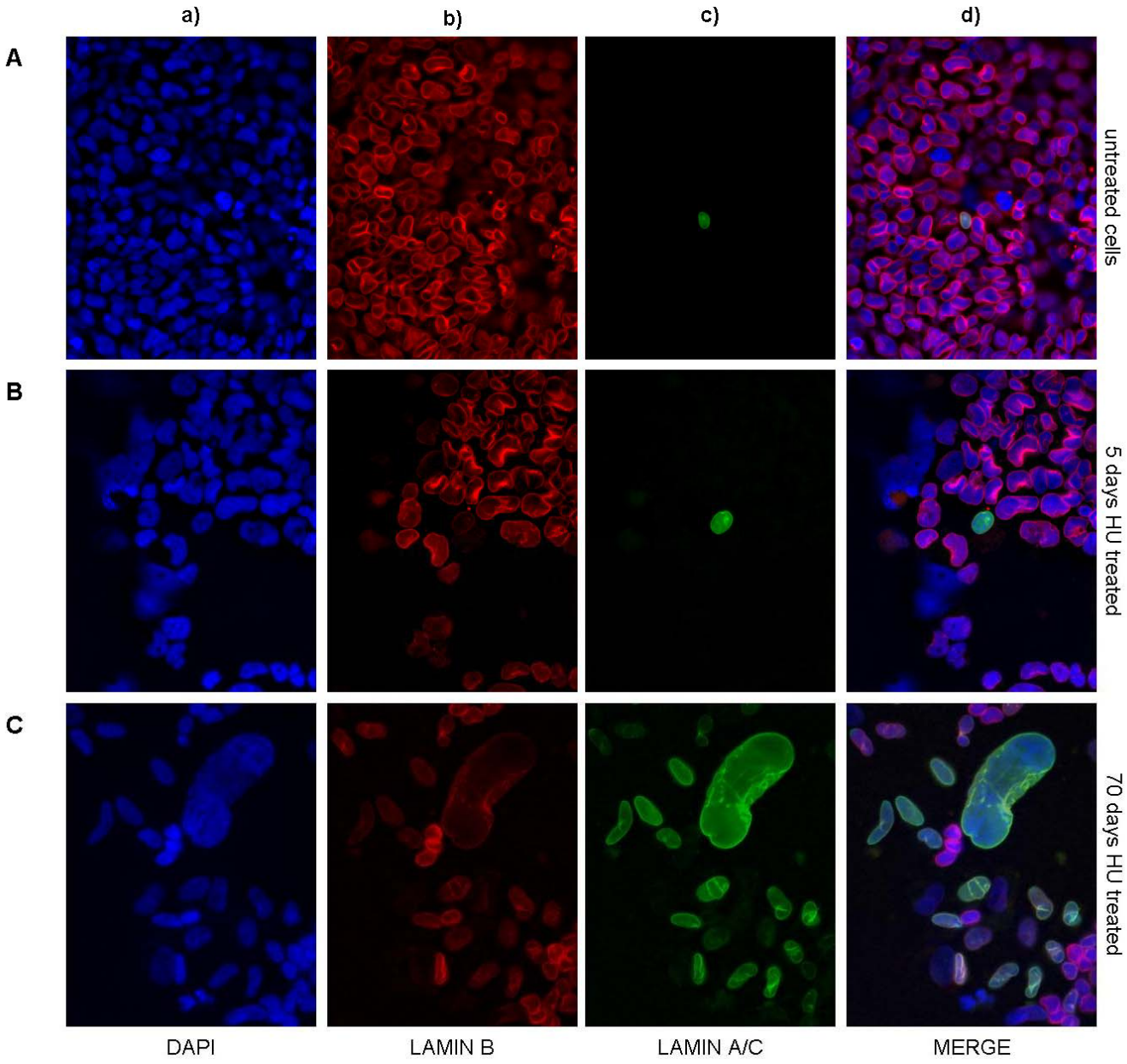

Figure 30 **Increasing lamin A/C positive population and morphology change along with HU treatment.** Images of untreated STA-NB-10 cells **A** were compared to cells induced with HU for 5 days **B** or 70 days **C**. Cytopreparations were stained for lamin A/C in green **a)** and for lamin B in red **b)**, DNA was stained with DAPI **c)**. The merged channel is shown in **d)**. Images were taken with a Zeiss Axioplan microscope with a 40x lens.

To quantitate the amount of lamin A/C positive cells at least 300 cells were counted per time point. The result is shown in Figure 31. A drastic increase in lamin A/C positive cells in the late time points of HU induction can be observed. Only 1.1% of the populations of time points 0 (untreated

cells) to 15 days of HU treatment were positive for lamin A/C. However, 67% of the cell population incorporated lamin A/C into the nuclear lamina after 8 weeks treatment (56 days). Surprisingly, of the population induced for 10 weeks 58% of the cells were lamin A/C positive whereas in another parallel population treated one day longer with HU 28% of the population was stained positive for lamin A/C.

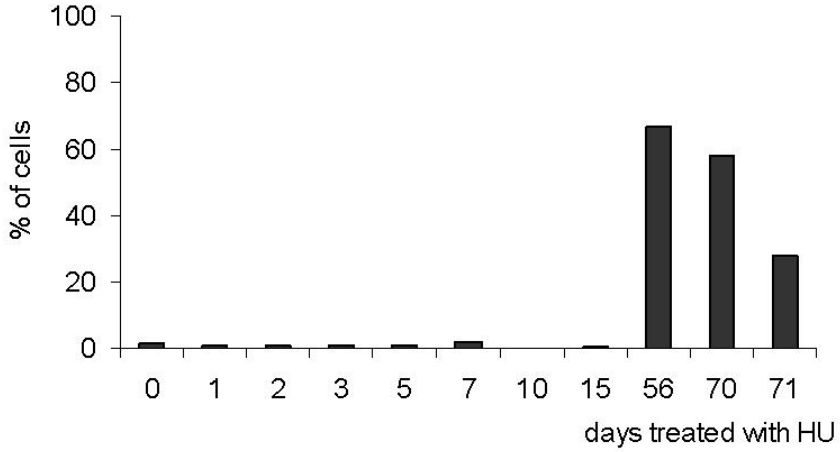

Figure 31 **Increase in lamin A/C positive cells with HU induction.** In the graph the percentage of lamin A/C positive cells are depicted per time point of HU induction. A minimum of 300 cells were analysed for positive lamin A/C staining per time point by counting with a Zeiss Axioplan microscope with a 40x lens.

To further investigate the composition of the nuclear lamina after 10 weeks treatment with HU, line trace profiles of lamin A/C positive cells were assessed. In Figure 32 a line trace profile through a lobulated nucleus is shown (white line). This cell pinches a micronucleus from the main nucleus off. Moreover, DAPI staining (a) shows differences in DNA density. Lamin B fluorescence intensity (b) is low, whereas lamin A/C intensity is high (c). The merged channels are depicted in (d). In Figure 32B the fluorescence profile along the white line is shown. Lamin B incorporation at the micronucleus is lower than 10% whereas the maximal intensity in the nucleus is 50%. Lamin A/C intensity correlates with DAPI intensity showing high percentage of intensity at the nuclear periphery and low intensity at the centre of the nuclei. Moreover, the lobulations are highly lamin A/C positive reaching 100% intensity.

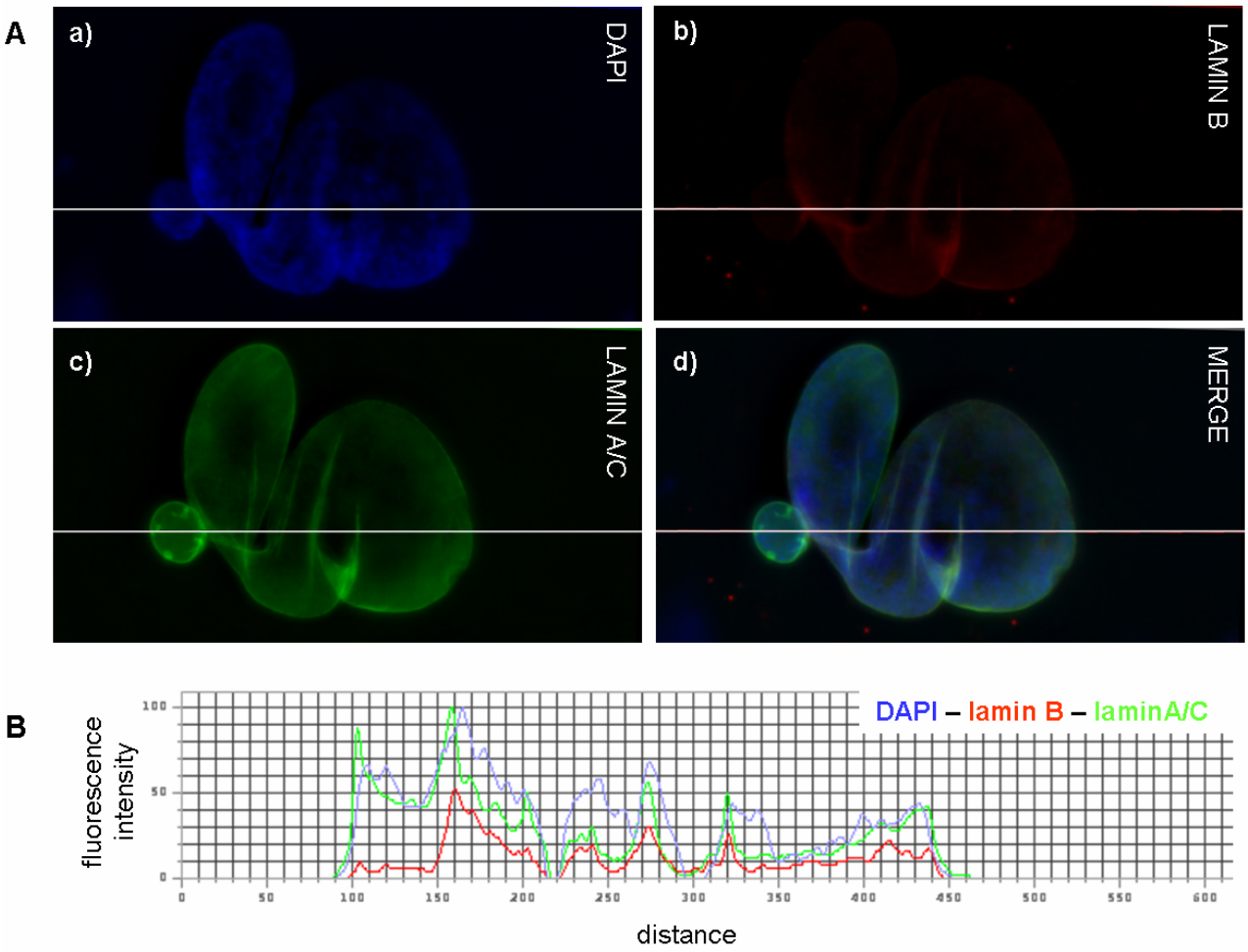

Figure 32 **Profile of lobulated 10 weeks HU induced STA-NB-10 cell**. **A** Cytospin preparations were stained for **a)** DNA with DAPI (blue), **b)** lamin B (red) and **c)** lamin A/C (green). Merged channels are shown in **d)**. The white line trace in A indicates the profile depicted in B. In **B** the profile of the lobulated cell is shown. The x-axis indicates the distance of the white line, whereas the y-axis corresponds to the fluorescence intensity of the different channels.

4.5 Analysis of the Senescence Pathway

From the time course experiment performed with HU induced STA-NB-10 cell populations, explained in detail in chapter 2.1.3, protein levels were analysed. In Figure 33 total protein lysates were prepared and probed for MYCN levels. Moreover, CDKIs (p21, p16) involved in the senescence pathway and their upstream and downstream interacting partners (p53, pRb) described in detail in chapter 1.2.3 were blotted.

MYCN, as product of the corresponding amplified gene in STA-NB-10 neuroblastoma cells decreases time dependent. After 56 days (8w) protein levels are negligible. Levels of tumour suppressor protein p53, which is a key regulator of genome integrity increase after 5 days (5d). The amount of p53 in cells after 56 days is again found decreased to a level comparable to untreated cells (0d). Additionally, with induction of p53, the levels of p21 - the downstream target of p53 - is

changed. p21 persists at high level after 56 days compared to untreated cells. p16 levels decrease until day 10 and afterwards increase again. p16 levels after 8 weeks are still lower than in untreated cells. pRb levels stay unchanged in the first three time points, whereas they decline slightly at day 10 and stay reduced. The blot for pRb showed at maximum four bands, where the uppermost is only present after 5 days. After 8 weeks only the lowest band shows strong signals. As loading control a ponceau staining was done and integrated density was measured by Image J, which is depicted in the lowest row. The loading of the different protein samples changes slightly. Highest loading differences are observed in protein samples of day 5 (1.2 fold the protein level of untreated cells) and day 10 (0.8 fold).

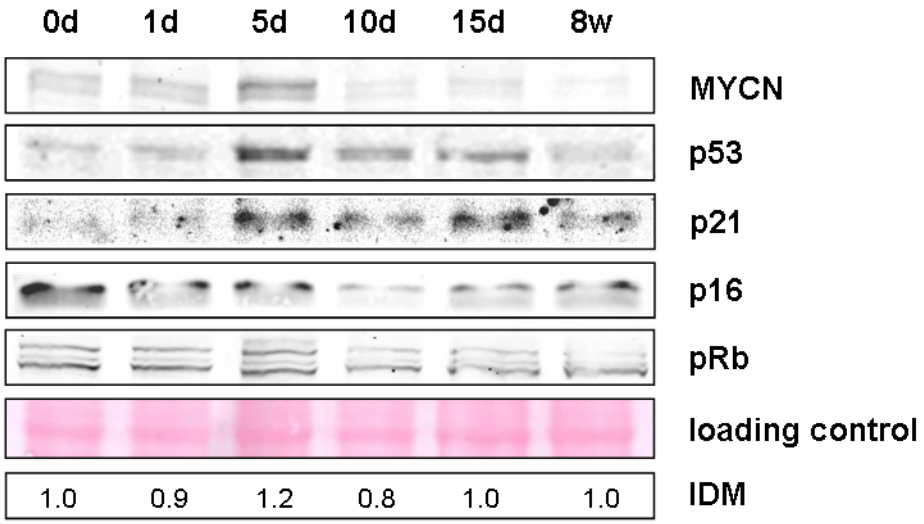

Figure 33 **Senescent pathway analysis by Western blot.** STA-NB-10 cells were HU induced and proteins were collected after 0 (0d), 1 (1d), 5 (5d), 10 (10d), 15 (15d) and after 56 days (8w). Totalprotein lysates were blotted and probed for MYCN, p53, cyclin dependent kinase inhibitor 1A (p21), cyclin dependent kinase inhibitor 2A (p16) and retinoblastoma protein (pRb). Ponceau staining was taken as loading control and integrated density measurements (IDM) is depicted as relative values to the STA-NB-10 untreated control lane (0d loading control).

5 Discussion

5.1 Markers of Senescence: Cell Morphology and SA-β-Gal Activity

Neuroblastoma cells are documented to show different types of cells: N-cells show a scant cytoplasm and high *MYCN* copy number. F-cells, occurring spontaneously show a flat morphology and SA-β-Gal activity (Ambros and Ambros 2000; Narath, Ambros et al. 2007). Time dependent, the amount of SA-β-Gal expressing neuroblastoma cells increased. These cells showed typical morphology of senescent cells with large, flat and granular cytoplasms. The population after 8 weeks of continuous HU treatment consisted primarily of senescent cells. The proportion of cells in G1-phase increased, while the proportion of cells in G2/M-and S-phase decreased. Dimri et al. showed that senescent fibroblasts and keratinocytes were positive for SA-β-Gal. Quiescent, presenescent or differentiated cells were negative for this enzyme (Dimri, Lee et al. 1995). In fibroblasts (REF52 and HFF) HU could induce proliferation arrest (Marusyk, Wheeler et al. 2007) and senescence (Yeo, Hwang et al. 2000). Human erythroleukemia K562 cells and rat heptoma cells got senescent and showed G1 arrest but neither differentiation nor programmed cell death was induced (Park, Jeong et al. 2000; Hong, Hong et al. 2004). In a previous study SA-β-Gal positive HU treated neuroblastoma cells showed decreased telomerase activity and shortened telomeres (Narath, Ambros et al. 2007). This lead to the assumption that long term low dose HU treatment of MNA neuroblastoma cells induces senescence which is marked by a flat morphology and SA-β-Gal activity.

With HU treatment not only senescent cells but also cells with neuronal features of differentiation appeared. HU is known to induce differentiation in erythroid precursor cells (Rencricca, Morse et al. 1975; Nagai, Tarumoto et al. 2003) and in erythroleukemias (Park, Choi et al. 2001), but in neuroblastoma cells usually retinoic acid is used for induction of differentiation. Interestingly, *MYCN* was shown to block terminal differentiation in retinoic acid induced MNA neuroblastoma cells (Thiele, Reynolds et al. 1985). Thus the reduced *MYCN* copy number, as well as its reduced expression and changes in the cell cycle machinery indicated by changes in CDKI levels (Figure 33) and cell cycle profile might be the cause for differentiation of a part of the population after HU treatment.

5.2 Proliferation, Growth and Cell Cycle Assay, *MYCN* Copy Number

5.2.1 HU Induced S-phase Arrest followed G1-arrest and Decline in Cell Population

Cell cycle analysis of untreated MNA neuroblastoma cells revealed a mean S-phase population of 27% while G1-phase accounted for 68% and G2/M population accounted for 5% (STA-NB-9 and STA-NB-10). This high amount of cells in S-phase of nearly 30% marks the highly proliferative character of the primary tumours from which the cell lines were generated. With HU treatment, up to 50% of the induced STA-NB-10 cells were found in S-phase of the cell cycle. There was a difference in the onset of the increase in S-phase in between the short term experiment lasting 10 days and the long term experiment lasting more than 8 weeks. S-phase increase peaked in the long term HU treatment after 5 days, with 42%, while in short term treatment increased S-phase was seen faster, after 1 day. Probably the experimental system of the two experiments, T25 flasks in the long-term treatment, 6-well plates in short term treatment, lead to this difference. Still, not the exact time point of S-phase increase, but information about the order of changes after induction was of our interest. Simultaneously to S-phase increase, the G1 population decreases and only in STA-NB-9 the G2/M population declines. This could account for either increased proliferation of cells or for arrest of cells in S-phase. The experiment measuring proliferation by BrdU incorporation over 24 hours elucidates this. As untreated and induced cells show the same amount of cells proliferating, the increase in the population in S-phase of the cell cycle profile must account for S-phase arrest. This is underlined by the fact that HU is known to deplete for dNTPs by blocking RRM, thus elongating the time needed for DNA replication (Schrell, Rittig et al. 1997; Szekeres, Fritzer-Szekeres et al. 1997). Together, this suggests that S-phase blockage occurs shortly after HU treatment.

Interestingly, after the population peaks in S-phase, a marked reduction of this population was observed, which is accompanied by increase of the G1-population. Moreover, a part of the cells treated with HU died continuously as indicated by the growth curve. This decrease in cell number could account for apoptosis of a part of the population. Also meningiomas (Schrell, Rittig et al. 1997) and melanomas (Krämer, Knauer et al. 2008) were found to undergo apoptosis after HU treatment, although drug doses were an order of magnitude higher compared to our study. Still, also low dose HU treatment leads to an increase in apoptosis as shown in COLO320 cells (Petit, Davidson et al. 1999). In studies with neuroblastoma cells members of the TNFR family (p75 and

CD95) and Bcl-2 were found to induce apoptosis (Dole, Nunez et al. 1994; Bunone, Mariotti et al. 1997; Fulda, Sieverts et al. 1997). Whether these genes are involved in HU mediated apoptosis or whether another cell death causing program (nekrosis, anoikis) is induced by HU in neuroblastoma cells has still to be elucidated.

Different effects of HU treatment may be dependent on the cell cycle phase of the individual cell of the asynchronous population. It was shown that HU depletes for dNTPs by blocking ribonucleotide reductase. dNTPs are necessary for replicating DNA and thus passing S-phase. Therefore S-phase arrest is suggested to occur by treatment with HU (Schrell, Rittig et al. 1997; Szekeres, Fritzer-Szekeres et al. 1997). This was approved here after 1-5 days low dose HU treatment. Moreover, HU is thought to induce replication fork stallings that lead to increased DNA damage (Ward and Chen 2001; Marusyk, Wheeler et al. 2007). The guardian of the genome, p53 is a key protein involved in the DDR. Here we could show an induction of p53 and its downstream target p21 after 5 days of treatment which would indicate a DDR induced by HU in MNA neuroblastoma cells. When an asynchronous population is thus treated with HU, primarily the cells in S-phase are impaired, which could account for a heterogeneity of the whole population.

5.2.2 HU Induced Loss of *MYCN* Copies in MNA Neuroblastoma Cells

Neuroblastoma cells which have an amplification of the transcription factor *MYCN* show aggressive growth characteristics and patients with this kind of tumour have a poor survival expectation (Nakagawara, Arima et al. 1992; Brodeur 2003). Low dose HU treatment accelerates the expulsion of amplified genes in the form of dmin from neoplastic cells in vitro (Snapka and Varshavsky 1983; Benner, Wahl et al. 1991; Von Hoff, Waddelow et al. 1991; Christen, Shalinsky et al. 1992; Von Hoff, McGill et al. 1992; Canute, Longo et al. 1996; Narath, Ambros et al. 2007) and in vivo (Raymond, Faivre et al. 2001). These dmin chromosomes were shown to be expulsed into micronuclei in cell lines (Von Hoff, McGill et al. 1992; Shimizu, Kanda et al. 1996; Narath, Ambros et al. 2007) and in primary neuroblastoma (Freeman-Edward, O'Neill et al. 2000; Valent, Benard et al. 2001). Here we show that the amplified *MYCN* gene is present in neuroblastoma cells STA-NB-9 and STA-NB-10 in the form of dmin. Additionally, we could show a time related loss of amplified *MYCN* copies during low dose HU treatment in MNA cell lines. The number of amplified cells is lower after 1 day, 10 days and 70 days of treatment compared to the untreated cells. Still, fewer non-amplified cells were found in the 10 days induced population than in the 70 days population. This increase in *MYCN* copies could account for different confluences of the starting

populations of each time point (flask) All flasks contained subconfluent cell populations but to different degrees which may be associated with differences in HU effectiveness. Moreover, with treatment the proportion of different cell types (N- and F-cells) varied. In the 70 days induced population, the flask contained more cells with differentiating phenotype than in the flask containing the 56-day induced population of the cell lines analysed.

The mechanisms by which dmin are expulsed are not yet known. However, dmin were shown to localize to the periphery of the nucleus (Freeman-Edward, O'Neill et al. 2000) and associate with lamins during S-phase (Tanaka and Shimizu 2000). Interestingly, we found amplified *MYCN* copies to localize preferentially to peripheral sites of the nucleus in the asynchronous cell populations.

Lamin B was found preferentially at sites of the nuclear lamina but also intranuclear association of signals occurred. The localisation of lamin B to dmin in certain cells might indicate that these cells are in S-phase of the cell cycle. For the first time we could show that lamin A/C was only expressed in neuroblastomas which show no *MYCN* amplification.

Treatment with HU accelerated expulsion of amplified extrachromosomal genes into micronuclei (Narath, Ambros et al. 2007). Additionally, HU induces premature senescence in several tumour cells (Park, Jeong et al. 2000; Hong, Hong et al. 2004; Kwak, Kim et al. 2004). Interestingly, also cells from patients with premature aging syndrome (Werner disease, Cockayne syndrome, Ataxia telangiectasia and Down syndrome) show an elevated formation of micronuclei (Weirich-Schwaiger, Weirich et al. 1994). In neuroblastoma cells treated with HU we found premature senescence to occur with the formation of micronuclei packed with *MYCN* (data not shown). Ultrastructural studies showed that micronuclei are surrounded by a double membrane with nuclear pores like normal nuclei (Gernand, Rutten et al. 2005). Not all micronuclei were found to be surrounded by a nuclear lamina, but the ones which did, were associated with the same lamina proteins as the nuclei from which they originated. These indications are solely descriptive and cannot account for conclusions about the formation of micronuclei during HU treatment.

Interestingly, during S-phase dmin were suggested to be selectively expulsed by budding (Itoh and Shimizu 1998; Shimizu, Itoh et al. 1998; Tanaka and Shimizu 2000). Thus, a correlation between the found S-phase propagation delay and selective expulsion of micronuclei might give a hint about the mechanism of HU as a micronuclei inducing substance.

5.3 Investigation of ROS Involving Mitochondrial Function in Neuroblastoma Cells Undergoing a Senescent Phenotype after HU Treatment

Mechanisms involving ROS were suggested to promote a senescence phenotype (chapter 1.2.2.4). Already in the 1950 Harman postulated that free radicals which were encountered throughout life damage cells by oxidation of cellular components. In turn cellular functions are impaired and the damaged cell starts senescing (Harman 1956). Reactive species, like ROS and RNS can have endogenous origin prevalently generated by leaking mitochondria or they are introduced into the cell by various environmental influences (IR, UV, cytokines, growth factors, chemotherapeutic drugs, and environmental toxins). Next to protein aggregation and lipid peroxidation which inactivates the function of these cellular building blocks, DNA as carrier of genetic information is damaged.

We hypothesized that HU induced cells show high amounts of cellular ROS which leads to a positive feed-back-loop involved in the onset of senescence. Therefore, the levels of ROS of neoplastic MNA neuroblastomas derived from aggressive primary tumours were assessed. Moreover, the timely correlation between ROS and senescence markers were monitored.

Recently new methods of measuring ROS were established. MitoSOX Red, a mitochondrial superoxide indicator, is targeted to the mitochondria and selectively oxidized by superoxide. Its fluorescence intensity is determined by live cell imaging using a fluorescence microscope or by flow cytometric analysis. The amount of mean fluorescence intensity in the mitochondria is correlated to the cellular superoxide status. It was shown not to be oxidized by other ROS- or RNS-generating systems and scavenging proteins like superoxide dismutase prevents oxidation of the dye. (Nieminen, Byrne et al. 1997; Maurer, Metelitsa et al. 1999; Konorev, Zhang et al. 2000; Melov 2000; Hardman, Afshari et al. 2001; Mawatari and Murakami 2001; Takahashi, Shibata et al. 2001; Batandier, Fontaine et al. 2002; Diaz, Liu et al. 2003; Scotti, Iamele et al. 2003).

In HU-induced MNA-NB cells changes in mitochondrial superoxide levels were observed. In STA-NB-9 cells the mitochondrial superoxide levels increase with HU induction already after 24 hours induction 1.7 fold. Moreover, treatment for 24 hours of MNA-NB cells with hydrogen peroxide, a ROS itself, mimics the effects of increased oxidative stress. Superoxide levels augment 1.7 fold, which equals the increase of superoxide of cells treated with HU. Moreover, untreated low passage MRC5 fibroblasts showed comparable levels of superoxide as untreated MNA neuroblastoma cells.

STA-NB-10 cells were less prone for oxidative stress, as they show lower amounts of mitochondrial superoxide level after 24 hours (1.2 fold) than STA-NB-9 cells. Moreover, with induction superoxide levels augment gradually to a final 13-fold increase compared to the untreated population. In comparison to the 13-fold increase found in senescent STA-NB-10 cells, the final 2.7 fold increase measured by flow cytometry in senescent STA-NB-9 cells seems low. Still, in the microscope, STA-NB-9 cells seem to increase more than the FACS measured value. Moreover, cell debris and dead cells were stained highly in STA-NB-9 cells which could raise basal levels of untreated cells and thus reduce the difference between control and senescent cells. From a biological point of view, the difference between the senescent STA-NB-9 cells and the senescent STA-NB-10 cells might be the used cultivation medium. STA-NB-9 cells were grown in HU-free medium, while STA-NB-10 cells were treated still with HU.

Measurements of cellular peroxide and peroxynitrite levels can be achieved by Dihydrorhodamine 123 (DHR) staining. This dye is oxidized by H_2O_2 and organic peroxides in the presence of catalysts like catalase and peroxidase, by peroxynitrite, by pyocyanin and phenazine methosulfate. NO or superoxide alone, the substances that in combination form peroxinitrite cannot oxidize DHR. Moreover, DHR is a an efficient singlet oxygen generator upon illumination and in cellular systems it produces singlet oxygen in mitochondria where it accumulates and induces oxidation of NAD(P)H (Briviba, Roussyn et al. 1996; Crow 1997; Sies, Sharov et al. 1997). HU treated STA-NB-9 MNA-NB cells show significantly increased levels of peroxide and its derivatives. Moreover, the levels of oxidized fluorescent DHR in untreated MNA neuroblastoma cells is comparable to low passage MRC5 fibroblasts. Thus, we could verify that with HU induction and with HU-linked senescence, the levels of cellular peroxide and derivatives increase.

The above mentioned leads us to the suggestion that HU may also be an inducer of oxidative stress, like H_2O_2. A study reported that in non-MNA neuroblastoma cell line SH-SY5Y cellular death was enhanced when treated with H_2O_2 (Castino, Bellio et al. 2007). Also in this study we see a high proportion of cells dying after induction with H_2O_2. Treatment with HU for 10 days also decimates the cell number of STA-NB-10 cells to half the starting population. Similar, induction of ROS in several *MYCN* amplified neuroblastoma cell lines leads to apoptosis by induction of PKC-δ (Domenicotti, Marengo et al. 2003; Marengo, Raffaghello et al. 2005; Ferretti, Marengo et al. 2007; Marengo, Balbis et al. 2008; Marengo, De Ciucis et al. 2008). Thus we suggest that low dose HU treatment increases cellular ROS levels which might be the reason for increased decline in cell population over time. The remaining cells might have a different redox-potential or a blocked apoptotic pathway which then triggers senescence.

10-N-nonyl acridine orange (NAO) is a dye that is incorporated into mitochondrial membrane protein cardiolipin. Its uptake is independent of transmembrane mitochondrial potential and it is an indicator for mitochondrial membrane mass (Leprat, Ratinaud et al. 1990; Oubrahim, Stadtman et al. 2001; Passos, Saretzki et al. 2007). HU induced MNA neuroblastoma cells which are presenescent, show slightly increased mitochondrial cardiolipin incorporation. However, induced senescent cells show a 3.4-fold increase in mitochondrial mass. This suggests that the amount or the size of mitochondria increases. As an increase in size of mitochondria was also seen in images of HU induced senescent MNA neuroblastoma cells taken with the electron microscope (not shown) we suggest that with ongoing senescence and HU treatment, mitochondria increase in size.

JC-1 is a lipophilic fluorescent cation that is selectively targeted to mitochondria and changes its fluorescence reversibly at different membrane potentials. This is achieved as the dye aggregates upon high membrane potential and emits a bright red-orange fluorescence at 590 nm. At low membrane potential, JC-1 is present in monomeric form and emits green fluorescence. The measured ratio determines mitochondrial membrane potential $\Delta\psi_m$ and thus is an indirect measure of the functionality of the mitochondrial membrane (Di Lisa, Blank et al. 1995; Salvioli, Ardizzoni et al. 1997; Passos, Saretzki et al. 2007). In MNA neuroblastoma cells induced with HU membrane potential decreases to half of the starting value. $\Delta\psi_m$ is again increased slightly when induced senescent cells are released into HU free medium. This might indicate that HU is involved in lowering the membrane potential and thus inducing dysfunctional mitochondria. In our experiments we could see a gradual, quick increase in ROS levels after HU treatment. It is known that oxidative stress damages primarily mtDNA which is essential for proper mitochondrial function. Consequently, dNTPS are essential for maintenance and repair of mtDNA damage. Ribonucleotide reductase small subunits RRM2 and p53 inducible RRM2B need iron molecules in order to convert NTPs into dNTPS (Terman and Brunk 2006; Voss and Siems 2006). HU is an iron chelator and is known to inactivate these rate limiting enzymes (Le and Richardson 2002; Lin, Belcourt et al. 2007). Moreover, reduced mtDNA copy numbers were observed in patients with MDS (mtDNA depletion syndrome, OMIM 251880) who had deletions or mutations in the RRM2B gene. Depletion of dNTP for mtDNA synthesis and repair with low dose HU could pose a reason for decreased membrane potential and increased ROS production. This in turn reduces mitochondrial function which leads to a higher amount of released intermediate radicals from the oxidative phosphorylation process (Passos and von Zglinicki 2005). Thus, HU might not only induce increased ROS levels but also be directly involved in mtDNA depletion and further mitochondrial

impairment.

Moreover, dysfunctional mitochondria lead to retrograde signaling, which raises the mitochondrial biogenesis leading to the generation of new functional mitochondria, which is also indicative for the increased mitochondrial mass we found in induced NB cells.

Increased ROS is suggested to lead to oxidative damage of cellular components bringing about a DNA damage response. This is suggested to lead to age dependent increase in genetic instability (Halliwell 2007) but is also involved in premature senescence (Passos, Saretzki et al. 2007).

In our model of tumor cell senescence, ROS increase may account for DNA damage. This suggestion is underlined, as p53 levels increased in early HU treated cells, which may account for a DNA damage response. This response may induce proliferation arrest and further ROS signaling may be the trigger for senescence.

Several tumors were found to use the potential of ROS to induce proliferation (Halliwell 2007). Contrary, here the amount of ROS in neuroblastoma increases steadily with HU treatment and with increase in SA-β-Gal positive cells. Moreover, an increase in G1 population of cells is observed. These are all indicatives that in neuroblastoma cells ROS signaling does not account for increased proliferation and increased tumorigenic potential, but for opposite mechanisms: senescence is induced with reduced proliferation, changes in morphology, SA-β-gal positivity and as shown before, with shortened telomeres (Narath, Ambros et al. 2007).

Moreover, NO - produced from HU - is a ROS itself and increases cellular oxidative stress (Wink and Mitchell 1998; King 2003; Pacher, Beckman et al. 2007). Moreover, NO was shown to act as important negative regulator of MYCN expression in neuroblastoma cells and it is suggested to negatively regulate proliferation by decreasing pRb phosphorylation (Ciani, Severi et al. 2004). In our experimental system the amount of MYCN expression decreases with HU treatment. Still, as only low doses of this substance are used, the amount of NO is assumed to be low. However, parallels can be seen in MYCN decrease and proliferation halt in HU treated NB cells. Thus perhaps different mechanism or the combined effects of superoxide, peroxide and NO induce MYCN downregulation and proliferation arrest.

Here we could for the first time show that the mechanism underlying HU induced senescence might involve increased superoxide and peroxide levels. Moreover, mitochondrial membrane potential decreased and mitochondrial mass increased which indicates dysfunction of this organelle. In MRC5 fibroblasts a feedback loop is started by uncoupling of mitochondria, which further increases cellular ROS production (Passos, von Zglinicki et al. 2006).

The connection between mitochondrial dysfunction and increased ROS in the onset of senescence

might involve telomere erosion (Passos and von Zglinicki 2005; Passos, Saretzki et al. 2007; Passos, Saretzki et al. 2007). In endothelial cells, mild chronic oxidative stress leads to loss of telomere integrity which is a major trigger for the onset of premature senescence (Kurz, Decary et al. 2004). In our experimental system shortened telomeres were shown after 6 weeks HU treatment (Narath, Ambros et al. 2007), which might indicate HU induced chronic oxidative stress to trigger premature senescence in MNA neuroblastoma cells.

5.4 Lamin and Associated Proteins

In normal individuals and also in mice, lamin A/C expression and incorporation into the lamina determines the state of differentiation. Lamin B is expressed in cells with a highly plastic potential, whereas lamin A/C is a marker of differentiation (Rober, Sauter et al. 1990). For the first time we observed an increase of lamin A/C expression in the induced senescent neuroblastoma cells which correlated negatively with lamin B expression. Coherent indications resulted from competitive microarray experiments done with STA-NB-9 and STA-NB-10, hybridizing cDNA from N-cells and HU induced senescent F-cells. There, *LMNA* was found to be expressed highly in F-cells while *LMNB1* was found to be expressed in N-cells only. Several types of tumours including lymphomas, skin cancers and adenocarcinomas were found deficient for lamin A/C (Prokocimer, Margalit et al. 2006). This suggests lamin A/C to have tumour suppressive functions (Nitta, Smith et al. 2007) as it keeps up a differential status with low plasticity. Here we could show for the first time that the N-cells of the neuroblastoma cell lines STA-NB-9 and STA-NB-10 are deficient in lamin A/C. Long term low dose treatment with HU indicates differentiation and loss of plasticity of neuroblastic tumour cells STA-NB-9 and STA-NB-10 which might indicate tumour suppressive functions as shown by Nitta et al (Nitta, Smith et al. 2007). Lamin A/C was shown to increase markedly after 56 days of HU induction. In cells treated for 70 or 71 days with HU, however, lamin A/C levels were lower again. This differences between the cell population treated for 56, 70 or 71 days might be caused because of high variations of different proportions of cell types present in the flasks of each time point. As different amounts of differentiated cells were present in the flask, this could make the high variation.

Lamin B is expressed ubiquitously in mammalian cells. The expression of this cellular component is associated with cell growth and survival. In our senescence induction system a decline in lamin B expression was observed together with an increase in G1 arrested cells and induction of SA-β-Gal activity. This underlines the changes in differentiation and tumour cell revertance of neuroblastoma cells after HU treatment (Narath, Ambros et al. 2007).

Several lines of evidence suggest an involvement of lamin A in physiological aging processes. The connection of lamin A expression and aging arose when premature aging in the HGPS was correlated with a mutation in the *LMNA* gene introducing a cryptic splicing site. This leads to the accumulation of a truncated, farnesylated prelamin A - progerin- in cells from HGPS patients. The same phenomena could be observed to a smaller extent in cells from old organisms (Haithcock, Dayani et al. 2005; Lans and Hoeijmakers 2006; Scaffidi and Misteli 2006; Cao, Capell et al. 2007; Dechat, Shimi et al. 2007).

In spontaneously occurring F-cells, which have comparable pheno- and genotype to induced senescencent neuroblastoma cells (Narath, Ambros et al. 2007), we could prove an increase in nuclear prelamin A. This together with the observed morphological changes, SA-β-Gal expression and strongly reduced proliferation activity suggests that cells from highly aggressive neuroblastoma are able to senesce prematurely.

Misshaped nuclei with lobes and invaginations were found in cells from *LMNA*$^{-/-}$ mice (Lammerding and Lee 2005), in *LMNA* mutated fibroblasts from lipodystrophic patients (Vigouroux, Auclair et al. 2001) and from HGPS patients (Oberdoerffer and Sinclair 2007), in lamin deficient cells from *Caenorhabditis elegans* (Liu, Rolef Ben-Shahar et al. 2000) and in cells from aged *C. elegans* (Haithcock, Dayani et al. 2005). A change in the ultrastructure of the cells shown by misshaping of the nuclei was also found in the spontaneously occurring F-cells and in the HU induced premature senescent neuroblastoma cells. Lobulated nuclei were found to not only restricted to lamin A/C expressing cells, but also were found in lamin B expressing cells. Thus, lobulation may not be indicative for incorporation of mature lamin but for accumulation of prelamin. These data suggest accumulation of prelamin A to account at least partially for the senescent phenotype in neuroblastoma cells.

Already low concentrations of prelamin A accumulation lead to a change in heterochromatin, with facultative inactive regions becoming transcribed (Shumaker, Dechat et al. 2006). Usually, heterochromatic regions are structurally fixed and linked to the nuclear lamina. Cells from HGPS patients, but also late passage fibroblasts show less heterochromatic markers which suggests lamin A to be associated with the epigenetic control of heterochromatin. Moreover, HGPS as well as late passage cells show a loss of heterochromatin (Shumaker, Kuczmarski et al. 2003; Gruenbaum, Margalit et al. 2005; Scaffidi and Misteli 2006). On the other hand, senescence-associated heterochromatic foci (SAHF), which consist of accumulated pRB proteins at sites of E2F promoters, are thought to lead to the irreversible proliferation arrest associated with senescence (Oberdoerffer and Sinclair 2007). This might suggest the involvement of prelamin A and lamin A/C

accumulation to indicate heterochromatic changes in HU treated neuroblastoma cells. A change in heterochromatic regions leads to changes in gene expression patterns as active chromatin gets silenced and vice versa. The high number of up- and down-regulated genes found in senescent neuroblastoma cells may indicate epigenetic regulation due to chromatin modifications to account for senescence: From 12982 genes analysed, 604 were upregulated and 786 were downregulated after 8 weeks of HU treatment. Still, further analysis investigating heterochromatic changes in induced senescent neuroblastoma cells and the involvement of lamins in this process have to be realised to give a clear answer.

Another interesting feature of HGPS cells is that they cannot be immortalized, even when telomere length was stabilized and telomerase was activated (Wallis, Sheerin et al. 2004). Neuroblastoma cell lines STA-NB-9 and STA-NB-10 showed abrogated telomerase activity and telomeres shorten to 50% of the previous length after 8 weeks of treatment with HU (Narath, Ambros et al. 2007). This phenomenon further points towards the possible importance of the nuclear lamina in tumour cell senescence of neuroblastoma cells.

In concordance with high proliferative and aggressive behaviour of MNA neuroblastoma (Brodeur, Seeger et al. 1985; Brodeur 2003), also other lamin A deficient cells were shown to proliferate highly (Van Berlo, Voncken et al. 2005). Neuroblastoma cells show increased expression and protein levels of p16. This, however was not related to *MYCN* amplification, pRb phosphorylation status or G1/S phase arrest (Diccianni, Omura-Minamisawa et al. 1999). In this study we investigated proteins involved in the senescence pathway by western blotting and lamin A/C expression by IF in the same cell population treated with HU for 8 weeks. We found p16 to be present in lamin A/C deficient, untreated neuroblastoma cells. With ongoing treatment, p16 levels decreased until day 10 and finally increased again slightly. At this last time point more than 2/3 of the cell population show lamin A/C incorporated into the nuclear lamina. These cells have an increase in their G1-population indicating G1 arrest. Also p16 is present. Contrary to our results, cells depleted for lamin A/C failed to G1 arrest after induction of p16 (Nitta, Jameson et al. 2006). The number of lamin A/C expressing cells, however, was markedly increased only after long-term treatment. This suggests that p16 and lamin A/C expression are regulated independently and do not together implicate in G1 arrest.

The protein connecting abrogation of growth and proliferation with loss of lamin A is suggested to be pRb. Hypophosphorylated, active pRb is an important factor involved in the senescence pathway (Itahana, Campisi et al. 2004). It binds E2F transcription factors which promote S-phase specific gene transcription when released from the complex. Moreover, pRb recruits chromatin remodelling

complexes to E2F specific gene promoters keeping them silenced and thus leading to G1 arrest of the cell cycle (Narita, Nuñez et al. 2003). In STA-NB-10 neuroblastoma cells HU treatment does not influence the pRb protein level markedly. On the other hand, early after HU induction cells accumulate in S-phase which might account for release of E2F-factors from the pRb complex which initiates S-phase specific gene transcription. Lamin A/C deficient cells showed high proliferative indices and could not be arrested in cell cycle (Nitta, Jameson et al. 2006). Untreated cells show high proliferation which increases at the beginning of treatment and further decreases. And lastly, *LMNA*$^{-/-}$ myoblasts showed impairment of fully differentiation. Combining these data with our data, a role for pRb has still to be investigated, as this is also one of the proteins involved in senescence pathways. Assuming no activity of pRb in lamin A/C deficient neuroblastoma cells, this could be the reason for unregulated proliferation, and thus a tumor promoting mechanism.

Lap2α is a protein binding DNA via its LEM domain and it shows a diffuse nuclear staining. In cells from aggressive, *MYCN* amplified neuroblastoma it seems to associate to DNA as DAPI staining and Lap2α staining resemble each other. Lamin A forms a complex with LAP2α and pRb which is supposed to retain hypophosphorylated pRb inside the nucleoplasm (Markiewicz, Dechat et al. 2002). In untreated neuroblastoma cells, in fact, lamin A is missing while a large amount of Lap2α is present in the cells.

LAP2α deficient cells showed impaired cell cycle arrest and impaired differentiation(Dorner, Vlcek et al. 2006). This in turn was suggested to repress E2F transcriptional activation of S-phase genes and thus G1 arrest (Dorner, Vlcek et al. 2006). Moreover, the spontaneous senescent cells were found deficient for LAP2α. This coheres with the effect that LAP2α siRNA depletion in HDFs leads to arrest in G1-phase of the cell cycle (Pekovic, Harborth et al. 2007). Moreover, cells from old individuals as well as from lamin A overexpressed or HGPS patients show downregulated LAP2s (Scaffidi and Misteli 2006; Scaffidi and Misteli 2008).

Therefore mechanisms different to retention of pRb in the nucleus could play a role in our experimental system. These could be the stabilizing effect of lamin A/C on pRb or the dephosphorylation activation, but still have to be elucidated.

A study depleting HeLa cells for ZMPSTE24, a zinc metallopeptidase cleaving prelamin A to lamin A, resulted in misshaped nuclei and micronuclei formation (Gruber, Lampe et al. 2005). Interestingly, HU is a substance accelerating the formation of micronuclei which contain extrachromosomally amplified genes (Von Hoff, McGill et al. 1992). In our experimental system we could observe dysmorphology of the nuclei with increased micronuclei formation after HU treatment. The micronuclei contained the amplified *MYCN* copies. Moreover, prelamin A increased

markedly in spontaneous senescent cells. These spontaneous F-cells contain only few, down to one copy of *MYCN* per cell. We assume that prelamin A also accumulates in HU induced senescent cells but this has to be verified.

As HU inhibits the active centres of zinc metalloproteinases (Campestre, Agamennone et al. 2006), this might be one possibility how ZMPSTE24 is inactivated. This might lead to accumulation of prelamin, which as a second step, might imply induction of a senescent phenotype. Papers report that PI inhibitors used for HIV treatment also block ZMPSTE24. Interestingly, these PI inhibitors induced oxidative stress in fibroblasts. This could also be seen in HU treated neuroblastoma cells. Another hint of possible relation between a change in nuclear lamina composition, oxidative stress and premature senescence is that neuroblastoma cells (SH-SY5Y) under oxidative stress were found to express lamin A/C (Nakamura, Yamada et al. 2006).

Lamin A/C mutation moreover was lately not only mentioned in context with Hutchinson Gilford progeria, a disease of premature aging, but also with physiological aging. It was suggested that cells of healthy old individuals show misshaped nuclei with lamin A incorporations similar to HGPS cells. Moreover, in HGPS the depletion of mesenchymal stem cells should be brought about by incorporated lamin A into the membrane, which is thought to be a cellular marker for differentiation and thus halts pluripotency (Scaffidi and Misteli 2008). Here, we could show that prelamin A accumulated in F-cells which might be the trigger for transformation of N-cells to F-cells. By induction of F-cells with HU, prelamin A might also accumulate leading to the premature senescent phenotype seen.

5.5 Analysis of the Senescence Pathway

MNA neuroblastoma was correlated to high MYCN protein levels (Nakagawara, Arima et al. 1992). In our time course experiments high MYCN levels were shown at time point 0 but with ongoing treatment, the level of MYCN reduced to unverifiable amounts (Figure 33). This was also correlated with *MYCN* dmin reduction seen in the FISH experiments. Although the amount of *MYCN* FISH spots per nucleus was higher as compared to the 10 days treated cells, protein levels were lowest in senescent cells. Interestingly, MYCN inhibition by peptide nucleic acid leads to diminished MDM2, stabilized p53 and apoptosis (Slack, Chen et al. 2005). In our experimental system, we could also see an increase in p53 protein levels related to MYCN decrease (Figure 33). For the first time we show that HU induces MYCN downregulation and p53 stabilization in MNA neuroblastoma cells.

The heterogeneity in the phenotypes after HU treatment - cells of one population undergo cell death, differentiation/maturation and senescence - might be the result of genetic differences

between treated cells. In another experimental system it was shown that p53 was needed for a HU-induced senescence (Marusyk, Wheeler et al. 2007), but not for all cells (Hong, Hong et al. 2004). Here we could demonstrate that p53 is induced by HU treatment after 5 days in MNA neuroblastoma cells (Figure 33). p53 on the other hand, is not only involved in the senescence pathway, but also in apoptosis induction by involvement of ROS (Polyak, Xia et al. 1997). Thus differences in the level of CDKIs may discriminate between senescence, apoptosis or differentiation. In cultured fibroblasts it was shown that the diversity in between one senescent population is high as cells expressing mainly p16 were found next to cells expressing primarily p21 (Itahana, Zou et al. 2003). Here, p21 levels peak after 5 days of HU treatment (Figure 33). This could be the result of increased p21 stability brought about by HU (Kim, Yeo et al. 2005) and/or by direct induction through its upstream effector p53.

p16 levels, on the other hand decrease with treatment and showed a minimum at day 10 of treatment, while later on levels increased again slightly. p16 expression as in our untreated MNA cells was correlated with aggressive tumour behaviour. Moreover, most of these primary neuroblastoma investigated showed no functional p16-pRb pathway (Omura-Minamisawa, Diccianni et al. 2001). Thus, it is not surprising that pRb protein levels show only slight differences, despite its activity in terms of phosphorylation was not determined. Perhaps the combined function of p16 and p21 discriminates the different pathways but to clarify this point more experiments have to be carried out. A significant reduction in cell proliferation, a G1 specific cell cycle arrest and an extensive neuronal differentiation of neuroblastoma cells (SK-N-BE) were also shown in cells depleted for cyclin D and CDK4 (Molenaar, Ebus et al. 2008).

List of Abbreviations

$1O_2$	singlet oxygen
8OHdG	8-hydroxy-2'-deoxyguanosine
ABCC1	ATP-binding cassette, sub-family C (CFTR/MRP), member 1
ALK	anaplastic lymphoma receptor tyrosine kinase
ALT	alternative lengthening of telomeres
APC	anaphase-promoting-complex
AT	ataxia-telangiectasia
ATM	ataxia-telangiectasia mutated
ATP	adenosin triphosphate
ATR	ataxia telangiectasia and Rad3 related
ATRIP	ataxia telangiectasia and Rad3 related interacting protein
BAF	barrier to autointegration factor
Bcl-2	B-cell CLL/lymphoma 2
bHLH-LZ	basic helix-loop-helix/leucine zipper motif
BLM helicase	bloom helicase
BR	basic DNA binding region
BrdU	bromodeoxyuridine
BSA	Bovine Serum Albumin
CCD	charge coupled device
CD44	Phagocytic Glycoprotein-1
cdc25a	cell division cycle 25 homolog A
CDC6	cell division cycle 6 homolog
CDK	cyclin dependent kinase
CDKN1A	cyclin dependent kinase inhibitor 1A, p21 (WAF1, CIP)
CDKN2A	cyclin dependent kinase inhibitor 1A, p14 (ARF), p16 (INK4A), p15
CHK	checkpoint kinase
COLO320	colorectal cancer cell line

DAPI	4'-6-Diamidino-2-phenylindole
DDX1	DEAD (Asp-Glu-Ala-Asp) box polypeptide 1
DDR	DNA damage response
DHR	dihydrorhodamine 123
DKK1	dickkopf homolog 1 (Xenopus laevis)
DKK3	dickkopf homolog 3 (Xenopus laevis)
dmin	double minute chromosome
DNA	deoxyribonucleic acid
dNTPs	deoxyribonucleotide triphosphate
DP-1 and -2	dimerization proteins 1 and 2
DSB	double strand breaks
DTT	dithiothreitol
E2F	elongation factor-2
EDTA	ethylene-diamine-tetra-acetic acid
EGFR	epidermal growth factor receptor
ERCC1	excision repair cross-complementation group 1
F-cells	flat-cells
FITC	fluorescein isothiocyanate
GPx1	glutathione peroxidase 1
GTPase	Small guanosine triphosphatases
H2AX	Histone 2A family member X
H_2O_2	hydrogen peroxide
HEPES	(4-(2-hydroxyethyl)-1-piperazineethanesulfonic acid)
HFF	human foreskin fibroblasts
HGPS	Hutchinson-Gilford Progeria Syndrome
HIV	human immunodeficiency virus
HLH	helix-loop-helix motif
HMGA1	high mobility group AT-hook 1

HNB1	hereditary neuroblastoma 1
HNO	nitroxyl
$HOCl^-$	hypochlorus acid
HP1	heterochromatin protein 1
HR	homologous recombination
hsr	homogenously staining region
HU	hydroxyurea
IFN-γ	interferon-gamma
iNOS	inducible nitric oxide
IR	ionizing radiation
LAP2	lamin associated protein 2
LBR	lamin B receptor
LEM domain	LAP2, emerin, MAN1 domain
MAD	MAX dimerization protein 1
MAPK	mitogen-activated protein kinase
MAX	MYC associated factor X
MCM7	minichromosome maintenance complex component 7
MDC1	mediator of DNA-damage checkpoint 1
MDM2	Mdm2 p53 binding protein homolog (mouse)
MDM2	double minute 2 protein
MDR1	ATP-binding cassette, sub-family B (MDR/TAP), member 1
MEK	map-erk kinase
MHC-1	major histocompatibility complex class 1
MNA	MYCN amplification
MORF4	mortality factor 4
MRN	Mre11/Rad50/Nbs1
mtDNA	mitochondrial DNA
MXI1	MAX interactor 1

MYC	v-myc myelocytomatosis viral oncogene homolog (avian)
MYCN	v-myc myelocytomatosis viral related oncogene, neuroblastoma derived (avian)
NAD(P)H	Nicotinamide adenine dinucleotide (phosphate)
NAG	neuroblastoma amplified gene
NAO	10-N-nonyl acridine orange
Nbs1	Nijmegen breakage syndrome 1
N-cells	neuronal cells
NHEJ	non-homologous end joining
NO^-	nitroxyl anion
NO_2	nitrogen dioxide
NO_2Cl	nitryl chloride
$NO^\cdot$	nitric oxide
NTPs	ribonucleotide triphosphate
$O_2^{\cdot}$-	superoxide radicals
$OH^\cdot$	hydroxyl radicals
$ONOO^-$	peroxynitrite
PARP-2	poly (ADP-ribose) polymerase family, member 2
PHOX2B	paired-like homeobox 2b
PIKK	phosphoinositide-3-kinase-related protein kinase
POT1	protection of telomeres 1 homolog
pRb	retinoblastoma protein
PTEN	phosphatase and tensin homolog
RAC1	Ras-related C3 botulinum toxin substrate 1
Rad51	RecA homolog, E. coli
RAF52 cells	rat embryo fibroblasts
Rap1	Repressor Activator Protein
RD	restrictive dermopathy
RNA	ribonucleic acid

RNR	ribonucleotide reductase
RNS	reactive nitrogen species
ROS	Reactive oxygen species
RRM1	ribonucleotide reductase large subunit
RRM2	ribonucleotide reductase small subunit
RRM2B	ribonucleotide reductase p53 inducible small subunit
RS	radical species
RT	room temperature
SA-β-Gal	senescence-associated -galactosidase
SAHF	senescent-associated heterochromatic foci
SCC	sodium chloride/sodium citrate, pH 7
SDS-PAGE	sodium dodecyl sulfate polyacrylamide gel electrophoresis
-SH	thiol group
SIPS	stress-induced premature senescence
SMAD3	mothers against decapentaplegic homolog 3
SMURF2	SMAD specific E3 ubiquitin protein ligase 2
SSB	single strand breaks
STA-NB-9/10	St. Anna Neuroblastoma 9/10
STAT5	signal transducer and activator of transcription 5
SV40	Simian virus 40
TBS	tris buffered saline
TERT	the catalytical subunit of telomerase
TGF-β	transforming growth factor
TIN2	TRF1-interacting factor
TMPO	thymopoietin
TPP1	tripeptidyl peptidase I
TRF1	telomeric repeat binding factor 1
TRF2	telomeric repeat binding factor 2

TRITC	tetramethylrhodamine isothiocyanate
TrkA	neurotrophic tyrosine kinase, receptor, type 1
TrkB	neurotrophic tyrosine kinase, receptor, type 2
TXT	Triton X-100
UTP	uridine triphosphate
UTR	untranslated region
UV	ultra violet radiation
WRN helicase	Werner's syndrome helicase
XPF	xeroderma pigmentosum, complementation group F
XMRK	Xiphophorus melanoma receptor kinase
Zmpste24	zinc metallopeptidase STE24 homolog
$\Delta\psi_m$	mitochondrial membrane potential
$^{-}OO^{\cdot}$	peroxyl radicals

List of Figures

List of Tables

Reference

Alberts Bruce , J. A., Lewis Julian ,Raff Martin ,Roberts Keith , and Walter Peter (2002). Molecular Biology of the Cell Garland Science, a member of the Taylor & Francis Group. **4th Edition**.

Ambros, I. M. and P. F. Ambros (2000). The Role of Schwann Cells in Neuroblastoma. Neuroblastoma. G. Brodeur, T. Sawada, Y. Tsuchida and P. A. Voûte, Elsevier Science**:** 229 - 243.

Ambros, I. M., S. Rumpler, et al. (1997). "Neuroblastoma cells can actively eliminate supernumerary MYCN gene copies by micronucleus formation--sign of tumour cell revertance?" Eur.J.Cancer **33**(12): 2043-2049.

Batandier, C., E. Fontaine, et al. (2002). "Determination of mitochondrial reactive oxygen species: methodological aspects." J Cell Mol Med **6**(2): 175-87.

Ben-Porath, I. and R. A. Weinberg (2004). "When cells get stressed: an integrative view of cellular senescence." J Clin Invest **113**(1): 8-13.

Ben-Porath, I. and R. A. Weinberg (2005). "The signals and pathways activating cellular senescence." Int J Biochem Cell Biol **37**(5): 961-76.

Benner, S. E., G. M. Wahl, et al. (1991). "Double minute chromosomes and homogeneously staining regions in tumors taken directly from patients versus in human tumor cell lines." Anticancer Drugs **2**(1): 11-25.

Bourdeaut, F., D. Trochet, et al. (2005). "Germline mutations of the paired-like homeobox 2B (PHOX2B) gene in neuroblastoma." Cancer Lett **228**(1-2): 51-8.

Bourdon, A., L. Minai, et al. (2007). "Mutation of RRM2B, encoding p53-controlled ribonucleotide reductase (p53R2), causes severe mitochondrial DNA depletion." Nat Genet **39**(6): 776-80.

Briviba, K., I. Roussyn, et al. (1996). "Attenuation of oxidation and nitration reactions of peroxynitrite by selenomethionine, selenocystine and ebselen." Biochem J **319 (Pt 1)**: 13-5.

Brodeur, G. M. (2003). "Neuroblastoma: biological insights into a clinical enigma." Nat Rev Cancer **3**(3): 203-16.

Brodeur, G. M., F. A. Hayes, et al. (1987). "Consistent N-myc copy number in simultaneous or consecutive neuroblastoma samples from sixty individual patients." Cancer Res **47**(16): 4248-53.

Brodeur, G. M., R. C. Seeger, et al. (1985). "Amplification of N-myc sequences in primary human neuroblastomas: correlation with advanced disease stage." Prog Clin Biol Res **175**: 105-13.

Bunone, G., A. Mariotti, et al. (1997). "Induction of apoptosis by p75 neurotrophin receptor in human neuroblastoma cells." Oncogene **14**(12): 1463-70.

Campestre, C., M. Agamennone, et al. (2006). "N-Hydroxyurea as zinc binding group in matrix metalloproteinase inhibition: mode of binding in a complex with MMP-8." Bioorg Med Chem Lett **16**(1): 20-4.

Campisi, J. (2005). "Senescent cells, tumor suppression, and organismal aging: good citizens, bad neighbors." Cell **120**(4): 513-22.

Campisi, J. and F. d'Adda di Fagagna (2007). "Cellular senescence: when bad things happen to good cells." Nat Rev Mol Cell Biol **8**(9): 729-40.

Canute, G. W., S. L. Longo, et al. (1996). "Hydroxyurea accelerates the loss of epidermal growth factor receptor genes amplified as double-minute chromosomes in human glioblastoma multiforme." Neurosurgery **39**(5): 976-83.

Cao, K., B. C. Capell, et al. (2007). "A lamin A protein isoform overexpressed in Hutchinson-Gilford progeria syndrome interferes with mitosis in progeria and normal cells." Proc Natl Acad Sci U S A **104**(12): 4949-54.

Caron, H. (1995). "Allelic loss of chromosome 1 and additional chromosome 17 material are both unfavourable prognostic markers in neuroblastoma." Med Pediatr Oncol **24**(4): 215-21.

Castino, R., N. Bellio, et al. (2007). "Cathepsin D-Bax death pathway in oxidative stressed

neuroblastoma cells." Free Radic Biol Med **42**(9): 1305-16.
Castle, V. P., K. P. Heidelberger, et al. (1993). "Expression of the apoptosis-suppressing protein bcl-2, in neuroblastoma is associated with unfavorable histology and N-myc amplification." Am J Pathol **143**(6): 1543-50.
Christen, R. D., D. R. Shalinsky, et al. (1992). "Enhancement of the loss of multiple drug resistance by hydroxyurea." Semin Oncol **19**(3 Suppl 9): 94-100.
Ciani, E., S. Severi, et al. (2004). "Nitric oxide negatively regulates proliferation and promotes neuronal differentiation through N-Myc downregulation." J Cell Sci **117**(Pt 20): 4727-37.
Cohn, S. L., H. Salwen, et al. (1990). "Prolonged N-myc protein half-life in a neuroblastoma cell line lacking N-myc amplification." Oncogene **5**(12): 1821-7.
Constantinescu, D., H. L. Gray, et al. (2006). "Lamin A/C expression is a marker of mouse and human embryonic stem cell differentiation." Stem Cells **24**(1): 177-85.
Corvi, R., L. C. Amler, et al. (1994). "MYCN is retained in single copy at chromosome 2 band p23-24 during amplification in human neuroblastoma cells." Proc Natl Acad Sci U S A **91**(12): 5523-7.
Crow, J. P. (1997). "Dichlorodihydrofluorescein and dihydrorhodamine 123 are sensitive indicators of peroxynitrite in vitro: implications for intracellular measurement of reactive nitrogen and oxygen species." Nitric Oxide **1**(2): 145-57.
de Lange, T. (2005). Shelterin: the protein complex that shapes and safeguards human telomeres. **19:** 2100-2110.
Dechat, T., A. Gajewski, et al. (2004). "LAP2alpha and BAF transiently localize to telomeres and specific regions on chromatin during nuclear assembly." J Cell Sci **117**(Pt 25): 6117-28.
Dechat, T., T. Shimi, et al. (2007). "Alterations in mitosis and cell cycle progression caused by a mutant lamin A known to accelerate human aging." Proc Natl Acad Sci U S A **104**(12): 4955-60.
Deng, X., L. Zhang, et al. (2006). "Double minute chromosomes in mouse methotrexate-resistant cells studied by atomic force microscopy." Biochem Biophys Res Commun **346**(4): 1228-33.
Deng, Y., S. S. Chan, et al. (2008). "Telomere dysfunction and tumour suppression: the senescence connection." Nat Rev Cancer **8**(6): 450-8.
Di Lisa, F., P. S. Blank, et al. (1995). "Mitochondrial membrane potential in single living adult rat cardiac myocytes exposed to anoxia or metabolic inhibition." J Physiol **486 (Pt 1)**: 1-13.
Di Micco, R., M. Fumagalli, et al. (2007). "Breaking news: high-speed race ends in arrest--how oncogenes induce senescence." Trends Cell Biol **17**(11): 529-36.
Diaz, G., S. Liu, et al. (2003). "Mitochondrial localization of reactive oxygen species by dihydrofluorescein probes." Histochem Cell Biol **120**(4): 319-25.
Diccianni, M. B., M. Omura-Minamisawa, et al. (1999). "Frequent deregulation of p16 and the p16/G1 cell cycle-regulatory pathway in neuroblastoma." Int J Cancer **80**(1): 145-54.
Dimri, G. P., X. Lee, et al. (1995). "A biomarker that identifies senescent human cells in culture and in aging skin in vivo." Proc Natl Acad Sci U S A **92**(20): 9363-7.
Dole, M., G. Nunez, et al. (1994). "Bcl-2 inhibits chemotherapy-induced apoptosis in neuroblastoma." Cancer Res **54**(12): 3253-9.
Domenicotti, C., B. Marengo, et al. (2003). "Role of PKC-delta activity in glutathione-depleted neuroblastoma cells." Free Radic Biol Med **35**(5): 504-16.
Dorner, D., S. Vlcek, et al. (2006). "Lamina-associated polypeptide 2alpha regulates cell cycle progression and differentiation via the retinoblastoma-E2F pathway." J Cell Biol **173**(1): 83-93.
Ferretti, C., B. Marengo, et al. (2007). "Effects of Agelas oroides and Petrosia ficiformis crude extracts on human neuroblastoma cell survival." Int J Oncol **30**(1): 161-9.
Foisner, R. (2001). "Inner nuclear membrane proteins and the nuclear lamina." J Cell Sci **114**(Pt

21): 3791-2.
Foley, K. P. and R. N. Eisenman (1999). "Two MAD tails: what the recent knockouts of Mad1 and Mxi1 tell us about the MYC/MAX/MAD network." Biochim Biophys Acta **1423**(3): M37-47.
Fong, L. G., J. K. Ng, et al. (2004). "Heterozygosity for Lmna deficiency eliminates the progeria-like phenotypes in Zmpste24-deficient mice." Proc Natl Acad Sci U S A **101**(52): 18111-6.
Ford, J. H., C. J. Schultz, et al. (1988). "Chromosome elimination in micronuclei: a common cause of hypoploidy." Am J Hum Genet **43**(5): 733-40.
Freeman-Edward, J., S. O'Neill, et al. (2000). "Expulsion of amplified MYCN from neuroblastoma tumor cells." Cancer Genet.Cytogenet. **116**(1): 87-88.
Fulda, S., H. Sieverts, et al. (1997). "The CD95 (APO-1/Fas) system mediates drug-induced apoptosis in neuroblastoma cells." Cancer Res **57**(17): 3823-9.
Funayama, R. and F. Ishikawa (2007). "Cellular senescence and chromatin structure." Chromosoma **116**(5): 431-40.
George, R. E., R. M. Kenyon, et al. (1996). "Investigation of co-amplification of the candidate genes ornithine decarboxylase, ribonucleotide reductase, syndecan-1 and a DEAD box gene, DDX1, with N-myc in neuroblastoma. United Kingdom Children's Cancer Study Group." Oncogene **12**(7): 1583-7.
Gernand, D., T. Rutten, et al. (2005). "Uniparental chromosome elimination at mitosis and interphase in wheat and pearl millet crosses involves micronucleus formation, progressive heterochromatinization, and DNA fragmentation." Plant Cell **17**(9): 2431-8.
Giannini, G., F. Cerignoli, et al. (2005). "High mobility group A1 is a molecular target for MYCN in human neuroblastoma." Cancer Res **65**(18): 8308-16.
Gilchrist, S., N. Gilbert, et al. (2004). "Altered protein dynamics of disease-associated lamin A mutants." BMC Cell Biol **5**(1): 46.
Goldstein, S. (1990). "Replicative senescence: the human fibroblast comes of age." Science **249**(4973): 1129-33.
Grandori, C. and R. N. Eisenman (1997). "Myc target genes." Trends Biochem Sci **22**(5): 177-81.
Gruber, J., T. Lampe, et al. (2005). "RNAi of FACE1 protease results in growth inhibition of human cells expressing lamin A: implications for Hutchinson-Gilford progeria syndrome." J Cell Sci **118**(Pt 4): 689-96.
Gruenbaum, Y., A. Margalit, et al. (2005). "The nuclear lamina comes of age." Nat Rev Mol Cell Biol **6**(1): 21-31.
Guo, X., Y. Deng, et al. (2007). "Dysfunctional telomeres activate an ATM-ATR-dependent DNA damage response to suppress tumorigenesis." Embo J **26**(22): 4709-19.
Haithcock, E., Y. Dayani, et al. (2005). "Age-related changes of nuclear architecture in Caenorhabditis elegans." Proc Natl Acad Sci U S A **102**(46): 16690-5.
Halliwell, B. (2007). "Oxidative stress and cancer: have we moved forward?" Biochem J **401**(1): 1-11.
Hanahan, D. and R. A. Weinberg (2000). "The hallmarks of cancer." Cell **100**(1): 57-70.
Hardman, R. A., C. A. Afshari, et al. (2001). "Involvement of mammalian MLH1 in the apoptotic response to peroxide-induced oxidative stress." Cancer Res **61**(4): 1392-7.
Harman, D. (1956). "Aging: A theory based on free radical and radiation " Journal of Gerontology: 288-300.
Hayflick, L. (1965). "The Limited in Vitro Lifetime of Human Diploid Cell Strains." Exp Cell Res **37**: 614-36.
Hayflick, L. and P. S. Moorhead (1961). "The serial cultivation of human diploid cell strains." Exp Cell Res **25**: 585-621.
Hiyama, E., K. Hiyama, et al. (1995). "Correlating telomerase activity levels with human neuroblastoma outcomes." Nat Med **1**(3): 249-55.

Holland, J., E. Frei, et al. (2003). Cancer Medicine. London, BC Decker Inc.
Hong, S. H., B. I. Hong, et al. (2004). "Involvement of mitogen-activated protein kinases and p21Waf1 in hydroxyurea-induced G1 arrest and senescence of McA-RH7777 rat hepatoma cell line." Exp Mol Med **36**(5): 493-8.
Itahana, K., J. Campisi, et al. (2004). "Mechanisms of cellular senescence in human and mouse cells." Biogerontology **5**(1): 1-10.
Itahana, K., J. Campisi, et al. (2007). "Methods to detect biomarkers of cellular senescence: the senescence-associated beta-galactosidase assay." Methods Mol Biol **371**: 21-31.
Itahana, K., Y. Zou, et al. (2003). "Control of the replicative life span of human fibroblasts by p16 and the polycomb protein Bmi-1." Mol Cell Biol **23**(1): 389-401.
Itoh, N. and N. Shimizu (1998). "DNA replication-dependent intranuclear relocation of double minute chromatin." J Cell Sci **111 (Pt 22)**: 3275-85.
Keshelava, N., R. C. Seeger, et al. (1997). "Drug resistance in human neuroblastoma cell lines correlates with clinical therapy." Eur J Cancer **33**(12): 2002-6.
Kim, H. S., E. J. Yeo, et al. (2005). "p21WAF/CIP1/SDI1 is upregulated due to increased mRNA stability during hydroxyurea-induced senescence of human fibroblasts." Mech Ageing Dev **126**(12): 1255-61.
King, S. B. (2003). "The nitric oxide producing reactions of hydroxyurea." Curr Med Chem **10**(6): 437-52.
Kirkwood, T. B. (2005). "Understanding the odd science of aging." Cell **120**(4): 437-47.
Kohl, N. E., N. Kanda, et al. (1983). "Transposition and amplification of oncogene-related sequences in human neuroblastomas." Cell **35**(2 Pt 1): 359-67.
Konorev, E. A., H. Zhang, et al. (2000). "Bicarbonate exacerbates oxidative injury induced by antitumor antibiotic doxorubicin in cardiomyocytes." Am J Physiol Heart Circ Physiol **279**(5): H2424-30.
Koppen, A., R. Ait-Aissa, et al. (2007). "Dickkopf-1 is down-regulated by MYCN and inhibits neuroblastoma cell proliferation." Cancer Lett **256**(2): 218-28.
Koppen, A., R. Ait-Aissa, et al. (2008). "Dickkopf-3 expression is a marker for neuroblastic tumor maturation and is down-regulated by MYCN." Int J Cancer **122**(7): 1455-64.
Krämer, O. H., S. K. Knauer, et al. (2008). "Histone deacetylase inhibitors and hydroxyurea modulate the cell cycle and cooperatively induce apoptosis." Oncogene **27**(6): 732-40.
Kudlow, B. A., B. K. Kennedy, et al. (2007). "Werner and Hutchinson-Gilford progeria syndromes: mechanistic basis of human progeroid diseases." Nat Rev Mol Cell Biol **8**(5): 394-404.
Kurz, D. J., S. Decary, et al. (2004). "Chronic oxidative stress compromises telomere integrity and accelerates the onset of senescence in human endothelial cells." J Cell Sci **117**(Pt 11): 2417-26.
Kwak, I. H., H. S. Kim, et al. (2004). "Nuclear accumulation of globular actin as a cellular senescence marker." Cancer Res **64**(2): 572-80.
Ladenstein, R., F. Berthold, et al., Eds. (2006). Neuroblastome. Pädiatrische Hämatologie und Onkologie. Heidelberg, Springer Medizin Verlag.
Lahoz, E. G., L. Xu, et al. (1994). "Suppression of Myc, but not E1a, transformation activity by Max-associated proteins, Mad and Mxi1." Proc Natl Acad Sci U S A **91**(12): 5503-7.
Lammerding, J. and R. T. Lee (2005). "The nuclear membrane and mechanotransduction: impaired nuclear mechanics and mechanotransduction in lamin A/C deficient cells." Novartis Found Symp **264**: 264-73; discussion 273-8.
Lans, H. and J. H. Hoeijmakers (2006). "Cell biology: ageing nucleus gets out of shape." Nature **440**(7080): 32-4.
Le, N. T. and D. R. Richardson (2002). "The role of iron in cell cycle progression and the proliferation of neoplastic cells." Biochim Biophys Acta **1603**(1): 31-46.
Leprat, P., M. H. Ratinaud, et al. (1990). "A new method for testing cell ageing using two

mitochondria specific fluorescent probes." Mech Ageing Dev **52**(2-3): 149-67.
Lin, Z. P., M. F. Belcourt, et al. (2007). "Excess ribonucleotide reductase R2 subunits coordinate the S phase checkpoint to facilitate DNA damage repair and recovery from replication stress." Biochemical Pharmacology **73**(6): 760-772.
Lisby, M., J. H. Barlow, et al. (2004). "Choreography of the DNA damage response: spatiotemporal relationships among checkpoint and repair proteins." Cell **118**(6): 699-713.
Lisby, M. and R. Rothstein (2004). "DNA damage checkpoint and repair centers." Curr Opin Cell Biol **16**(3): 328-34.
Lisby, M. and R. Rothstein (2005). "Localization of checkpoint and repair proteins in eukaryotes." Biochimie **87**(7): 579-89.
Liu, B. and Z. Zhou (2008). "Lamin A/C, laminopathies and premature ageing." Histol Histopathol **23**(6): 747-63.
Liu, J., T. Rolef Ben-Shahar, et al. (2000). "Essential roles for Caenorhabditis elegans lamin gene in nuclear organization, cell cycle progression, and spatial organization of nuclear pore complexes." Mol Biol Cell **11**(11): 3937-47.
Mallette, F. A. and G. Ferbeyre (2007). "The DNA damage signaling pathway connects oncogenic stress to cellular senescence." Cell Cycle **6**(15): 1831-6.
Marengo, B., E. Balbis, et al. (2008). "GSH loss per se does not affect neuroblastoma survival and is not genotoxic." Int J Oncol **32**(1): 121-7.
Marengo, B., C. De Ciucis, et al. (2008). "Mechanisms of BSO (L-buthionine-S,R-sulfoximine)-induced cytotoxic effects in neuroblastoma." Free Radic Biol Med **44**(3): 474-82.
Marengo, B., L. Raffaghello, et al. (2005). "Reactive oxygen species: biological stimuli of neuroblastoma cell response." Cancer Lett **228**(1-2): 111-6.
Markiewicz, E., T. Dechat, et al. (2002). "Lamin A/C binding protein LAP2alpha is required for nuclear anchorage of retinoblastoma protein." Mol Biol Cell **13**(12): 4401-13.
Marusyk, A., L. J. Wheeler, et al. (2007). "p53 mediates senescence-like arrest induced by chronic replicational stress." Mol Cell Biol **27**(15): 5336-51.
Mattout, A., T. Dechat, et al. (2006). "Nuclear lamins, diseases and aging." Curr Opin Cell Biol **18**(3): 335-41.
Maurer, B. J., L. S. Metelitsa, et al. (1999). "Increase of ceramide and induction of mixed apoptosis/necrosis by N-(4-hydroxyphenyl)- retinamide in neuroblastoma cell lines." J Natl Cancer Inst **91**(13): 1138-46.
Mawatari, S. and K. Murakami (2001). "Effects of ascorbate on membrane phospholipids and tocopherols of intact erythrocytes during peroxidation by t-butylhydroperoxide: comparison with effects of dithiothreitol." Lipids **36**(1): 57-65.
McKusick, V. A. (2007). "Mendelian Inheritance in Man and its online version, OMIM." Am J Hum Genet **80**(4): 588-604.
Melov, S. (2000). "Mitochondrial oxidative stress. Physiologic consequences and potential for a role in aging." Ann N Y Acad Sci **908**: 219-25.
Molenaar, J. J., M. E. Ebus, et al. (2008). "Cyclin D1 and CDK4 activity contribute to the undifferentiated phenotype in neuroblastoma." Cancer Res **68**(8): 2599-609.
Moreau, L. A., P. McGrady, et al. (2006). "Does MYCN amplification manifested as homogeneously staining regions at diagnosis predict a worse outcome in children with neuroblastoma? A Children's Oncology Group study." Clin Cancer Res **12**(19): 5693-7.
Naetar, N., S. Hutter, et al. (2007). "LAP2alpha-binding protein LINT-25 is a novel chromatin-associated protein involved in cell cycle exit." J Cell Sci **120**(Pt 5): 737-47.
Nagai, T., T. Tarumoto, et al. (2003). "Oxidative stress is involved in hydroxyurea-induced erythroid differentiation." Br J Haematol **121**(4): 657-61.
Nakagawara, A., M. Arima, et al. (1992). "Inverse relationship between trk expression and N-myc amplification in human neuroblastomas." Cancer Res **52**(5): 1364-8.

Nakagawara, A., C. G. Azar, et al. (1994). "Expression and function of TRK-B and BDNF in human neuroblastomas." Mol Cell Biol **14**(1): 759-67.
Nakamura, M., M. Yamada, et al. (2006). "Phosphoproteomic profiling of human SH-SY5Y neuroblastoma cells during response to 6-hydroxydopamine-induced oxidative stress." Biochim Biophys Acta **1763**(9): 977-89.
Narath, R., I. M. Ambros, et al. (2007). "Induction of senescence in MYCN amplified neuroblastoma cell lines by hydroxyurea." Genes Chromosomes Cancer **46**(2): 130-42.
Narita, M., S. Nuñez, et al. (2003). "Rb-Mediated Heterochromatin Formation and Silencing of E2F Target Genes during Cellular Senescence." Cell **113**(6): 703-716.
Nieminen, A. L., A. M. Byrne, et al. (1997). "Mitochondrial permeability transition in hepatocytes induced by t-BuOOH: NAD(P)H and reactive oxygen species." Am J Physiol **272**(4 Pt 1): C1286-94.
Nitta, R. T., S. A. Jameson, et al. (2006). "Stabilization of the retinoblastoma protein by A-type nuclear lamins is required for INK4A-mediated cell cycle arrest." Mol Cell Biol **26**(14): 5360-72.
Nitta, R. T., C. L. Smith, et al. (2007). "Evidence that proteasome-dependent degradation of the retinoblastoma protein in cells lacking A-type lamins occurs independently of gankyrin and MDM2." PLoS ONE **2**(9): e963.
Nordlund, P., B. M. Sjoberg, et al. (1990). "Three-dimensional structure of the free radical protein of ribonucleotide reductase." Nature **345**(6276): 593-8.
Norris, M. D., S. B. Bordow, et al. (1997). "Evidence that the MYCN oncogene regulates MRP gene expression in neuroblastoma." Eur J Cancer **33**(12): 1911-6.
Obe, G. and D. Vijayalaxmi, Eds. (2007). Chromosomal alterations
Methods, Results and Importance in Human Health. Heidelberg, Springer-Verlag.
Oberdoerffer, P. and D. A. Sinclair (2007). "The role of nuclear architecture in genomic instability and ageing." Nat Rev Mol Cell Biol **8**(9): 692-702.
Omura-Minamisawa, M., M. B. Diccianni, et al. (2001). "p16/p14(ARF) cell cycle regulatory pathways in primary neuroblastoma: p16 expression is associated with advanced stage disease." Clin Cancer Res **7**(11): 3481-90.
Oubrahim, H., E. R. Stadtman, et al. (2001). "Mitochondria play no roles in Mn(II)-induced apoptosis in HeLa cells." Proc Natl Acad Sci U S A **98**(17): 9505-10.
Oue, T., M. Fukuzawa, et al. (1996). "In situ detection of DNA fragmentation and expression of bcl-2 in human neuroblastoma: relation to apoptosis and spontaneous regression." J Pediatr Surg **31**(2): 251-7.
Pacher, P., J. S. Beckman, et al. (2007). "Nitric oxide and peroxynitrite in health and disease." Physiol Rev **87**(1): 315-424.
Park, J. I., H. S. Choi, et al. (2001). "Involvement of p38 kinase in hydroxyurea-induced differentiation of K562 cells." Cell Growth Differ **12**(9): 481-6.
Park, J. I., J. S. Jeong, et al. (2000). "Hydroxyurea induces a senescence-like change of K562 human erythroleukemia cell." J Cancer Res Clin Oncol **126**(8): 455-60.
Passos, J. F., G. Saretzki, et al. (2007). "Mitochondrial dysfunction accounts for the stochastic heterogeneity in telomere-dependent senescence." PLoS Biol **5**(5): e110.
Passos, J. F., G. Saretzki, et al. (2007). "DNA damage in telomeres and mitochondria during cellular senescence: is there a connection?" Nucleic Acids Res **35**(22): 7505-13.
Passos, J. F. and T. von Zglinicki (2005). "Mitochondria, telomeres and cell senescence." Exp Gerontol **40**(6): 466-72.
Passos, J. F. and T. Von Zglinicki (2006). "Oxygen free radicals in cell senescence: are they signal transducers?" Free Radic Res **40**(12): 1277-83.
Passos, J. F., T. von Zglinicki, et al. (2006). "Mitochondrial dysfunction and cell senescence: cause or consequence?" Rejuvenation Res **9**(1): 64-8.

Pekovic, V., J. Harborth, et al. (2007). "Nucleoplasmic LAP2alpha-lamin A complexes are required to maintain a proliferative state in human fibroblasts." J Cell Biol **176**(2): 163-72.
Petit, T., K. Davidson, et al. (1999). "Elimination of extrachromosomal c-myc genes by hydroxyurea induces apoptosis." Apoptosis **4**(3): 163-7.
Polyak, K., Y. Xia, et al. (1997). "A model for p53-induced apoptosis." Nature **389**(6648): 300-305.
Pontarin, G., P. Ferraro, et al. (2007). "p53R2-dependent ribonucleotide reduction provides deoxyribonucleotides in quiescent human fibroblasts in the absence of induced DNA damage." J Biol Chem **282**(23): 16820-8.
Prokocimer, M., A. Margalit, et al. (2006). "The nuclear lamina and its proposed roles in tumorigenesis: projection on the hematologic malignancies and future targeted therapy." J Struct Biol **155**(2): 351-60.
Raymond, E., S. Faivre, et al. (2001). "Effects of hydroxyurea on extrachromosomal DNA in patients with advanced ovarian carcinomas." Clin Cancer Res **7**(5): 1171-80.
Reiter, J. L. and G. M. Brodeur (1996). "High-resolution mapping of a 130-kb core region of the MYCN amplicon in neuroblastomas." Genomics **32**(1): 97-103.
Reiter, J. L. and G. M. Brodeur (1998). "MYCN is the only highly expressed gene from the core amplified domain in human neuroblastomas." Genes Chromosomes Cancer **23**(2): 134-40.
Rencricca, N. J., B. S. Morse, et al. (1975). "Hydroxyurea-induced erythroid differentiation." Proc Soc Exp Biol Med **149**(4): 1052-4.
Rober, R. A., H. Sauter, et al. (1990). "Cells of the cellular immune and hemopoietic system of the mouse lack lamins A/C: distinction versus other somatic cells." J Cell Sci **95 (Pt 4)**: 587-98.
Roninson, I. B. (2003). "Tumor cell senescence in cancer treatment." Cancer Res **63**(11): 2705-15.
Ross, R. A., J. L. Biedler, et al. (2003). "A role for distinct cell types in determining malignancy in human neuroblastoma cell lines and tumors." Cancer Lett **197**(1-2): 35-9.
Ross, R. A., B. A. Spengler, et al. (1983). "Coordinate morphological and biochemical interconversion of human neuroblastoma cells." J.Natl.Cancer Inst. **71**(4): 741-747.
Salvioli, S., A. Ardizzoni, et al. (1997). "JC-1, but not DiOC6(3) or rhodamine 123, is a reliable fluorescent probe to assess delta psi changes in intact cells: implications for studies on mitochondrial functionality during apoptosis." FEBS Lett **411**(1): 77-82.
Scaffidi, P. and T. Misteli (2006). "Lamin A-dependent nuclear defects in human aging." Science **312**(5776): 1059-63.
Scaffidi, P. and T. Misteli (2008). "Lamin A-dependent misregulation of adult stem cells associated with accelerated ageing." Nat Cell Biol **10**(4): 452-9.
Schiffmann, D. and U. De Boni (1991). "Dislocation of chromatin elements in prophase induced by diethylstilbestrol: a novel mechanism by which micronuclei can arise." Mutat Res **246**(1): 113-22.
Schmitt, C. A., J. S. Fridman, et al. (2002). "A senescence program controlled by p53 and p16INK4a contributes to the outcome of cancer therapy." Cell **109**(3): 335-46.
Schoenlein, P. V., J. T. Barrett, et al. (2003). "Radiation therapy depletes extrachromosomally amplified drug resistance genes and oncogenes from tumor cells via micronuclear capture of episomes and double minute chromosomes." Int J Radiat Oncol Biol Phys **55**(4): 1051-65.
Schrell, U. M., M. G. Rittig, et al. (1997). "Hydroxyurea for treatment of unresectable and recurrent meningiomas. I. Inhibition of primary human meningioma cells in culture and in meningioma transplants by induction of the apoptotic pathway." J Neurosurg **86**(5): 845-52.
Schwab, M., K. Alitalo, et al. (1983). "Amplified DNA with limited homology to myc cellular oncogene is shared by human neuroblastoma cell lines and a neuroblastoma tumour." Nature **305**(5931): 245-8.
Scotti, C., L. Iamele, et al. (2003). "Lack of molecular relationships between lipid peroxidation and mitochondrial DNA single strand breaks in isolated rat hepatocytes and mitochondria." Mitochondrion **2**(5): 361-73.

Seeger, R. C., G. M. Brodeur, et al. (1985). "Association of multiple copies of the N-myc oncogene with rapid progression of neuroblastomas." N Engl J Med **313**(18): 1111-6.
Serrano, M., A. W. Lin, et al. (1997). "Oncogenic ras provokes premature cell senescence associated with accumulation of p53 and p16INK4a." Cell **88**(5): 593-602.
Shao, J., B. Zhou, et al. (2006). "Ribonucleotide reductase inhibitors and future drug design." Curr Cancer Drug Targets **6**(5): 409-31.
Shimizu, N., N. Itoh, et al. (1998). "Selective entrapment of extrachromosomally amplified DNA by nuclear budding and micronucleation during S phase." J Cell Biol **140**(6): 1307-20.
Shimizu, N., T. Kanda, et al. (1996). "Selective capture of acentric fragments by micronuclei provides a rapid method for purifying extrachromosomally amplified DNA." Nat.Genet. **12**(1): 65-71.
Shohet, J. M., M. J. Hicks, et al. (2002). "Minichromosome maintenance protein MCM7 is a direct target of the MYCN transcription factor in neuroblastoma." Cancer Res **62**(4): 1123-8.
Shumaker, D. K., T. Dechat, et al. (2006). "Mutant nuclear lamin A leads to progressive alterations of epigenetic control in premature aging." Proc Natl Acad Sci U S A **103**(23): 8703-8.
Shumaker, D. K., E. R. Kuczmarski, et al. (2003). "The nucleoskeleton: lamins and actin are major players in essential nuclear functions." Curr Opin Cell Biol **15**(3): 358-66.
Sies, H., V. S. Sharov, et al. (1997). "Glutathione peroxidase protects against peroxynitrite-mediated oxidations. A new function for selenoproteins as peroxynitrite reductase." J Biol Chem **272**(44): 27812-7.
Slack, A., Z. Chen, et al. (2005). "The p53 regulatory gene MDM2 is a direct transcriptional target of MYCN in neuroblastoma." Proc Natl Acad Sci U S A **102**(3): 731-6.
Slack, A. and J. M. Shohet (2005). "MDM2 as a critical effector of the MYCN oncogene in tumorigenesis." Cell Cycle **4**(7): 857-60.
Slamon, D. J., T. C. Boone, et al. (1986). "Identification and characterization of the protein encoded by the human N-myc oncogene." Science **232**(4751): 768-72.
Smith, R. A., G. F. Kelso, et al. (2003). "Using mitochondria-targeted molecules to study mitochondrial radical production and its consequences." Biochem Soc Trans **31**(Pt 6): 1295-9.
Snapka, R. M. and A. Varshavsky (1983). "Loss of unstably amplified dihydrofolate reductase genes from mouse cells is greatly accelerated by hydroxyurea." Proc Natl Acad Sci U S A **80**(24): 7533-7.
Snyers, L., S. Vlcek, et al. (2007). "Lamina-associated polypeptide 2-alpha forms homo-trimers via its C terminus, and oligomerization is unaffected by a disease-causing mutation." J Biol Chem **282**(9): 6308-15.
Spengler, B. A., D. L. Lazarova, et al. (1997). "Cell lineage and differentiation state are primary determinants of MYCN gene expression and malignant potential in human neuroblastoma cells." Oncol.Res. **9**(9): 467-476.
Starcevic, S. L., N. M. Diotte, et al. (2003). "Oxidative DNA damage and repair in a cell lineage model of human proliferative breast disease (PBD)." Toxicol Sci **75**(1): 74-81.
Stock, C., E. Bozsaky, et al. (2008). "Genes proximal and distal to MYCN are highly expressed in human neuroblastoma as visualized by comparative expressed sequence hybridization." Am J Pathol **172**(1): 203-14.
Suzuki, M. and D. A. Boothman (2008). "Stress-induced Premature Senescence (SIPS)." J Radiat Res (Tokyo).
Suzuki, T., E. Bogenmann, et al. (1993). "Lack of high-affinity nerve growth factor receptors in aggressive neuroblastomas." J Natl Cancer Inst **85**(5): 377-84.
Szekeres, T., M. Fritzer-Szekeres, et al. (1997). "The enzyme ribonucleotide reductase: target for antitumor and anti-HIV therapy." Crit Rev Clin Lab Sci **34**(6): 503-28.
Takahashi, M., M. Shibata, et al. (2001). "Estimation of lipid peroxidation of live cells using a

fluorescent probe, diphenyl-1-pyrenylphosphine." Free Radic Biol Med **31**(2): 164-74.
Tanaka, T. and N. Shimizu (2000). "Induced detachment of acentric chromatin from mitotic chromosomes leads to their cytoplasmic localization at G(1) and the micronucleation by lamin reorganization at S phase." J Cell Sci **113 (Pt 4)**: 697-707.
Terman, A. and U. T. Brunk (2006). "Oxidative stress, accumulation of biological 'garbage', and aging." Antioxid Redox Signal **8**(1-2): 197-204.
Thiele, C. J., C. P. Reynolds, et al. (1985). "Decreased expression of N-myc precedes retinoic acid-induced morphological differentiation of human neuroblastoma." Nature **313**(6001): 404-6.
Thompson, P. M., B. A. Seifried, et al. (2001). "Loss of heterozygosity for chromosome 14q in neuroblastoma." Med Pediatr Oncol **36**(1): 28-31.
Toussaint, O., E. E. Medrano, et al. (2000). "Cellular and molecular mechanisms of stress-induced premature senescence (SIPS) of human diploid fibroblasts and melanocytes." Exp.Gerontol. **35**(8): 927-945.
Valent, A., J. Benard, et al. (2001). "In vivo elimination of acentric double minutes containing amplified MYCN from neuroblastoma tumor cells through the formation of micronuclei." Am.J.Pathol. **158**(5): 1579-1584.
Van Berlo, J. H., J. W. Voncken, et al. (2005). "A-type lamins are essential for TGF-beta1 induced PP2A to dephosphorylate transcription factors." Hum Mol Genet **14**(19): 2839-49.
van Noesel, M. M. and R. Versteeg (2004). "Pediatric neuroblastomas: genetic and epigenetic `Danse Macabre'." Gene **325**: 1-15.
Vigouroux, C., M. Auclair, et al. (2001). "Nuclear envelope disorganization in fibroblasts from lipodystrophic patients with heterozygous R482Q/W mutations in the lamin A/C gene." J Cell Sci **114**(Pt 24): 4459-68.
Vlcek, S. and R. Foisner (2007). "Lamins and lamin-associated proteins in aging and disease." Curr Opin Cell Biol **19**(3): 298-304.
Von Hoff, D. D., J. R. McGill, et al. (1992). "Elimination of extrachromosomally amplified MYC genes from human tumor cells reduces their tumorigenicity." Proc.Natl.Acad.Sci.U.S.A **89**(17): 8165-8169.
Von Hoff, D. D., T. Waddelow, et al. (1991). "Hydroxyurea accelerates loss of extrachromosomally amplified genes from tumor cells." Cancer Res. **51**(23 Pt 1): 6273-6279.
von Zglinicki, T., G. Saretzki, et al. (2005). "Human cell senescence as a DNA damage response." Mech Ageing Dev **126**(1): 111-7.
Voss, P. and W. Siems (2006). "Clinical oxidation parameters of aging." Free Radic Res **40**(12): 1339-49.
Wallis, C. V., A. N. Sheerin, et al. (2004). "Fibroblast clones from patients with Hutchinson-Gilford progeria can senesce despite the presence of telomerase." Exp Gerontol **39**(4): 461-7.
Ward, I. M. and J. Chen (2001). "Histone H2AX is phosphorylated in an ATR-dependent manner in response to replicational stress." J Biol Chem **276**(51): 47759-62.
Weirich-Schwaiger, H., H. G. Weirich, et al. (1994). "Correlation between senescence and DNA repair in cells from young and old individuals and in premature aging syndromes." Mutat Res **316**(1): 37-48.
Weiss, M. J., C. Guo, et al. (2000). "Localization of a hereditary neuroblastoma predisposition gene to 16p12-p13." Med Pediatr Oncol **35**(6): 526-30.
Wenzel, A., C. Cziepluch, et al. (1991). "The N-Myc oncoprotein is associated in vivo with the phosphoprotein Max(p20/22) in human neuroblastoma cells." Embo J **10**(12): 3703-12.
Wenzel, A. and M. Schwab (1995). "The mycN/max protein complex in neuroblastoma. Short review." Eur J Cancer **31A**(4): 516-9.
White, P. S., J. M. Maris, et al. (1997). "Molecular analysis of the region of distal 1p commonly deleted in neuroblastoma." Eur J Cancer **33**(12): 1957-61.
Wimmer, K., X. X. Zhu, et al. (1999). "Co-amplification of a novel gene, NAG, with the N-myc

gene in neuroblastoma." Oncogene **18**(1): 233-8.
Wink, D. A. and J. B. Mitchell (1998). "Chemical biology of nitric oxide: Insights into regulatory, cytotoxic, and cytoprotective mechanisms of nitric oxide." Free Radic Biol Med **25**(4-5): 434-56.
Wu, C. H., R. Apweiler, et al. (2008). "The universal protein resource (UniProt)." Nucleic Acids Res **36**(Database issue): D190-5.
Yeo, E. J., Y. C. Hwang, et al. (2000). "Senescence-like changes induced by hydroxyurea in human diploid fibroblasts." Exp Gerontol **35**(5): 553-71.
Zhang, H. (2007). "Molecular signaling and genetic pathways of senescence: Its role in tumorigenesis and aging." J Cell Physiol **210**(3): 567-74.
Zhou, B. B. and S. J. Elledge (2000). "The DNA damage response: putting checkpoints in perspective." Nature **408**(6811): 433-9.

Curriculum Vitae

Lebenslauf	Heide-Marie Binder
Persönliche Daten	geboren am 25. Februar 1982 in Linz, Oberösterreich
	Wohnadresse: Haberlgasse 51/11, 1160 Wien
	Email: heidi.binder@ccri.at Telefonnummer: +43(1)40470-4050 Mobiltelefon: +43(699)8128 1646
Ausbildung	
2007 – 2008	Diplomarbeit am CHILDREN'S CANCER RESEARCH INSTITUTE, St. Anna Kinderkrebsforschung
2007	Kurze Wissenschaftlich Arbeit bei Prof. T. von Zglinicki im Henry Wellcome Laboratory for Biogerontology Research, Newcastle upon Tyne, England
2006	Auslandssemester an der UAM, Madrid, Spanien mit Praktikum bei María Ángeles Muñoz-Fernández, PhD, MD im Laboratorio de Inmuno-Biología Molecular des Universitätskrankenhaus Gregorio Marañon
2000 - 2008	Diplomstudium der molekularen Biologie an der Universität Wien
1992 - 2000	AHS, International School Linz-Auhof mit internationalem Baccalaureat und österreichischer Matura abgeschlossen
1988 - 1992	Volksschule Linz